Spatial Organization of CD28 Modulates T-cell Activation

Haoqian Chen

Submitted in partial fulfillment of the
Requirements for the degree of
Doctor of Philosophy
In the Graduate School of Arts and Sciences

COLUMBIA UNIVERSITY
2016

ABSTRACT

Spatial Organization of CD28 Modulates T-cell Activation

Haoqian Chen

T-cells are central to our success as a species. They confer specific and long-term immunity in a process known as adaptive immunity. During adaptive immune response, pathogen ingested by peripheral sentinel cells are brought to the local lymph nodes and presented to T-cells. T-cell recognizes the antigen via its receptor complex (TCR-CD3). The high affinity binding primes the cell for activation. With a positive costimulationary signal from CD28, the T-cell is fully activated, resulting in IL-2 secretions and cellular proliferation. Clinicians are increasingly harnessing the adaptive immune system to combat diseases such as cancer. Specifically, T-cells are activated and expanded ex vivo for adoptive immunotherapies. The ability to modulate T-cell activation is crucial in engineering appropriate effector cell populations for therapeutics. The focus of this thesis is to address the functional impact of CD28 spatial organization on T-cell activation.

It has been observed that the spatial segregation of CD3 and CD28 by a few microns has resulted in poor activation of human T-cells. Lck, a Src family kinase (SFK) emerges as the

instigator of the phenomenon. The kinase is associated with both CD3 and CD28 signal cascades. We propose a reaction diffusion model to describe the delicate balance between protein mobility and Lck de-activation. The work in this dissertation describes two probes to investigate Lck kinase activity, which permit real-time imaging of both the initiation of pLck activity and its duration. A FRET reporter is constructed to study the spatial and temporal initiation of the kinase activity. Embedded with the Lck membrane domain and contained a substrate for pLck to phosphorylate, the FRET biosensor reports the Lck kinase activity in real-time. Using microprinting to control CD3 and CD28 spatial organizations, the FRET reporter reveals that while T-cells require CD28 for significant IL-2 secretion, CD3 engagement is essential to initiate cellular activation through a spike in pLck kinase activity. Spatially, the reporter shows heightened kinase activity concentrated at the center of the cells upon CD3 engagement.

To study the duration of pLck activity, a recruitment reporter is made. CD3 is found ubiquitously throughout the cellular membrane. And its activation by pLck induces the recruitment of a pair of tandem SH2-domain. The recruitment probe (also containing a pair of tandem SH2-domain) revealed curtailed pLck kinase activity due to CD3-CD28 segregation. Ultimately, understanding CD28 modulation of T-cell activation is clinically relevant as it provides new opportunities and targets for the development of therapeutics.

Table of Contents

List of Figures

Figure 1.3: Plasticity of T-cell differentiation. The ability of T-cell lineages to be reconditioned has important implications for immunotherapeutics. From (Zhou, Chong et al. 2009).

Figure 1.4: MHC-TCR-independent activation of engineered T-cells achieved with antibody receptor genetically engineered against a target antigen. The receptor is then coupled to a signaling domain intracellularly. Adapted from (Maus, Grupp et al. 2014) and (Restifo, Dudley et al. 2012).

Figure 1.5: A. Immunological synapse is the site of critical ligand interactions. T-cells are primed when TCRs recognize specific peptide-loaded MHC. Then costimulatory signal is given by APC via its binding to either CD28 or CTLA-4 receptors. The signaling structure is further stabilized by adhesive receptor LFA-1, which binds to ICAM-1 on APCs. From (Abbas, Lichtman et al. 2007). B. The high sensitivity of T-cell recognition is made possible by the formation of spatially discrete zones within the SMAC. Adapted from (Dustin, Chakraborty et al. 2010).

Figure 1.6: The effect of CD80 on TCR spatial organization. A. The APC presents only MHC-II and LFA-1. CD80 is necessary for TCR migration to the cSMAC. Its absence results in loss of spatial segregation as TCR (red) mixes with LFA-1 (blue). B. With full-length CD80, one observes segregation of CD80FL from TCR clusters. C. With tail deleted CD80, CD80TL colocalizes with TCR. Scale bar = 2μm. From (Tseng, Liu et al. 2005)

Figure 1.7: A. Mouse T-cells respond robustly to peripheral presentation of CD28. From (Shen, Thomas et al. 2008). B. Human T-cells respond most potently to colocalized presentation

of CD3 and CD28, and also peripheral presentation of the proteins. From (Bashour, Tsai et al. 2014).

Figure 1.8: A. Well established is the role of pLck in TCR/CD3 complex-associated signaling. Lck phosphorylates ITAMs on CD3. Then pITAMs act as docking sites for ZAP70 by interacting with the ZAP70 SH2 domains. ZAP70 initiates a network of signaling proteins with diverse functions. Adapted from (Koretzky and Myung 2001). B. Less understood is the role of pLck in CD28-associated signaling. Two signaling pathways have been discovered for CD28. One is a PI3K (the p86-p110 heterodimer)-dependent pathway, and another is an adaptor protein (Grb2 or GADS)-dependent pathway. Suspect of phosphorylating the YMNM motifs on CD28, Lck is known also to activate PDK1. Adapted from (Boomer and Green 2010).

Figure 1.9: A. Stainings in mouse T-cells revealed pLck to be localized throughout the interface, regardless of the patterned surfaces. From (Bashour, Tsai et al. 2014). B. Human T-cell stainings of Lck revealed a preference for CD3, with lesser overlap on CD28. From (Bashour, Tsai et al. 2014). C. Translocation of Lck between TCR-CD3 complex and CD28 to initiate signaling cascade will be a function of Lck diffusion and pLck dephosphorylation. Please note: pLck staining was performed with pY394 antibody, which is unable to distinguish between pLck and pFyn. Thus, it's referred to as pSFK.

Figure 2.1: Autoinhibited kinase is characterized by the activating Y416 being buried in the active site cleft. This is achieved by two intramolecular interactions: pY527 binding

with R175 and SH2-SH3-kinase linker packing against the back of the catalytic domain . In the activated form, pY416 pins the active site open. Adapted from (Boggon and Eck 2004).

Figure 2.2: A. Diagram of the constructs. CLckY-1 is a fully functional Lck. Y505F, having removed the autoinhibitory tyrosine, is the 'open' form. Y394F cannot be phosphorylated, is the 'closed' form. Finally ECYFP is a positive control for FRET response. B. Spectral emission in JCam1.6 for the four constructs. Adapted from (Stirnweiss, Hartig et al. 2013).

Figure 2.3: The HindII digestion of pHR-ZIP. The enzyme digested the plasmid into eight fragments. The largest fragment 7758-11197 contained the ZIP reporter. And the second largest fragment 238-3473 had the bacterial origin of replication and ampicillin resistance for selection. The two pieces were recovered and religated together.

Figure 2.4: A. Schematic of the Src FRET reporter: membrane-targeting domain (MGCIKSKRKDNLNDDE), donor (eCFP), SH2 domain, flexible linker, substrate, and acceptor (eYFP). B. FRET response upon Src activation. Adapted from (Wang, Botvinick et al. 2005).

Figure 2.5: ITAMs in CD3ζ. The motifs are well conserved between the species. Differences are highlighted in white. ITAM3 is identical between human and mouse.

Figure 3.3: Representative images of transfected mouse splenocytes. Images were taken in Brightfield, interference reflection microscopy (IRM), and epifluorescence (for GFP). IRM reports cellular adhesion, a good indicator of cellular viability. Red arrows point to apoptotic cells. Scale Bar = 10µm.

Figure 3.4: Representative images of transfected mouse splenocytes. Images were taken in Brightfield, IRM, and epifluorescence (for GFP or YPET and mCherry). Mouse spleenocytes tolerated GFP, but not LckR_FRET. Scale Bar = 10µm.

Figure 3.5: Representative images of transfected human peripheral blood CD4+ T-cells. Images were taken in Brightfield, IRM, and epifluorescence (for YPET and mCherry). While transfection was achieved at 2200mV and 3.5ug of mRNA, the cell was not viable as seen in IRM. Scale Bar = 10µm.

Figure 3.6: Representative images of transfected human peripheral blood Cd4+ T-cells using the Amaxa system. Images were taken in Brightfield, IRM, and epifluorescence (for GFP or YPET and mCherry). Despite a large quantity of LckR_FRET mRNA, the transfection efficiency was still poor. Scale Bar = 10µm.

Figure 3.7: A. mouse transgenic splenic T-cell were activated by APCs from B10.BR mice. From (Lee, Holdorf et al. 2002). B. Jurkat cells were seeded onto activating surfaces. All the cells are fixed at the indicated time, perforated, blocked and stained with pLck.

Figure 3.8: Cellular response to micropatterned surface. A. mouse splenocytes favored peripheral presentation of CD28. From (Shen, Thomas et al. 2008). B. Human peripheral blood lymphocytes favored co-presentation of CD3 and CD28. From (Bashour, Tsai et al. 2014). C. Jurkat cells, while like human primary cells responded most strongly to COL surfaces, had significant IL-2 secretion on SEG patterns.

Figure 3.9: PLck staining of mouse naïve T-cells, human primary T-cells, and Jurkat cells. While pLck was found throughout the mouse T-cell –glass interface, pLck preferentially co-localize with CD3 in human primary cells. From (Bashour, Tsai et al. 2014). In human lymphoblastic cell line, Jurkat E6.1, pLck also favored CD3. However, there existed a low concentration of pLck throughout the cell-glass interface.

Figure 3.10: Plots of a representative null cell bouncing on the glass surface. The cell is not in contact with any micropatterned proteins (-------- trace of closest micropatterned dot). And the FRET ratio is sensitive to cells stepping on and off the glass surface.

Figure 3.11: A. Plots of a representative null cell landing and spreading on the glass surface. Again the cell is not in contact with any micropatterned proteins (-------- closest micropatterned surface). B. FRET ratio traces of null cells.

Figure 3.12: A cell interacting intermittently with the micropatterned proteins (-------- αCD3-dot).

Figure 3.13: Montage of a Jurkat cell interacting with a COL micropatterned glass coverslide. A. Only the donor (YPET) intensity was shown. B. Heat map of FRET ratios. Scale bar = 5µm.

function of the differences in refractive induces of the interface, and its intensity decays exponentially. From (Mattheyses, Simon et al. 2010).

Figure 4.4: Schematic of reporter redesign from a pLck FRET reporter to a Zap70 recruitment biosensor.

Figure 4.5: A. SH2_YPET transfected Jurkat cell on surface completely coated with activating antibodies. Clusters of ZH2_YPET were laterally static. B. In contrast, SH2_YPET was very fluid in Jurkat cell exposed to micropatterns C. The fully coated surface was used to check whether SH2_YPET molecules were stably bound to pITAM. Its recovery in about 2 minutes suggested active exchange between bleached and unbleached pools of SH2_YPET. Scale bar = 5µm.

Figure 4.6: SH2_YPET distribution is unique from both pZap70 and pLck. Its distribution more closely resembles that of pLck than pZap70. While pZap70 has mostly disappeared 15 minutes after seeding, pLck concentrated on the micropatterned protein dots with some found throughout the cell. Scale bar = 5µm.

Figure 4.7: Null cells transfected with SH2_YPET mRNA were seeded on micropatterned surfaces. No intense increases in TIRF of SH2_YPET (in green) was observed beyond the initial cell landing and spreading. Epifluorescence of SH2_YPET (in red) remained largely unchanged. Scale bar = 5µm.

Figure 4.8: Jurkat cell transfected with LckR_FRET on α-CD3 (blue) only surface with YPET in green and mCherry in red. The FRET reporter was unable to detect a high concentration of kinase activity on the α-CD3 dot as seen in the color map. Scale bar = 5μm.

Figure 4.9: Jurkat cell transfected with SH2_YPET on α-CD3 (blue) only surface. When a cell only interacts with micropatterned surface at the lamellipodia, the recruitment ratio exhibits spatial distortion. Note the gradient in epifluorescence intensity (red) as a function of cell radius. Scale bar = 5μm.

Figure 4.10: Jurkat cell transfected with SH2_YPET (TIRF intensity in green and epifluorescence intensity in red) on COL pattern (blue). The cell lands and spreads around the stamped protein. Initially, pLck was found throughout the interface, with heightened kinase activity on the α-CD3/α-CD28 dot. While pLck activity gradually dropped off across the interface, recruitment remained strong at the dot. A trace of averaged intensities on the dot was plotted. Scale bar = 5μm.

Figure 4.11: TIRF/Epifluorescence ratio of Jurkat cells on COL surfaces.

Figure 4.12: Jurkat cell on SEG pattern (blue for α-CD28 and pink for α-CD3). As previously discussed, the cell initiated contact with α-CD3 dot and increased recruitment of reporter was observed near the center of the cell. Scale bar = 10μm.

Figure 4.13: Normalized TIRF intensity of Jurkat cells on COL (in green) and SEG (in red) patterns. The decay in signal was slower on COL patterns versus SEG patterns.

List of Tables

List of Abbreviations

APC	—	Antigen Presenting Cell
COL	—	Colocalized pattern
CTL	—	Cytotoxic T-Cells
FLIM	—	Fluorescence-Lifetime Imaging Microscopy
FRAP	—	Fluorescence Recovery after Photobleaching
FRET	—	Förster/Fluorescence Resonance Energy Transfer
IL	—	Interleukin
IS	—	Immunological Synapse
ITAM	—	Immunoreceptor Tyrosine-Based Activation Motif
LAT	—	Linker for Activation of T-cells
Lck	—	Lymphocyte-specific Protein Kinase
MDSC	—	Myeloid Derived Suppressor Cell
MHC	—	Major Histocompatibility Complex
PRR	—	Pattern Recognition Receptor

PTK	—	Protein Tyrosine Kinases
SEG	—	Segregated pattern
SLP-76	—	SH2-domain containing Leukocyte Phosphoprotein of 76kDa
SMAC	—	SupraMolecular Activation Clusters
TCR	—	T-Cell Receptor
Tfh	—	Follicular T-cells
Th	—	T Helper Cells
TIL	—	Tumor-Infiltrating Lymphocyte
TIRFM	—	Total Internal Reflection Fluorescence Microscopy
Treg	—	Regulatory T-cells

Chapter 1

1. Introduction

1.1 Cancer and Personalized Medicine

Cancer is the abnormal growth of host cells. While clinically easy to describe, the group of more than 100 diseases arises from complex combinations of genetic and environmental factors. In 2011, the heterogeneous body of diseases accounts for roughly $88.7 billion in direct cost (Soni 2014). Despite costly healthcare expenditure and substantial funding for cancer research, the overall rate of cancer mortality has only decreasing around 1.6% from 2002-2011 (National Cancer Institute 2015). In contrast, mortality rate of cardiovascular disease has decreased by 30.8% during the same period (Mozaffarian, Benjamin et al. 2015).

One contributing factor is the broad-brush approach to treatment. In an effort to contain the malignant cells, healthy host cells are sacrificed in invasive nonspecific procedures such as radiation, surgery, and chemotherapy. With increasing understanding of genetic and molecular

biological mechanisms governing malignancy, the field is exploring and investing in personalized treatments, in an effort to limit collateral damages to healthy cells. And most recently, clinicians are interested in harnessing the patient's own immune system to combat cancerous cell in a treatment known as immunotherapy.

1.2 Immune System

Central to our success as a species has been the ability of our immune system to identify and defend against foreign invaders. The host resistances are multi-step, sequential, and inter-communicating. Beyond the first lines of defense, physical barriers and intrinsic immunity, is the innate immunity. The system functions continuously, thus able to respond instantaneously to a foreign pathogen. This is achieved nonspecifically through the binding of common pathogenic motifs to the pattern recognition receptors (PRRs). The activation of PRRs results in cytokines being secreted by the infected cells to attract local sentinel cells. The sentinel cells initiate inflammation to disrupt pathogen expansions into healthy cells. The innate immunity is nonspecific and without memory: every infection is 'new' and the response is identical.

In contrast, adaptive immune response is specific and long-term. Also recruited to the site of infection are antigen-presenting cells (APCs), critical links between innate and adaptive immune systems. In a week, the APCs, having ingested the microbes, migrate to the local lymph nodes. APCs load the pathogen fragments onto receptors to be presented to the T- and B-lymphocytes. The adaptive response has three distinct phases: recognition, amplification, and control (Janeway 2005). First, specific lymphocytes are activated for each pathogen. Then the activated

lymphocytes differentiate and multiply into different effector cell types to combat the pathogen. Finally the system reestablishes homeostasis as T-cells undergo apoptosis, leaving behind memory cells for swift and augmented responses during subsequent infections with the same pathogen (Fig. 1.1).

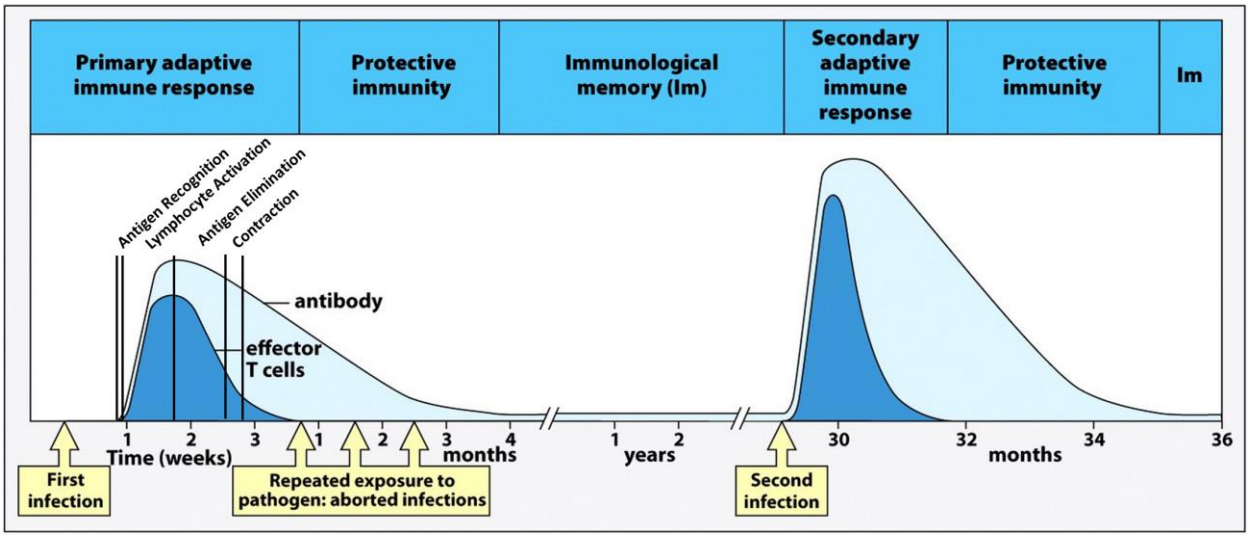

Figure 1.1: Primary adaptive immunity response initiates a week after primary infection. It is a specific defense with memory. Years after the primary infection, exposure to the same pathogen results in an accelerated and more robust immune response. Adapted from (Parham and Janeway 2009).

In the context of immunotherapy, much of the research focuses on the initial recognition and activation of T-lymphocytes. Two major subsets of T-cells exist, distinguished by its interaction with two classes of antigen presenting receptors, or major histocompatibility complexes (MHCs), on APCs. MHC class I receptors bind to CD8+ cytotoxic T lymphocytes (CTLs), which as the name suggests directly engage and kill pathogens. CD4+ helper T-cells, binding to MHC class II receptors, are the master coordinators of adaptive immunity. The CD4+ helper T-cells communicate through cytokine secretions and interactions with other immune cells to shape the effector responses.

1.3 CD4+ Helper T-cell

Crucial to CD4+ T-cell coordination of an appropriate response is its plasticity to shape an effective defense (Fig. 1.2). Canonical T-cell effector roles include humoral and cell-mediated immunities. With increasing understanding of helper T-cells, more lineages have been identified.

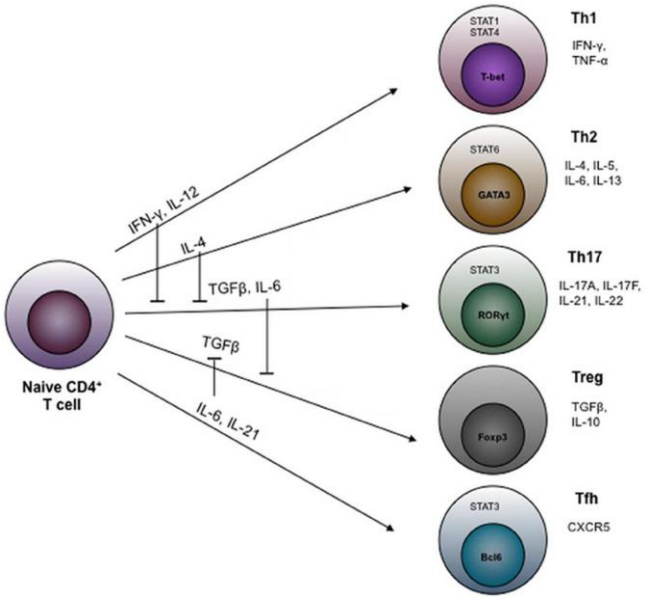

Figure 1.2: T helper cell traditional lineages. Five well-characterized lineages are Th1, Th2, Th17, Treg, and Tfh. Th1 defends against intracellular parasites. Th2 controls parasites and extracellular pathogens; negatively, it is associated with allergy and asthma. Th17 is most known for its destructive effects: autoimmunity, cancer, and transplantation rejection. Treg participates in immune homeostasis and maintains tolerance. Finally Tfh residing in B-cell follicles of secondary lymphoid organs aids in B-cell antibody production. Adapted from (Sethi, Kulkarni et al. 2013).

In cell-mediated immunity, CD4+ T Helper 1 (Th1) cells recruit CTLs, macrophages, neutrophils, and other effector cells to kill intracellular pathogens and tumor cells. In humoral immunity,

CD4+ T Helper 2 (Th2) cells help B-cells to produce antibody and to undergo affinity maturation. Th2 cells mediate an effective B-cell response against blood circulating pathogens and toxins, which are neutralized and marked by antibodies for phagocytosis and elimination by the complement system (Zhu and Paul 2010). Less understood, but known for much longer are Th17 cells. Interleukin-17 (IL-17) is the signature cytokine; it is highly inflammatory (Tesmer, Lundy et al. 2008). Believed to be important for protection against extracellular bacteria and some fungi before the advent of modern sanitation, Th17 is better known for its inflammatory effects in diverse group of autoimmune diseases such as rheumatoid arthritis, transplantation rejection, and cancer (Tesmer, Lundy et al. 2008). Regulatory T-cells (Tregs) suppress the activation and expansion of B- and T-cells that bind strongly to self-antigen through direct cell contact; thus disruption in Treg functions results in autoimmunity and inflammatory diseases. During adaptive immune response, the delicate balance between effector cells (T- and B-cells) and Tregs is crucial in shaping an appropriate response: a proper immune reaction of suitable quality and magnitude versus tolerance for self-antigens (Sakaguchi, Yamaguchi et al. 2008). Finally, follicular helper T (Tfh) cells are located in the secondary lymphoid organ: such as lymph nodes, tonsils, spleen, and Peyer's patches. Tfh regulates B-cell immunity by aiding in antibody production by activating affinity maturation and antibody class switching (Fazilleau, Mark et al. 2009).

New potential lineages are Type 1 regulatory T (Tr1) cells, T helper 3 (Th3) cells, and T Helper 9 (Th9) cells. Tr1 cells are CD4+ T-cells that secrete predominately IL-10 and some TGF-β, both are immunosuppressive cytokines. IL-10 is important for immune tolerance and the dampening of autoimmune diseases (Pot, Apetoh et al. 2011). Th3 cells are specifically involved in mucosal

immunity, while secreting predominately TGF-β and some IL-10. TGF-β is important to induce the production of IgA; the immunoglobulin is a noninflammatory complex that's a poor activator of the complement system, thus weakly phagocytosed. Th3 cells through IgA also suppress Th1 and Th2 cells in the mucosal surfaces (Weiner 2001). As the mucosal membrane is constantly being exposed to pathogens, sustained inflammation of the gut is undesirable. Finally, Th9 cells are defined by the secretion of IL-9, a proliferative cytokine. And it's been associated with human allergic diseases such as asthma and allergic rhinitis (Soroosh and Doherty 2009).

The heterogeneous population of effector and regulatory T-cells demonstrates T helper cell plasticity and crossover of functional roles, crucial to its ability to effectively combat a diverse range of pathogens (Fig. 1.3) (O'Shea and Paul 2010).

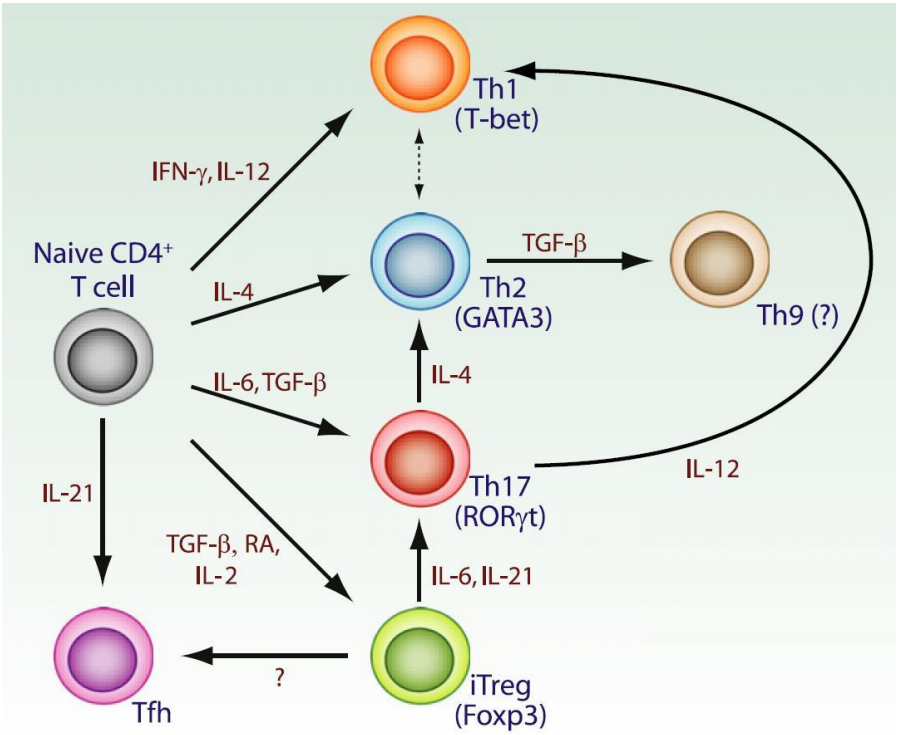

Figure 1.3: Plasticity of T-cell differentiation. The ability of T-cell lineages to be reconditioned has important implications for immunotherapeutics. From (Zhou, Chong et al. 2009).

The ability to understand the mechanisms governing T-cell activation and differentiation is critical for cellular-based immunotherapy, specifically to modify and modulate host responses to diseases such as cancer.

1.4 Adoptive Immunotherapy

Clinicians, in an effort to harness the adaptive immune system to combat tumors, have attempted two fundamentally different strategies: therapeutic vaccination and passive immunization (June 2007). Initially, therapeutic vaccination was an attractive approach, trying to booster a patient's reactivity to tumor cells with low toxicities. However, a review by Klebanoff and colleagues summarized seven years of clinical researches in the Surgery Branch of the National Cancer Institute. They found that in only less than 4% of patients, were the tumors induced to regress (Klebanoff, Acquavella et al. 2011). Three major factors contribute to the failure of therapeutic vaccinations. One, the tumor cells recruit Tregs and induce the differentiation of myeloid derived suppressor cells (MDSCs). Two, the tumor-specific T-cells are prone to immunological exhaustion and senescence. In a healthy host, the intricate balance of immunostimulatory and immunosuppressive T-cells insure proper clonal expansion to eliminate pathogens and contraction to prevent autoimmunity. Contraction to homeostasis is reestablished by inducing cell exhaustion and apoptosis. In cancer patients, between the recruitment of Treg and chronic nature of the tumor-bearing state, T-cells are immunologically exhausted, poorly functional and weakly proliferative. Moreover, T-cells enter into senescence,

cell cycle arrest, and non-responsiveness (Yao and Moorman 2013). Finally, tumors are highly mutagenic, resulting in immune evasion (Klebanoff, Acquavella et al. 2011)

Recent years experimental treatments with passive immunization, also known as adoptive T-cell therapy, appear to have the potential to enhance host anti-tumor immunity. Briefly, T-cells are isolated (autologous or allogeneic) and expanded *ex vivo* before being infused into the patient. Three distinct strategies have been explored: CTL therapy, tumor-infiltrating lymphocyte (TIL) therapy, and engineered T-cells. CTL therapy clinically has been investigated in melanoma patients. Infusion of CTLs specific for Melanoma-associated Antigen Recognized by T-cells 1 (MART-1) was effective. However, it resulted in outgrowth of MART-1–negative tumor masses. This illustrates one fundamental flaw with *ex vivo*-activated lymphocytes. Because lymphocytes are highly specific for an antigen, the technique permits the outgrowth of antigen escape variants. Instead of tumor regression, in a vaccine-like response, the tumor mutates and continues to expand with epitopes not recognized by the infused CTLs (June 2007). A possible solution is the generation of a broader repertoire of tumor-specific CTLs.

Another strategy, recognizing the limitation of CTL therapy, is TIL therapy. Instead of *ex vivo* activation of selective antigen-specific CTLs, TIL therapy isolates diverse types of immune cells from tumor masses already sensitized to the cancerous cells. The *ex vivo* culturing of the immune cells remove them from the immunosuppressive microenvironment generated by both the tumor cells and MDSCs. In a study by Rosenberg and colleagues, metastatic melanoma patients underwent TIL therapy. Of the 93 patients, 20 patients were responsive: achieved complete tumor regression. The response was durable, with 19 patients having complete

regressions beyond 3 years (Rosenberg, Yang et al. 2011). However most patients were non-responsive due to a few critical factors: telomere shortening, reduced expression of CD27+ CTLs, and poor persistence of TILs in circulation a month after infusion. In general, the clinical study illustrates one large limitation to TIL therapy: the technical difficulty of culturing TILs. Only 30-40% of the biopsied specimens yielded satisfactory T-cell population (June 2007). Lymphocyte culturing is both labor and resources intensive, requiring ~6 weeks. The lengthy lymphocyte culturing is associated with telomere shortening, which induces cellular senescence, and reduction of CD27 and CD28 in TILs, which is crucial for a robust immune response (Tran, Zhou et al. 2008).

Another strategy is engineered T-cells. Depending on the types of cancer, many different approaches have been made to engineer T-cells. One extremely successful method has been to use chimeric antigen receptors (CARs), pioneered by Carl June, our clinical collaborator. The June group specializes in treating chronic lymphocytic leukemia (CLL). Not a solid tumor, CCL directly affects B-cells. The condition is life-threatening; however, people can live without their B-cells. Thus the June group targeted a B-cell specific marker, CD19. Using this tissue-differentiation antigen is only possible because B-cells are not essential for life. CARs are constructed to bypass MHC-T-cell Receptor (MHC-TCR) engagement using a genetically engineered activating receptor against CD19. Intracellularly, the receptor is coupled to a TCR signaling domain CD3ζ and a costimulatory domain CD137 or CD28 (Kalos, Levine et al. 2011)(Fig. 1.4). Clinically, the CARS therapy was administrated into both children and adult

patients with acute lymphoblastic leukemia (ALL) and CLL. Complete remission was achieved for 90% of the patients with ALL (Maude, Frey et al. 2014).

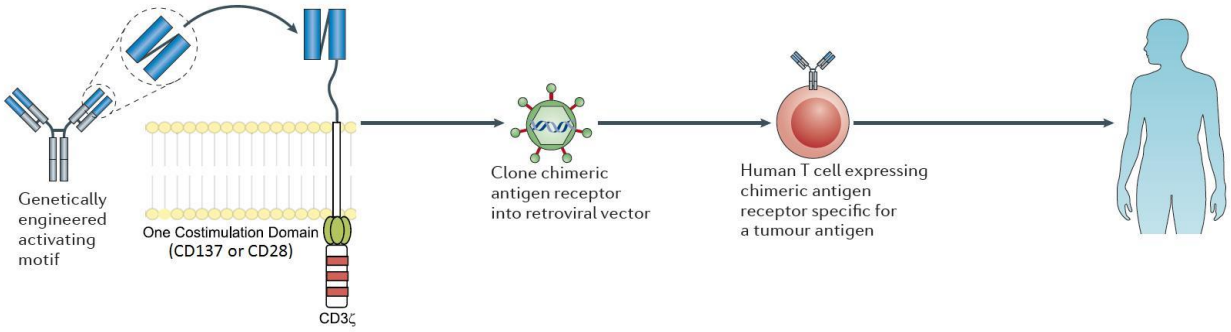

Figure 1.4: MHC-TCR-independent activation of engineered T-cells achieved with antibody receptor genetically engineered against a target antigen. The receptor is then coupled to a signaling domain intracellularly. Adapted from (Maus, Grupp et al. 2014) and (Restifo, Dudley et al. 2012).

Our collaboration with the June group looks to improve T-cell activation and expansion before genetic engineering. The clinical gold-standard for cell expansion is polystyrene beads with magnetic cores. The bead is coated with activating antibodies and removed before infusion into patients. Unfortunately, the removal is imperfect, thus work in our lab explores alternative expansion platforms.

1.5 T-cell Activation

As APCs traffic into local lymph nodes, they interact with naïve T-cells. And T-cell activation is initiated at the immunological synapse (IS), the interface between T-cells and APCs. Specificity is conferred when T-cell receptors (TCR) recognize and bind to peptides loaded onto MHC-II receptors (pHMCs). With less than 10 specific pHMC complexes being presented on the APC

surface, the naïve T-cell is primed. Costimulatory signal is necessary to sustain the interaction. Here the response polarizes as APCs bind to either positive or negative costimulatory signals (Fig. 1.5A). Activation is boosted by CD28 binding during an infection and diminished by CTLA-4 binding during peripheral tolerance. The high sensitivity of T-cell recognition is achieved by extensive membrane protein reorganization at the IS into spatially discrete zones of supramolecular activation clusters (SMACs), which resembles a bull's-eye (Fig. 1.5B). Sustained signaling in a mature IS for CD4+ T-cell is mediated by TCRs in small clusters of 5-30 molecules moving centripetally toward central SMAC (cSMAC)(Dustin, Chakraborty et al. 2010). Costimulatory receptors CD28 and co-receptor CD4 and Cd8 are also found in the cSMAC. Cluster size regulates protein sorting at the IS. And larger ectodomains are relegated to the peripheral SMAC (pSMAC). Noted is the segregation of integrin receptor, LFA-1, to the pSMAC. The adhesive receptor binds to ICAM-1 on APCs to further stabilize the IS by creating a seal. CD45, a protein tyrosine phosphatase that has net negative effect on downstream signaling event is further segregated to the distal SMAC (dSMAC).

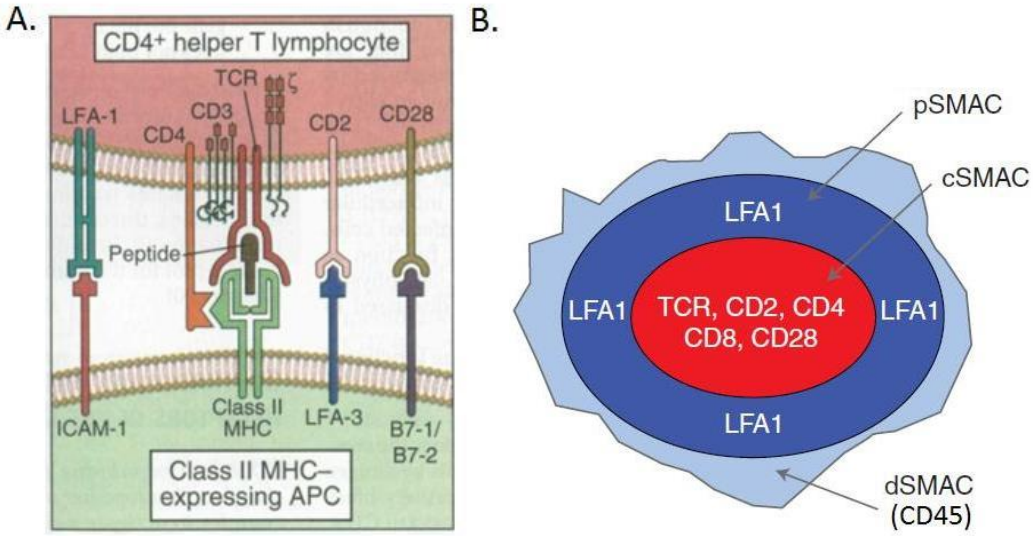

Figure 1.5: A. Immunological synapse is the site of critical ligand interactions. T-cells are primed when TCR recognize specific peptide-loaded MHC. Then costimulatory signal is given by APC via its binding to either CD28 or CTLA-4 receptors. The signaling structure is further stabilized by adhesive receptor LFA-1, which binds to ICAM-1 on APCs. From (Abbas, Lichtman et al. 2007). B. The high sensitivity of T-cell recognition is made possible by the formation of spatially discrete zones within the SMAC. Adapted from (Dustin, Chakraborty et al. 2010).

Intracellularly, TCR has no cytosolic signaling domains. Its signal is propagated by the CD3 complex through the phosphorylation of immunoreceptor tyrosine-based activation motifs (ITAMs) by lymphocyte-specific protein tyrosine kinases (Lck) for further downstream signaling. Positive costimulation induces signaling cascade critical to proliferation and differentiation; and understanding the interplay between CD3 and CD28 is the key to improving and modulating *ex vivo* T-cell expansion for adoptive immunotherapy.

1.6 The Spatial and Functional Interactions in T-cell Activation

Beyond size exclusion, Michael Dustin's group studied the effect of APC costimulatory presentation on T-cell spatial segregation and function. The Dustin group generated an artificial APC with either a full-length CD80 (CD80FL) or a cytoplasmic tail deleted mutant (CD80TL), both tagged with yellow fluorescent proteins (YFPs). Peptide-loaded MHC-II (specifically the I-E^k pMHC complex), ICAM-1 and either one of the CD80 constructs were inserted into Chinese hamster ovary (CHO) cells functioning as an artificial APCs for mouse T-cells. To assess functional differences, the Dustin group measured proliferation both via [^{3}H] thymidine

incorporation and IL-2 secretion. Functionally, the assays revealed that CD80FL induces superior proliferation than CD80TL. However CD80TL still performs better than MHC-II alone without CD28 engagements (Tseng, Liu et al. 2005).

The Dustin group decided to examine the spatial distribution within the IS. Without CD80 engagement, TCR does not migrate to the cSMAC and mixes with LFA-1 at the interface (Fig. 1.6A). With CD80 engagement, TCRs move into the cSMAC. For CD80FL, CD80/CD28 is segregated from TCR-CD3 clusters (Fig. 1.6B); however CD80TL colocalizes with TCR (Fig. 1.6C). The study revealed that functional impairments affect spatial organizations.

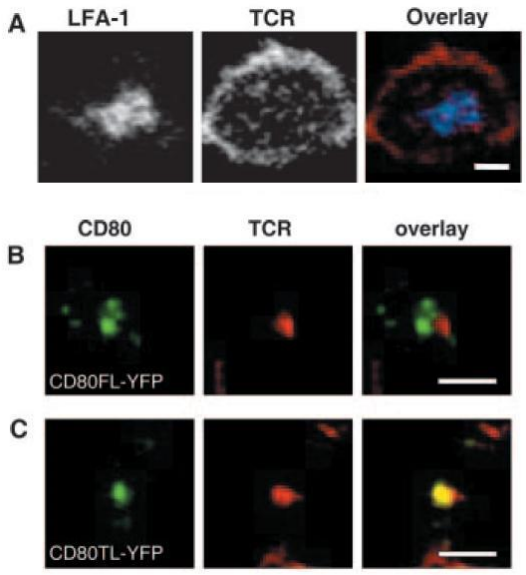

Figure 1.6: The effect of CD80 on TCR spatial organization. A. The APC presents only MHC-II and LFA-1. CD80 is necessary for TCR migration to the cSMAC. Its absence results in loss of spatial segregation as TCR (red) mixes with LFA-1 (blue). B. With full-length CD80, one observes segregation of CD80FL from TCR clusters. C. With tail deleted CD80, CD80TL colocalizes with TCR. Scale bar = 2µm. From (Tseng, Liu et al. 2005)

Our group attempted to invert the relationship. We wanted to understand if *ex vivo* T-cell exposure to activating proteins in different spatial arrangements can modulate T-cell

activations. Our group recapitulated the spatial cues with activating antibodies printed on glass surfaces. To induce functional impairments with TCR-CD3/CD28 colocalization (Fig. 1.6C), antibodies activating CD3 and CD28 were mixed together and absorbed onto 2μm-dot stamps; then the proteins were printed onto clean glass surfaces. To elicit a strong activation by spatially segregating the TCR-CD3 and CD28 proteins (Fig. 1.6B), we coated and stamped 2μm-dot stamps with anti-CD3 antibody (α-CD3) and 1μm-dot stamps with anti-CD28 antibody (α-CD28). And to assess T-cell activation in response to the different patterns, again IL-2 secretion was measured.

We were able to demonstrate that inversely spatial cues affect T-cell activations. And our results concur with the CD80 study from the Dustin group. Without CD28 engagement (CD3-only), IL-2 secretion was very weak. Colocalized (COL) surface exhibited slightly stronger secretion. And segregated (SEG) surface demonstrated strongest IL-2 secretion, 2- to 3- fold higher than the COL patterns. To better understand the spatial effect of CD3 and CD28 on T-cell activation, 2 additional surfaces were examined. One tested if the positive modulation was purely due to the separation of CD3 and CD28 by creating a reverse segregated surface (REV-SEG). 2μm-dot stamps were coated with α-CD28 while 1μm-dots were coated with α-CD3. A marked decrease in IL-2 secretion was observed on REV-SEG patterns. Finally, to test if peripheral presentation of CD28 is the key to strong IL-2 secretion, mixture of CD28 and CD3 coated 1μm-dot stamp (REV-COL). And it gave the strongest response (Fig. 1.7A). We concluded that peripheral presentation of CD28 induces robust response, and not the segregation of CD3 and CD28 signals (Shen, Thomas et al. 2008).

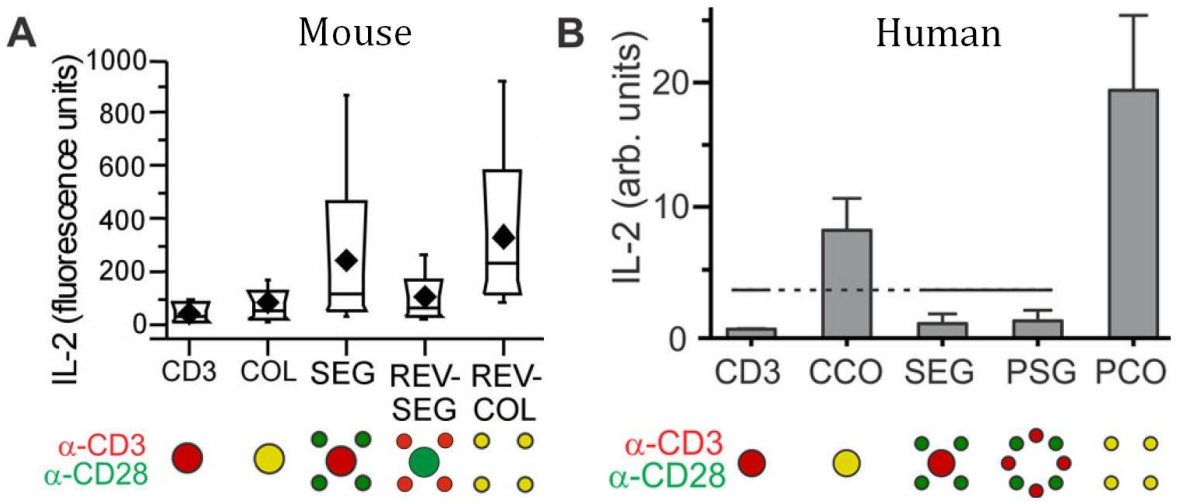

Figure 1.7: A. Mouse T-cells respond robustly to peripheral presentation of CD28. From (Shen, Thomas et al. 2008). B. Human T-cells respond most potently to colocalized presentation of CD3 and CD28, and also peripheral presentation of the proteins. From (Bashour, Tsai et al. 2014).

More relevant to adoptive T-cell immunotherapy would be human T-cell and its response to spatial cues. Thus similar experiments were conducted on naïve peripheral blood human T-cells. As with mouse T-cells, CD3 only patterns resulted in minimal IL-2 secretion. However, unlike mouse T-cells, human cells did not tolerate CD3/CD28 separation, as seen on SEG and peripheral SEG (PSG) patterns. In terms of IL-2 secretion, SEG and PSG exhibited similar response to CD3 only patterns. And like mouse T-cells, peripheral presentation enhanced IL-2 secretion, as seen on centrally COL (CCO) versus peripheral COL (PCO) patterns (Fig. 1.7B). In fact, PCO patterns generated comparable quantity of IL-2 as fully coated surfaces. The results have significant implication for pharmaceutical research. Certainly, it may help to explain why many drug candidates that appeared promising in mouse preclinical immunological studies utterly fail in human clinical trials.

Next we sought out a protein or a pathway to explain the observed differences in mouse and human T-cells. One protein that interacts with both CD3 and CD28 is Lck. As alluded to previously, the effect of activated Lck or phospho-Lck (pLck) on CD3-associated signaling is well understood (Fig. 1.8A). PLck phosphorylates ITAMs (pITAMs) on the CD3 complexes. PITAMs become a binding site for the SH2 domains on ZAP-70. Its recruitment to pITAM results in ZAP70 activation/phosphorylation by pLck. Activated ZAP70 phosphorylates scaffold proteins LAT and SLP-76 for the recruitment of PLCγ, initiating extensive signaling networks (Alegre, Frauwirth et al. 2001, Koretzky and Myung 2001). PLck role in CD28 signaling is less understood. PLck is one of the two candidates shown to phosphorylate the YMNM motif on CD28. Lck is also recruited to PYAP to activate PDK1 (Fig. 1.8B) (Boomer and Green 2010).

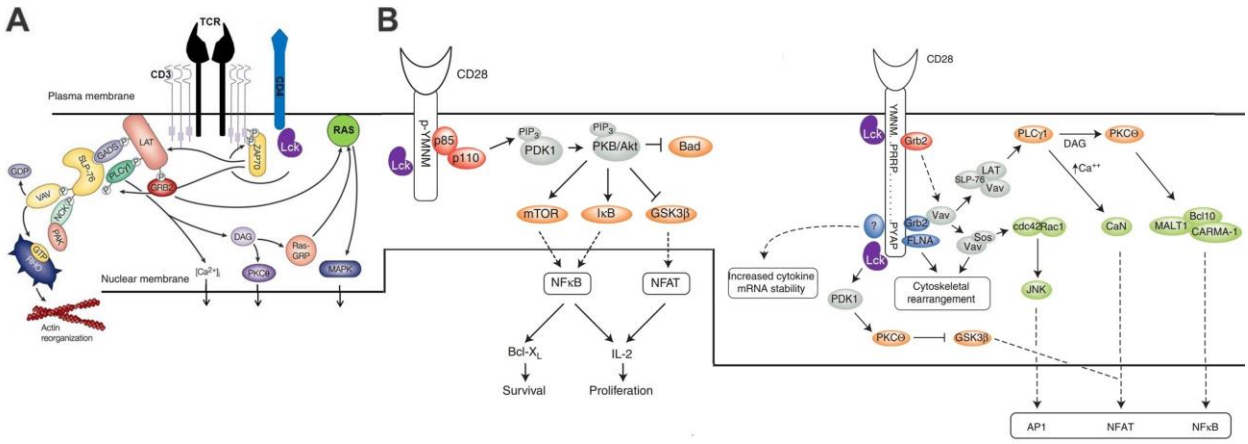

Figure 1.8: A. Well established is the role of pLck in TCR/CD3 complex-associated signaling. Lck phosphorylates ITAMs on CD3. Then pITAMs act as docking sites for ZAP70 by interacting with the ZAP70 SH2 domains. ZAP70 initiates a network of signaling proteins with diverse functions. Adapted from (Koretzky and Myung 2001). B. Less understood is the role of pLck in CD28-associated signaling. Two signaling pathways have been discovered for CD28. One is a PI3K (the p86-p110 heterodimer)-dependent pathway, and another is an adaptor protein (Grb2 or GADS)-dependent pathway. Suspect of phosphorylating the YMNM motifs on CD28, Lck is known also to activate PDK1. Adapted from (Boomer and Green 2010).

Fixed stainings of pLck on patterned surfaces revealed a difference between mouse and human T-cells. In mouse T-cells, pLck is distributed throughout the interface regardless of the patterned surfaces (Fig. 1.9A). In human T-cell, pLck preferentially localizes to TCR-CD3 with minor overlap on CD28 (Fig. 1.9B). In contrast, total Lck is distributed evenly across the interface (not shown) (Bashour, Tsai et al. 2014). Many models have been formulated to explain cellular regulation of pLck activity. In this case, because pLck must translocate between CD3 and CD28 to initiate signaling cascade, a balance must exist between Lck diffusion and pLck dephosphorylation (Fig. 1.9C). A former lab member, Keenan Bashour, studied Lck diffusion via fluorescence recovery after photobleaching (FRAP). He found diffusion to be faster in mouse T-cells, at about 0.37 ± 0.017 $\mu m^2/s$. PLck diffusion in human T-cells clocked in at 0.04 ± 0.02 $\mu m^2/s$, 8-folds slower.

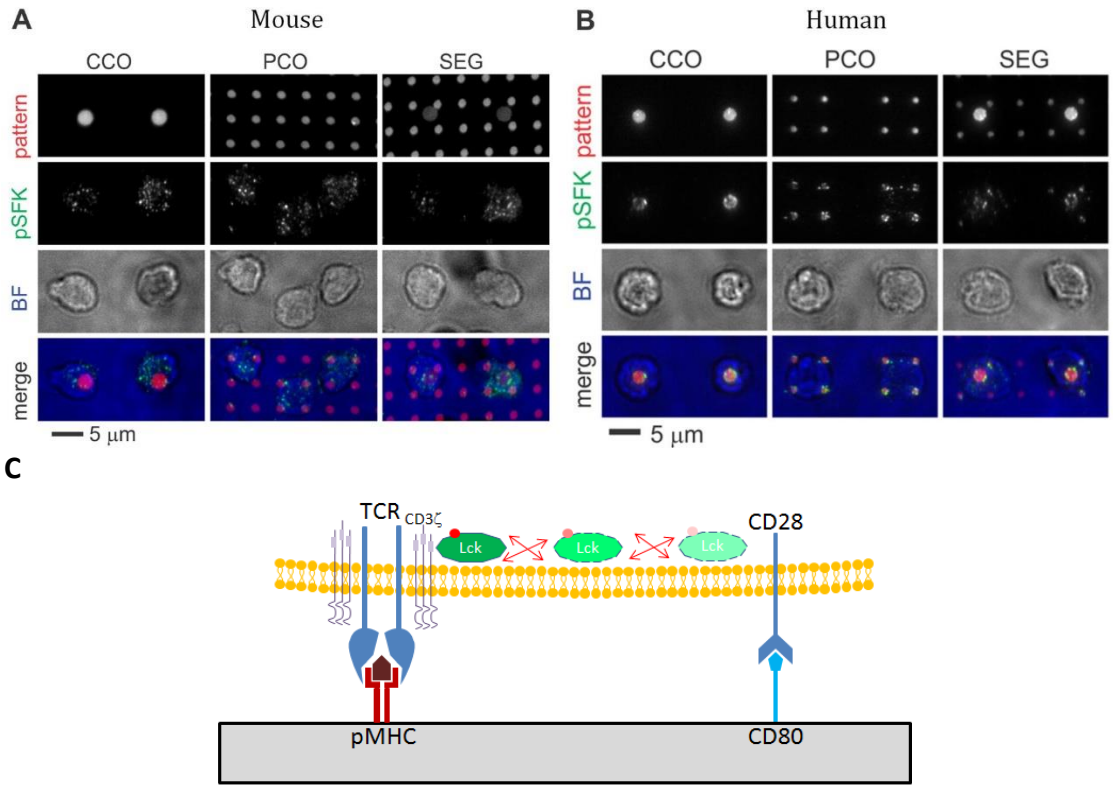

Figure 1.9: A. Stainings in mouse T-cells revealed pLck to be localized throughout the interface, regardless of the patterned surfaces. From (Bashour, Tsai et al. 2014). B. Human T-cell stainings of pLck revealed a preference for CD3, with lesser overlap on CD28. From (Bashour, Tsai et al. 2014). C. Translocation of Lck between TCR-CD3 complex and CD28 to initiate signaling cascade will be a function of Lck diffusion and pLck dephosphorylation. Please note: pLck staining was performed with pY394 antibody, which is unable to distinguish between pLck and pFyn. Thus, it's referred to as pSFK.

While the rate of Lck diffusion could partial account for the differential responses between the species, it still does not address the role of phosphatase activity on Lck kinase activity. Thus, this dissertation focuses on creating reporters of Lck kinase activity.

1.7 Significance

Adoptive Immunotherapy is a promising treatment to combat certain types of cancers. And the plasticity of CD4+ T helper cells makes it an attractive target for cellular immunotherapy. Critical to the modulation of T helper cell activation and differentiation is the costimulatory signal. And a deeper understanding of the pathways governing the process is crucial to better engineer or direct the immune responses against cancerous cells.

Lck arose as a master initiator of intracellular signaling cascades. And the acute differences in mouse and human T-cell activations hopefully will help to elucidate the means of cellular control and modulation.

Chapter 2

2. Designing a Reporter of Lck Kinase Activity

2.1 Introduction

Lck is a member of the Src family kinases (SFK). The family is highly conserved and present in essentially all metazoan cells, in response to external stimuli. Another SFK relevant to immune response is Fyn, which is difficult to differentiate from Lck, and will be discussed in detail later.

As an essential kinase in T-cell activation, Lck activity is highly regulated by conformational changes. Specifically, the kinase activity is controlled via phosphorylation and dephosphorylation of two regulatory tyrosine residues. To understand this conformational regulation, it's important to understand the structure of Lck. In general, SFKs share a number of conserved domains. At the N-terminus is a SH4 domain. Lck SH4 domain is both myristoylated

and palmitoylated for membrane-targeting. Next are the SH3, SH2, and kinase (SH1) domains. The hallmarks of SFK are an autoinhibitory tyrosine at the C-terminus just downstream of the SH1 domain and an activating tyrosine in the kinase activation loop in the SH1 domain.

The autoinhibitory tyrosine (Y527 in Src or Y505 in Lck) is phosphorylated by Csk or its homolog Chk and dephosphorylated byCD45 (Rossy, Williamson et al. 2012). Phosphorylated Y527 binds with Arg175 in the SH2 domain (Fig. 2.1). And the steric and electrostatic factors result in an intramolecular interaction between SH2, SH3, and the linker segment to the kinase domain (Fig. 2.1). These two intramolecular bindings pack against the back of the catalytic domain. Without sterically occluding the catalytic cleft, the interactions result in the active site is locked into an inactive conformation (Fig. 2.1). The activating tyrosine (Y416 in c-Src or Y394 in Lck) is buried into the cleft, unable to be phosphorylated (Boggon and Eck 2004), which necessary for its kinase activity.

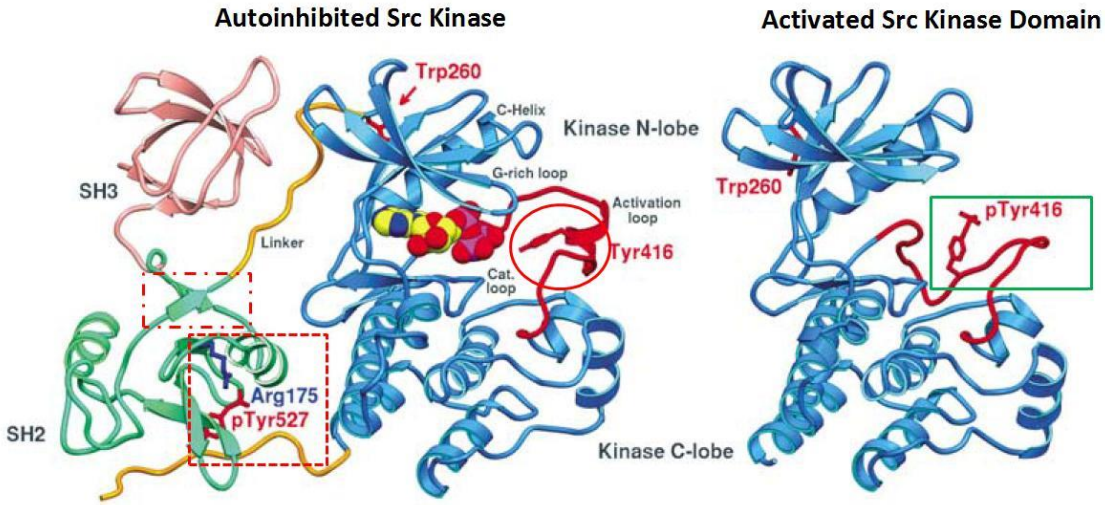

Figure 2.1: Autoinhibited kinase is characterized by the activating Y416 being buried in the active site cleft . This is achieved by two intramolecular interactions: pY527 binding with R175 and SH2-SH3-kinase linker packing against the back of the catalytic domain . In the activated form, pY416 pins the active site open .

Adapted from (Boggon and Eck 2004).

In contrast, pY416 pins the activation loop in an active conformation (Fig. 2.1). Y416 phosphorylation is achieved in a process known as trans-autophosphorylation. And its dephosphorylation is carried out by CD45. (Rossy, Williamson et al. 2012). Consensus within literature is that CD45 has a predominately negative effect on Lck activity. Kinetically, high level of CD45 is required to dephosphorylate Y394 and suppress Lck activity. Meanwhile low level of CD45 favors Y505 dephosphorylation, which enhances Lck activity. Under basal conditions, CD45 concentration is very high thus restraining Lck activity. However, during IS formation, CD45 is segregated to dSMAC. It's inferred to favor Y505 dephosphorylation and to enhance Lck kinase activity.

Stirnweiss and colleagues constructed a Förster resonance energy transfer (FRET) biosensor to study Lck conformational change (Stirnweiss, Hartig et al. 2013). The group studied Lck in JCAM1.6, a Jurkat mutant with no Lck activity. And Jurkat is a leukemic T-cell line. The reporter had a fully functional Lck. Its insertion into JCAM1.6 restores cellular signaling. To report Lck conformation, Stirnweiss inserted a donor (eCFP) between the membrane targeting domain and the SH3 domain; then the acceptor (eYFP) was placed at the tail end (Fig. 2.2A CLckY-1).

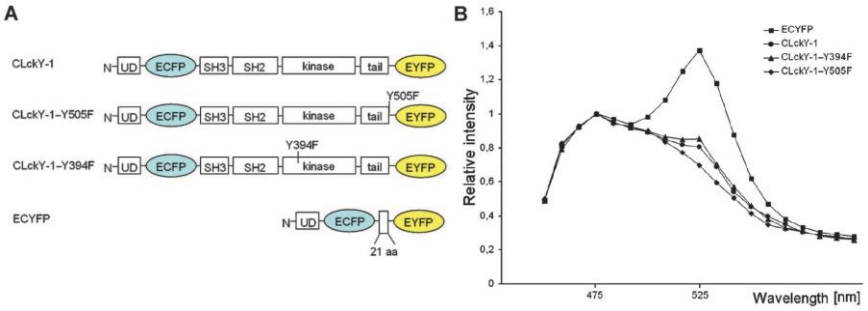

Figure 2.2: A. Diagram of the constructs. CLckY-1 is a fully functional Lck. Y505F, having removed the autoinhibitory tyrosine, is the 'open' form. Y394F cannot be phosphorylated, is the 'closed' form. Finally ECYFP is a positive control for FRET response. B. Spectral emission in JCam1.6 for the four constructs. Adapted from (Stirnweiss, Hartig et al. 2013).

When the protein is in the autoinhibited and closed state, FRET intensity will increase as SH2-SH3-tail domains pack together, against the back of the catalytic domain. When Lck is activated, the SH2-SH3 clamp releases and Y505 is dephosphorylated, thus separating the donor and the acceptor fluorescent proteins and quenching the FRET response. To explore the dynamic range of the reporter, the authors also produced two mutants. One removed the autoinhibitory tyrosine, thus always in the 'open' conformation (Fig. 2.2A CLckY-1-Y505F). Another removed the activating tyrosine, thus always in the 'closed' conformation (Fig. 2.2A CLckY-1-Y394F). As expected, the 'closed' or inactive form (CLckY-1-Y394F) had the strongest FRET response, while 'open' or active form (CLckY-1-Y505F) had the weakest (Fig. 2.2B). In unstimulated JCAM1.6 cells, CLckY-1 reported that 16% of the constructs exhibited an 'open' conformation. Upon α-CD3 stimulation, the biosensor reported a 20% increase at the plasma membrane (Stirnweiss, Hartig et al. 2013). However, not much is revealed about Lck kinase activity.

Table 2.1: Four functional forms of Lck in T-cells. JCAM1.6 is a mutant from of Jurkat cells. From (Nika, Soldani et al. 2010).

	Relative Proportion of Lck Forms in Unstimulated Cells			
	Closed-Inactive	Primed	pY394-Active	DPho-Active
Human $CD4^+$ T cells	14%	48%	17%	21%
Jurkat cells	23%	25%	23%	29%

To complicate the story of Lck conformational regulation, there are two additional protein states. The canonical forms are closed, inactive Lck (pY505) and active Lck (pY394). When both

tyrosines are dephosphorylated it's referred to as 'primed'. And when both tyrosines are phosphorylated (DPho), the protein is enzymatically active (Nika, Soldani et al. 2010). In naïve human T-cells ~38% of total Lck was constitutively activated (Table 2.1).

Other studies reported that Lck activation was independent of TCR engagement. It's the dynamic regulation of Lck to the IS that regulates Lck kinase activity (Nika, Soldani et al. 2010). Thus, a real-time spatiotemporal reporter of Lck kinase activity is needed to study the modulatory effect of CD28 on T-cell activation.

2.2 Materials and Method

2.2.1 ZIP Plasmid Preparation.

ZIP reporter from the Vale group was purchased from Addgene (Cambridge, MA), a nonprofit plasmid repository. The sequence was inserted into a pHR vector with ampicillin resistance. And each domain was flanked with unique restriction enzymes for ease of manipulation. CD3ζ and eGFP was removed by a double digest of AscI and MscI (New England Biolab, R0534 and R0558). Because MscI is *dcm* methylation sensitive, ZIP was cloned in a bacteria strain that is deficient in the methylase. Thus ZIP was expanded in INV110 (Invitrogen, C7171-03) before enzymatic digestions.

2.2.2 Custom Plasmid Preparation

A custom plasmid was synthesized by Invitrogen via GeneArt: in a pMK-RQ backbone with Kanamycin resistance, plus AscI and MscI recognition sites to flank the 1030bp sequence of interest. Like ZIP reporter, the construct was expanded in INV110 and double digested by restriction enzymes AscI and MscI.

2.2.3 Building Lck Kinase Activity FRET reporter (LckR_FRET)

To construct the Lck kinase activity FRET reporter, the two fragments from ZIP and GeneArt custom plasmid were ligated together. The ligation was completed using a T4 DNA Ligase (New England Biolab, M0202) at a 1:9 molar ratio of ZIP: custom plasmid fragments. To prevent self-ligation of the ZIP fragments, they were treated with Antarctic Phosphatase (New England Biolab, M0289) to dephosphorylate the 5'-ends. The original plan was to introduce the religated plasmid into cells via electroporation. The pHR-LckR_FRET plasmid was about 11.45kb, too large for a viable and efficient cellular transfection. To trim the vector, the retroviral machinery was removed using a HindIII digestion of full length ZIP plasmid (Fig. 2.3). And the largest two fragments contained both the ZIP reporter and the bacteria replication machinery, which were religated together. The final LckR_FRET reporter was trimmed to 6.3kb. The plasmid was sequenced to validate its DNA fidelity using 10 primers: CTGCTTCTCGCTTCTGTTC, AGTACAGCCACCAAGGACAC, CGTCCTTGAAGAAGATGGTC, CATCAAGGCCAACTTCAAGA, ATGATGGCCATGTTATCCTC, AGTTCATGTACGGCTCCAAG, TAGGTGGTCTTGACCTCAGC, TCGCACCGGTATACAAGTTT, CGAGTAGAACTCGCAGAGC, and GGTGGAGAAGCTCATTGCTA.

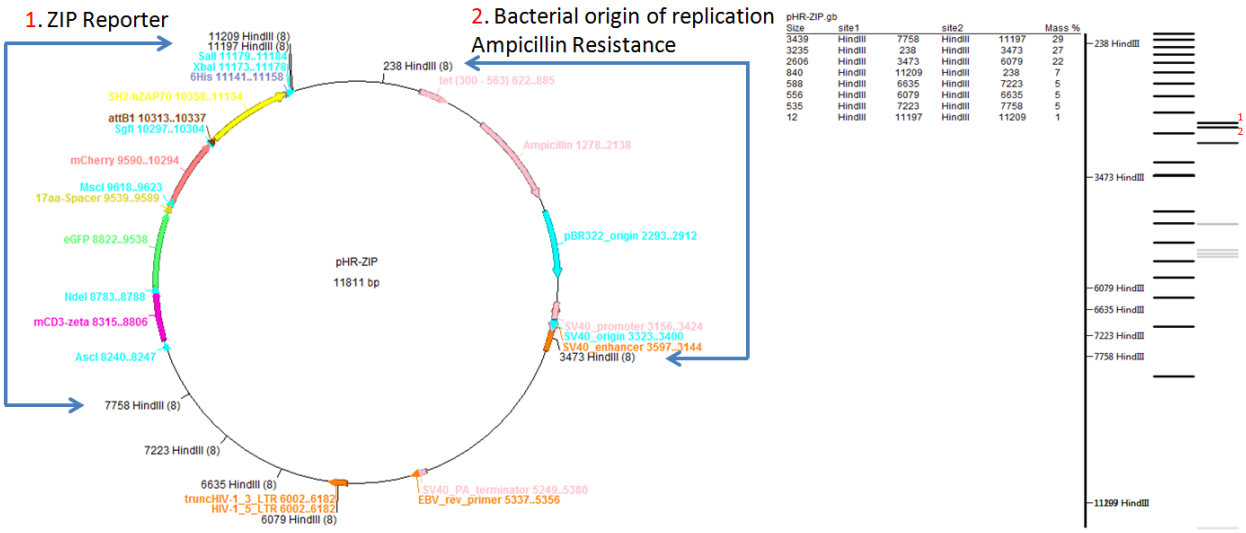

Figure 2.3: The HindII digestion of pHR-ZIP. The enzyme digested the plasmid into eight fragments. The largest fragment 7758-11197 contained the ZIP reporter. And the second largest fragment 238-3473 had the bacterial origin of replication and ampicillin resistance for selection. The two pieces were recovered and religated together.

2.2.4 Glass Substrate Preparation.

Glass coverslips were cleaned in hot detergent (Linbro 7X, diluted with deionized water), rinsed with MilliQ-grade water, and then baked at 450°C for 6 h.

NIH 3T3 cells naturally adhere to glass thus does not require the coverslides to be treated with adhesive proteins. Jurkat E6.1 cells are suspension cells, and will only adhere and spread upon its activation. Thus glass coverslips were incubated with 5µg/mL : 5µg/mL : 2µg/mL mixture of α-CD3 (clone OKT3 from M Sheetz' laboratory, Columbia University) : α-CD28 (clone 9.3 from BioXCell, BE0248) : human ICAM-1 (R&D Systems CD54 Fc Chimera Protein) for 2h.

2.2.5 NIH 3T3 and Jurkat Cell Culturing

Mouse NIH3T3 embryonic fibroblast (gift of Emily Moore, Christopher Jacobs' laboratory at Columbia University) was maintained in DMEM (Sigma, D6429) with 10% FBS (Hyclone SH30071.03) and 50 U/mL Penicillin & Streptomycin. Jurkat E6.1, human leukemic T-lymphoblast (American Type Culture Collection, TIB-152) was maintained in RPMI 1640 (Gibco 32404), 10% FBS, 10mM HEPES, 50 U/mL Penicillin & Streptomycin, 2mM L-glutamine, and 50μM β-Mercaptoethanol. For live cell imaging, to minimize autofluorescent interference, media without phenol red were used (Gibco 11835). And to maintain the condition at 37°C, LiveCell™ heating chamber was mounted onto the microscope, connect to a 5% CO_2 air tank.

2.2.6 Nucleic Acid Transfection

Transfection was performed in the Neon Transfection System (Invitrogen), using the recommended settings. Post transfection, cells recovered in the appropriate prewarmed media. For DNA-transfection, NIH3T3 cells were left to recover overnight.

Despite trimming the vector to 6.3Kb, the Jurkat could not tolerate the large vector. Using CellScript (Madison, WI), mRNA transcription of LckR_FRET was performed *in vitro*. Post mRNA-transfection, cells were ready after a 5 h recovery.

2.2.7 Lck Activity FRET Reporter Dynamic Study

Jurkat cells expressing LckR_FRET mRNA were incubated on glass precoated with activating antibody for 15 min, fixed, and imaged. For PP2 studies, Jurkat cells were preincubated with the antagonist (Calbiochem 529573) for 30min at 10µM.

Cells were fixed with 1:1 mixture of 4% paraformaldehyde: PHEM buffer for 15 minutes. Then washed with PBS before imaging.

2.2.8 Data Acquisition

All images were collected via an Olympus IX81 inverted microscope equipped with 20x, 60x, and 100x objectives. Images were collected using Andor iXon3 EM-CCD. LckR_FRET was imaged using TIRF microscopy (excitation 480nm, 100x/1.45 oil immersion objective): donor emitter filter S535/40M and acceptor emitter filter S610/40M.

The MetaMorph software for Olympus was used to acquire the images. Image processing was done on both MetaMorph and ImageJ. Functions used include, but are not limited to: overlaying multiple channels, background subtraction, and median filtration. Where appropriate, certain functions of image analysis were performed in Matlab.

2.2.9 Data Analysis for LckR_FRET

The analysis was adapted from Na and colleagues (Na and Wang 2008). Subtraction of background signal was performed with MetaMorph. Using Matlab, alignment was performed pixel-by-pixel maximizing the normalized cross-correlation coefficient of YPET and mCherry.

With proper background subtraction, no mask was needed. FRET ratio was defined as mCherry/YPET intensity on TIRF. FRET ratio was measured averaging 1-4 regions of interest (ROIs) per cell. The FRET ratio was then analyzed using standard ANOVA and performed with the OriginPro 8 software.

Below is the Matlab codes for analyzing FRET ratio on fixed samples, across 1-4 ROIs.

```
FRET_fixed_all.m

clear; clc;

%%  Pre-treating the data using MetaMorph%%
% select an area as the background using trace region icon
% BACKGROUND SUBTRACTION
% Go to 'Process' menu
% --> Background and Shading Correction...
% --> select source image
%     select full stack (subtract background from each image of the
stack)
% --> Operation: -> Statistical Correction
% --> Parameters: -> Region Statistics -> Average -> Region number: 1

Sample = '08.tif';
Raw = 'L_08.tif';
%%______CHANGE NAME

figure
num_image = max(size(imfinfo(Sample)));
[YFPcr rect] = imcrop(imadjust(imread(Sample,1))); % YFPcr: adjusted
image intensity (like in imageJ)
title('Crop the YFP/Donor image');
[isize jsize] = size(YFPcr);

% Initialize variables
offsets = zeros(num_image,3);
offsets1 = zeros(num_image,3);
```

```
YFPcrop = imcrop(imread(Sample,1), rect); % YFPcrop: intensity
unadjusted image

mFP = imadjust(imread(Sample,2)); % Read in the mCherry image as the
base
A = normxcorr2(YFPcrop,mFP); % Template is YFP cropped image, base is
mCherry

[max_A, imax] = max(abs(A(:)));
[ipeak, jpeak] = ind2sub(size(A),imax(1));
corr_offset1 = [ (ipeak-size(YFPcrop,1)) (jpeak-size(YFPcrop,2)) ]; %
How the template image needs to translate [i distance, j distance]
offsets(1,1:2) = corr_offset1;
offsets(1,3) = max_A;
rect_new = [corr_offset1(2)+.51, corr_offset1(1)+.51,rect(3),rect(4)];
mFPcrop = imcrop(imread(Sample,2), rect_new); % Crop the mCherry image
unadjusted

% Calculate FRET ratio, mCherry/YFP on a pixel-by-pixel basis
FRETratio = (double(mFPcrop) ./ double(YFPcrop));
%unadjusted/unadjusted
FRETratio(isnan(FRETratio)) = 0;
FRETratio(isinf(FRETratio)) = 0;

EPI_YPET = imcrop(imread(Raw,5),rect);
EPI_mCherry = imcrop(imread(Raw,6),rect);

EPIratio = (double(EPI_YPET ) ./ double(EPI_mCherry));
%unadjusted/unadjusted
EPIratio(isnan(EPIratio)) = 0;
EPIratio(isinf(EPIratio)) = 0;

%%%%%~~~~~~~~~~~~~~~~~~~~~~~~~~~~~~~~~~~~~~~~~~~~~~~~~~~~~~~~~~~~~~~

FRET_fixed_ROI.m

%  Define ROI of the cell body
figure
bg2 = imcrop(imadjust(imread(Sample,1)),rect);
im2 = imcrop(imadjust(imread(Sample,3)),rect);
imshow(bg2, 'Border', 'tight');
```

```
hold on
iim2 = image(im2,'XData',[0 0]S,'YData',[0 0]);
alpha(iim2, 0.4);

title('Select cells')
[ROI1 xi1body yi1body]=roipoly;

title('Select cells')
[ROI2 xi2body yi2body]=roipoly;

title('Select cells')
[ROI3 xi3body yi3body]=roipoly;

FRET1 = FRETratio.*ROI1;
EPI1 = EPIratio.*ROI1;
FRETmean1 = mean2(FRET1(ROI1==1));
EPImean1 = mean2(EPI1(ROI1==1));

FRET2 = FRETratio.*ROI2;
EPI2 = EPIratio.*ROI2;
FRETmean2 = mean2(FRET2(ROI2==1));
EPImean2 = mean2(EPI2(ROI2==1));

FRET3 = FRETratio.*ROI3;
EPI3 = EPIratio.*ROI3;
FRETmean3 = mean2(FRET3(ROI3==1));
EPImean3 = mean2(EPI3(ROI3==1));

FRETmean = (FRETmean1+FRETmean2+FRETmean3)/3;
EPImean = (EPImean1+EPImean2+EPImean3)/3;

Close
```

2.3 Results

2.3.1 Designing the Lck Activity Reporter

To develop a FRET-based indicator of Lck kinase activity, existing SFK biosensors were examined. Wang and colleagues constructed a reporter for Src, the prototype SFK (Wang, Botvinick et al. 2005). The reporter had six main domains. First is the membrane-targeting domain from Lyn. Next is the FRET donor, a cyan fluorescent protein (eCFP). Then is a SH2 domain to bind to the substrate. A flexible linker connects the SH2 domain to the substrate. Finally at the C-terminus is the FRET acceptor, a yellow fluorescent protein (eYFP). The substrate is what informs the Src kinase activity. WMED**Y**D**Y**VHLOG is derived from p130cas; it is the peptide that Src phosphorylates *in vivo.* Upon double tyrosine phosphorylation, SH2-domain of the reporter binds to the substrate to change the FRET response (Fig. 2.4A).

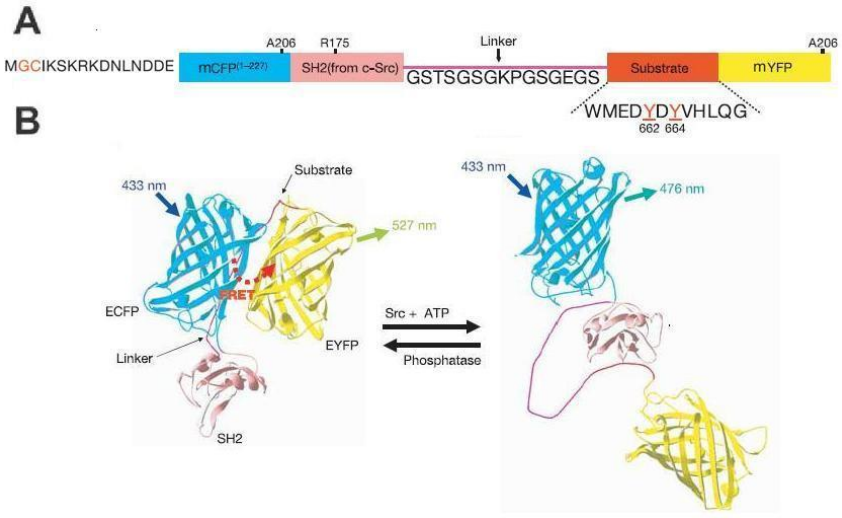

Figure 2.4: A. Schematic of the Src FRET reporter: membrane-targeting domain (MGCIKSKRKDNLNDDE), donor (eCFP), SH2 domain, flexible linker, substrate, and acceptor (eYFP). B. FRET response upon Src activation. Adapted from (Wang, Botvinick et al. 2005).

In a traditional FRET reporter, FRET intensity increases with enzyme activity. In the case of Src, it is the opposite. Without Src the donor and acceptor couple for a positive FRET response. Upon Src activation, substrate-SH2 interaction separates the two fluorescent proteins for a negative FRET response (Fig. 2.4B)

For Lck kinase activity, a good substrate is ITAM on CD3ζ. ITAM sequences from both human and mouse CD3ζ (Table 2.2 and Table 2.3) were assessed to find a consensus between the two species.

Table 2.2: Consensus sequence for mouse CD3ζ (Consensus CDS).

Mouse CD3ζ - 495nt

```
  1 ATGAAGTGGA AAGTGTCTGT TCTCGCCTGC ATCCTCCACG TGCGGTTCCC
 51 AGGAGCAGAG GCACAGAGCT TTGGTCTGCT GGATCCCAAA CTCTGCTACT
101 TGCTAGATGG AATCCTCTTC ATCTACGGAG TCATCATCAC AGCCCTGTAC
151 CTGAGAGCAA AATTCAGCAG GAGTGCAGAG ACTGCTGCCA ACCTGCAGGA
201 CCCCAACCAG CTCTACAATG AGCTCAATCT AGGGCGAAGA GAGGAATATG
251 ACGTCTTGGA GAAGAAGCGG GCTCGGGATC CAGAGATGGG AGGCAAACAG
301 CAGAGGAGGA GGAACCCCCA GGAAGGCGTA TACAATGCAC TGCAGAAAGA
351 CAAGATGGCA GAAGCCTACA GTGAGATCGG CACAAAAGGC GAGAGGCGGA
401 GAGGCAAGGG GCACGATGGC CTTTACCAGG GTCTCAGCAC TGCCACCAAG
451 GACACCTATG ATGCCCTGCA TATGCAGACC CTGGCCCCTC GCTAA
```

Table 2.3: Consensus sequence for human CD3ζ (Consensus CDS)

Human CD3ζ - 492nt

```
  1 ATGAAGTGGA AGGCGCTTTT CACCGCGGCC ATCCTGCAGG CACAGTTGCC
 51 GATTACAGAG GCACAGAGCT TTGGCCTGCT GGATCCCAAA CTCTGCTACC
101 TGCTGGATGG AATCCTCTTC ATCTATGGTG TCATTCTCAC TGCCTTGTTC
151 CTGAGAGTGA AGTTCAGCAG GAGCGCAGAC GCCCCCGCGT ACCAGCAGGG
201 CCAGAACCAG CTCTATAACG AGCTCAATCT AGGACGAAGA GAGGAGTACG
251 ATGTTTTGGA CAAGAGACGT GGCCGGGACC CTGAGATGGG GGGAAAGCCG
301 AGAAGGAAGA ACCCTCAGGA AGGCCTGTAC AATGAACTGC AGAAAGATAA
351 GATGGCGGAG GCCTACAGTG AGATTGGGAT GAAAGGCGAG CGCCGGAGGG
401 GCAAGGGGCA CGATGGCCTT TACCAGGGTC TCAGTACAGC CACCAAGGAC
451 ACCTACGACG CCCTTCACAT GCAGGCCCTG CCCCCTCGCT AA
```

Mouse CD3ζ

```
  1 MKWKVSVLAC ILHVRFPGAE AQSFGLLDPK LCYLLDGILF IYGVIITALY
 51 LRAKFSRSAE TAANLQDPNQ LYNELNLGRR EEYDVLEKKR ARDPEMGGKQ
101 QRRRNPQEGV YNALQKDKMA EAYSEIGTKG ERRRGKGHDG LYQGLSTATK
151 DTYDALHMQT LAPR
```

Human CD3ζ

```
  1 MKWKALFTAA ILQAQLPITE AQSFGLLDPK LCYLLDGILF IYGVILTALF
 51 LRVKFSRSAD APAYQQGQNQ LYNELNLGRR EEYDVLDKRR GRDPEMGGKP
101 RRKNPQEGL YNELQKDKMA EAYSEIGMKG ERRRGKGHDG LYQGLSTATK
150 DTYDALHMQA LPPR
```

CD3ζ is well-conserved. Almost identical in length, the human CD3ζ has a deletion of a glutamine at Q101. Structurally there are 3 major domains. First, the signaling domain, underline above, targets CD3ζ for the cytoplasmic membrane. Next is the transmembrane domain, highlighted in blue. Finally, CD3ζ has 3 ITAMs, in green. Focusing on the ITAMs, the third one is the best candidate for the substrate domain of the reporter because it's identical between the two species (Fig. 2.5).

	ITAM 1	ITAM 2	ITAM 3
Mouse	NQ LYNELNLGRR EEYDVLEKK	EGV YNALQKDKMA EAYSEIGTK	DG LYQGLSTATK DTYDALHMQ
Human	NQ LYNELNLGRR EEYDVLDKR	EGL YNELQKDKMA EAYSEIGMK	DG LYQGLSTATK DTYDALHMQ

Figure 2.5: ITAMs in CD3ζ. The motifs are well conserved between the species. Differences are highlighted in white. ITAM3 is identical between human and mouse.

In vivo, SH2 domain of ZAP70 binds to the phosphorylated ITAMs, thus a natural candidate for the reporter. And the species does not matter. The reporter should also migrate with the target protein, thus Lck membrane target domain (MGCGCSSNPE), also known as Lck10, should be added to the biosensor.

2.3.2 Building the Lck Activity Reporter

Instead of building the reporter from scratch, fragments were salvaged from other FRET reporters. The Vale group made a FRET biosensor to report on CD3 zeta chain ITAM phosphorylation, or ZIP^{WT} (Yudushkin and Vale 2010). The construct had a full length CD3ζ, donor fluorescent protein (eGFP), linker (GPGSASGEGLPGSAGPG), acceptor fluorescent protein (mCherry), and SH2 from human ZAP70 (residues 1-259) (Fig. 2.6A, Table 2.4). Instead of measuring the intensities of donor and acceptor fluorescent proteins, the Vale group utilized fluorescent-lifetime imaging microscopy (FLIM). FRET response was measured via eGFP lifetime; upon energy transfer, the length of the eGFP lifetime was shortened. Looking at the dynamic range of the ZIP reporter, two other mutants were explored. One construct removed all the tyrosines in ITAM (ZIP^{YF}), another removed the arginines in SH2, which bind to the phosphorylated tyrosines on ITAMs (ZIP$^{R37K/R180K}$) (Fig. 2.6B).

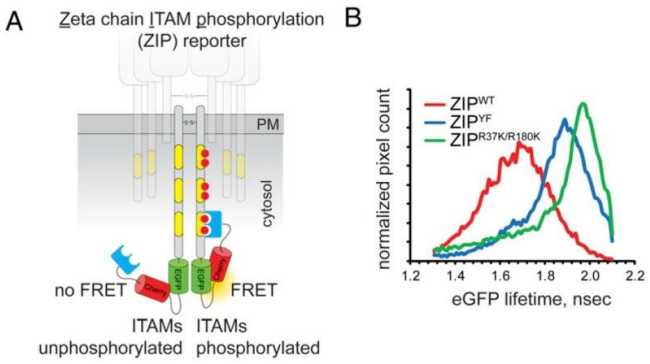

Figure 2.6: A. Diagram of the ZIP reporter. It contains full-length CD3ζ, eGFP, linker, mCherry, and human SH2. B. Jurkat transfected with ZIP^{WT}, ZIP^{YF}, and $ZIP^{R37K/R180K}$; the cells adhered onto glass precoated with α-CD3 antibody for 10min before being fixed and measured using TCSPC-FLIM. From (Yudushkin and Vale 2010).

As expected, ZIP^{WT} exhibited shortening of eGFP lifetime upon α-CD3 activation. ZIP^{YF} and $ZIP^{R37K/R180K}$, unable to form an intramolecular interaction between the SH2 domain and the ITAMs had extended eGFP lifetime (Fig. 2.6B).

Table 2.4: Sequence for ZIP^{WT}. It contains five discrete domains: CD3ζ, eGFP, linker, mCherry, and SH2.

```
-121                                                    GGCGC GCCagtcctc
 -61 cgacagactg agtcgcccgg gggggatctg gagctctcga gaattctcac gcgtgccacc
   1 ATGaagtgga aagtgtctgt tctcgcctgc atcctccacg tgcggttccc aggagcagag
  61 gcacagagct ttggtctgct ggatcccaaa ctctgctact tgctagatgg aatcctcttc
 121 atctacggag tcatcatcac agccctgtac ctgagagcaa aattcagcag gagtgcagag
 181 actgctgcca acctgcagga ccccaaccag ctctacaatg agctcaatct agggcgaaga
 241 gaggaatatg acgtcttgga gaagaagcgg gctcgggatc cagagatggg aggcaaacag
 301 cagaggagga ggaaccccca ggaaggcgta tacaatgcac tgcagaaaga caagatggca
 361 gaagcctaca gtgagatcgg cacaaaaggc gagaggcgga gaggcaaggg gcacgatggc
 421 ctttaccagg gtctcagcac tgccaccaag gacacctatg atgccctgCA TATGcagacc
 481 ctggcccctc gcccaccggt cgccaccATG gtgagcaagg gcgaggagct gttcaccggg
 541 gtggtgccca tcCTGGTCGA GCTGGACGGC GACGTAaacg gccacaagtt cagcgtgtcc
 601 ggcgagggcg agggcgatgc cacctacggc aagctgaccc tgaagttcat ctgcaccacc
 661 ggcaagctgc ccgtgccctg gcccaccctc gtgaccaccc tgacctacgg cgtgcagtgc
 721 ttcagccgct accccgacca catgaagcag cacgacttct tcaagtccgc catgcccgaa
 781 ggctacgtcc aggagcgcac catcttcttc aaggacgacg gcaactacaa gacccgcgcc
 847 gaggtgaagt tcgagggcga caccctggtg aaccgcatcg agctgaaggg catcgacttc
 901 aaggaggacg gcaacatcct ggggcacaag ctggagtaca actacaacag ccacaacgtc
 961 tatatcatgg ccgacaagca gaagaacggc atcaaggtga acttcaagat ccgccacaac
1021 atcgaggacg gcagcgtgca gctcgccgac cactaccagc agaacacccc catcggcgac
1081 ggccccgtgc tgctgcccga caaccactac ctgagcaccc agtccgccct gagcaaagac
1141 cccaacgaga agcgcgatca CATGGTCCTG CTGGAGTTCG TGaccgccgc cgggatcact
1201 ctcggcatgg acgagctgta caaggacca ggatcggcgt ctggggaagg actgccagga
```

1261 tcagccggac cagga**atggt gagcaagggc gaggaggata acaTGGCCAt catcaaggag**
1321 **ttcatgcgct tcaaggtgca catggagggc tccgtgaacg gccacgagtt cgagatcgag**
1381 **ggcgagggcg agggccgccc ctacgagggc acccagaccg ccaagctgaa ggtgaccaag**
1441 **ggtggccccc tgcccttcgc ctgggacatc ctgtcccctc agttcatgta cggctccaag**
1501 **gcctacgtga agcaccccgc cgacatcccc gactacttga agctgtcctt ccccgagggc**
1561 **ttcaagtggg agcgcgtgat gaacttcgag gacggcggcg tggtgaccgt gacccaggac**
1621 **tcctccctgc aggacggcga gttcatctac aaggtgaagc tgcgcggcac caacttcccc**
1681 **tccgacggcc ccgtaatgca gaagaagacc atgggctggg aggcctcctc cgagcggatg**
1741 **taccccgagg acggcgccct gaagggcgag atcaagcaga ggctgaagct gaaggacggc**
1801 **ggccactacg acgctgaggt caagaccacc tacaaggcca agaagcccgt gcagctgccc**
1861 **ggcgcctaca acgtcaacat caagttggac atcacctccc acaacgagga ctacaccatc**
1921 **gtggaacagt acgaacgcgc cgagggccgc cactccaccg gcggcatgga cgagctgtac**
1981 aa**GCGATCGC** accggtatac aagtttgtac aaaaaagcag gctccgcggc cgccccttc
2041 acc**atgccag accccgcggc gcacctgccc ttcttctacg gcagcatctc gcgtgccgag**
2101 **gccgaggagc acctgaagct ggcgggcatg gcggacgggc tcttcctgct gcgccagtgc**
2161 **ctgcgctcgc tgggcggcta tgtgctgtcg ctcgtgcacg atgtgcgctt ccaccacttt**
2221 **cccatcgagc gccagctcaa cggcacctac gccattgccg gcggcaaagc gcactgtgga**
2281 **ccggcagagc tctgcgagtt ctactcgcgc gaccccgacg ggctgccctg caacctgcgc**
2341 **aagccgtgca accggccgtc gggcctcgag ccgcagccgg gggtcttcga ctgcctgcga**
2401 **gacgccatgg tgcgtgacta cgtgcgccag acgtggaagc tggagggcga ggccctggag**
2461 **caggccatca tcagccaggc cccgcaggtg gagaagctca ttgctacgac ggcccacgag**
2521 **cggatgccct ggtaccacag cagcctgacg cgtgaggagg ccgagcgcaa actttactct**
2581 **ggggcgcaga ccgacggcaa gttcctgctg aggccgcgga aggagcaggg cacatacgcc**
2641 **ctgtccctca tctatgggaa gacggtgtac cactacctca tcagccaaga caaggcgggc**
2701 **aagtactgca ttcccgaggg caccaagttt gacacgctct ggcagctggt ggagtatctg**
2761 **aagctgaagg cggacgggct catctactgc ctgaaggagg cctgccccaa cagcagtgcc**
2821 ccagggcacc atcatcatca tcatTAAgcg gccgcgac**TC** **TAGAGTCGAC** ctgcaggcat
2881 gcaagc

The linker, mCherry, and SH2 from Vale's construct were salvaged. Modifications were made at the N-terminus to ensure that the probe would diffuse with the Lck proteins. Thus the full-length CD3ζ domain was replaced with the Lck membrane targeting domain (Lck10), and a substrate peptide (ITAM3) (Table 2.5). Instead of FLIM, which captures eGFP lifetime, FRET

response was quantified using the intensities of acceptor versus donor fluorescent proteins. YPET was selected as the donor because with a 450nm excitation laser, the fluorescent protein would more strongly excited, thus more electrons would be available for nonradiative energy transfer. YPET was a better candidate, since it's more blue-shifted (Fig. 2.7) and has greater brightness (product of extinction coefficient and quantum yield) than eGFP (Shaner, Steinbach et al. 2005). Finally, looking at the spectra overlap between donor and acceptor proteins, YPET-mCherry overlap was not much less than eGFP-mCherry overlap (Fig. 2.6). So YPET replaced eGFP.

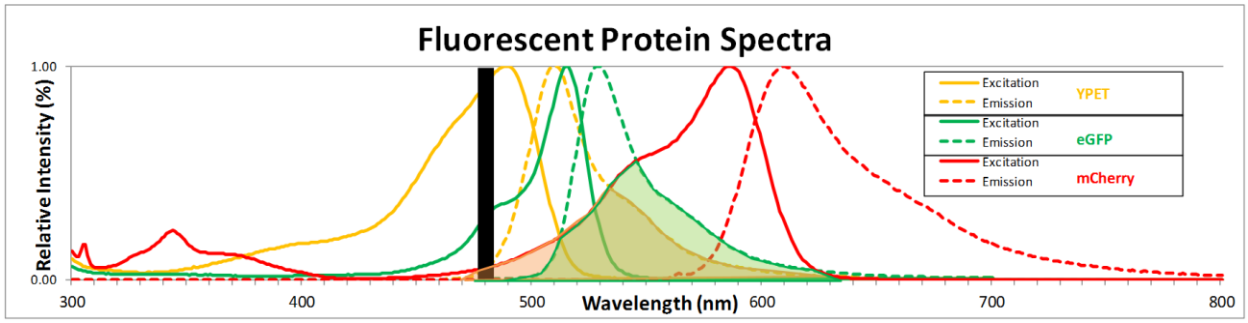

Figure 2.7: Spectra for YPET, eGFP and mCherry. YPET has a 30nm blue shift in excitation when compared to eGFP. And because mCherry has a wide excitation spectrum, minimal loss experienced in overlap with YPET. Black vertical bar denotes the excitation laser wavelength.

Table 2.5: Sequence for Lck FRET reporter. It contains three domains different from ZIP: Lck10, ITAM3, and YPET

```
241                                                  G GCGCGCCagt cctccgacaa
 301  TAATACGACT CACTATAGGG agacaagctt cgaattATGg gctgtggctg cagctcaaac
 361  cctgaaccag atccgggaca gATGaaaggc gagcgccgga ggggcaaggg gcacgatggc
 421  ctttaccagg gtctcagtac agccaccaag gacacctacg acgccttCA TATGcaggcc
 481  ctgccccctc gcccaccggt cgccaccATG gtgagcaaag gcgaagagct gttcaccggc
 541  gtggtgccca tcctggtgga gctggacggc gacgtgaacg gccacaagtt cagcgtgagc
 601  ggcgagggcg agggcgacgc cacctacggc aagctgaccc tgaagctgct gtgcaccacc
 661  ggcaagctgc ccgtgccctg gcccaccctg gtgaccaccc tgggctacgg cgtgcagtgc
 721  ttcgcccggt accccgacca catgaagcag cacgacttct tcaagagcgc catgcccgag
 781  ggctacgtgc aggagcggac catcttcttc aaggacgacg gcaactacaa gacccgggcc
```

```
 847 gaggtgaagt tcgagggcga caccctggtg aaccggatcg agctgaaggg catcgacttc
 901 aaggaggacg gcaacatcct gggccacaag ctggagtaca actacaacag ccacaacgtg
 961 tacatcaccg ccgacaagca gaagaacggc atcaaggcca acttcaagat ccggcacaac
1021 atcgaggacg gcggcgtgCA GCTGgccgac cactaccagc agaacacccc catcggcgac
1081 ggccccgtgc tgctgcccga caaccactac ctgagctacc agagcgccct gttcaaggac
1141 cccaacgaga agcgggacca catggtgctg ctggagttcc tgaccgccgc cggcatcacc
1201 gagggcatga acgagctcta taaggacca ggatcggcgt ctggggaagg actgccagga
```

2.3.3 Lck Activity FRET Reporter Transfection into Cells

Before sequencing, subclones were transfected into mouse embryonic fibroblasts, a cell type very easy to transfect to check for proper ligation without out-of-frame mutations (Fig. 2.8).

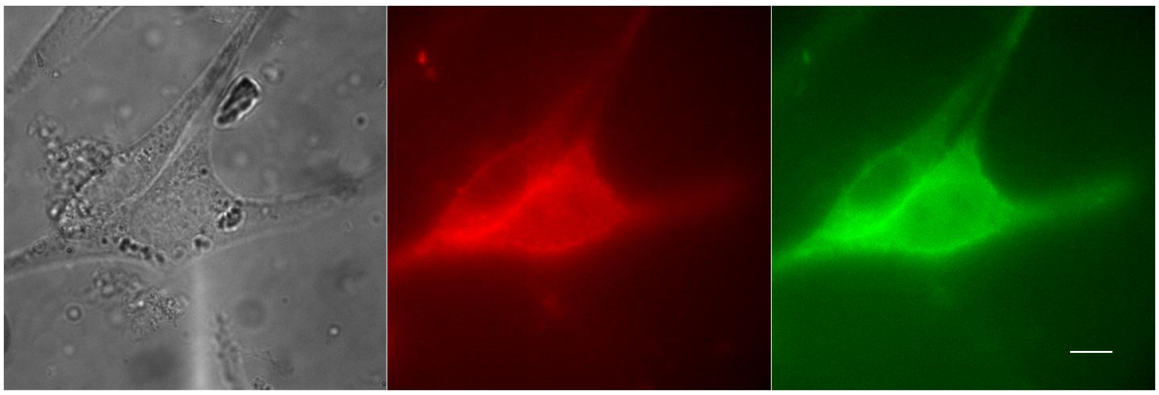

Figure 2.8: Plasmid transfection of LckR_FRET into NIH 3T3 cells to check for out-of-frame mutations. Scale bar = 10µm.

Then the final plasmid for LckR-FRET was sequenced.

```
   1 MGCGCSSNPE PDPGQMKGER RRGKGHDGLY QGLSTATKDT YDALHMQALP PRPPVATMVS
  61 KGEELFTGVV PILVELDGDV NGHKFSVSGE GEGDATYGKL TLKLLCTTGK LPVPWPTLVT
 121 TLGYGVQCFA RYPDHMKQHD FFKSAMPEGY VQERTIFFKD DGNYKTRAEV KFEGDTLVNR
 181 IELKGIDFKE DGNILGHKLE YNYNSHNVYI TADKQKNGIK ANFKIRHNIE DGGVQLADHY
 241 QQNTPIGDGP VLLPDNHYLS YQSALFKDPN EKRDHMVLLE FLTAAGITEG MNELYKGPGS
 301 ASGEGLPGSA GPGMVSKGEE DNMAIIKEFM RFKVHMEGSV NGHEFEIEGE GEGRPYEGTQ
```

```
361  TAKLKVTKGG PLPFAWDILS PQFMYGSKAY VKHPADIPDY LKLSFPEGFK WERVMNFEDG
421  GVVTVTQDSS LQDGEFIYKV KLRGTNFPSD GPVMQKKTMG WEASSERMYP EDGALKGEIK
481  QRLKLKDGGH YDAEVKTTYK AKKPVQLPGA YNVNIKLDIT SHNEDYTIVE QYERAEGRHS
541  TGGMDELYKR SHRYTSLYKK AGSAAAPFTM PDPAAHLPFF YGSISRAEAE EHLKLAGMAD
601  GLFLLRQCLR SLGGYVLSLV HDVRFHHFPI ERQLNGTYAI AGGKAHCGPA ELCEFYSRDP
661  DGLPCNLRKP CNRPSGLEPQ PGVFDCLRDA MVRDYVRQTW KLEGEALEQA IISQAPQVEK
721  LIATTAHERM PWYHSSLTRE EAERKLYSGA QTDGKFLLRP RKEQGTYALS LIYGKTVYHY
781  LISQDKAGKY CIPEGTKFDT LWQLVEYLKL KADGLIYCLK EACPNSSAPG HHHHHH
```

Two approaches were available to investigate the dynamic range of the LckR_FRET reporter. Wang and colleagues studied the Src reporter using the purified protein. Emission ratios of donor/acceptor were measured via cuvettes after the addition of ATPs. Unfortunately this method was abandoned because Lck10 resulted in the LckR_FRET reporters being translocated to the bacterial cellular membrane, thus very difficult to isolate.

Another approach was the method utilized by the Vale group. Briefly, Vale transfected the ZIP reporter into Jurkat cells. The cells were either preincubated with PP2, a SFK antagonist, or not. Then the cells were permit to adhere onto activating glass coverslips before being fixed and imaged via FLIM.

The Jurkat cell line is difficult to transfect, as immune cells are naturally adverse to take up foreign genetic materials, because it mimics a viral infection. The Vale group opted to use lentiviral transductions. However, the methodology is incompatible with naïve primary T-cells,

the focus of our group's work on micropatterned surfaces. Thus electrophoresis was used to transfect cells with *in vitro* transcribed LckR_FRET mRNA.

Jurkat cells were stably transfecting LckR_FRET. After fixing, images were acquired for both donor and acceptor fluorescent proteins in TIRF with a 480nm excitation. The FRET ratio for activated Jurkat was 0.424 ± 0.203 (mean ± standard deviation). And the FRET ratio for PP2 preincubated Jurkat was 0.320 ± 0.140 (mean ± standard deviation) (Fig. 2.9). The differences were statistically significant ($p = 0.012$).

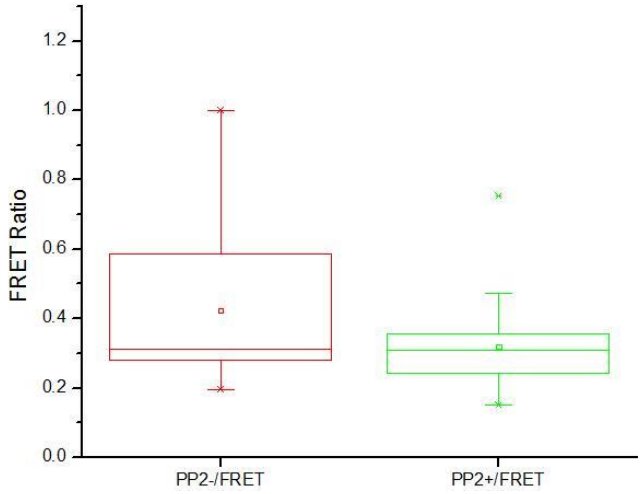

Figure 2.9: The effect of PP2 on LckR_FRET biosensor. Box and whisker diagram of FRET ratio for Jurkat cells transfected with LckR_FRET. P < 0.05.

2.4 Discussion

Two fundamentally different approaches can be used to study Lck dynamics. One focuses on the phosphorylation states of the regulatory tyrosines, and another on the Lck kinase activity. Typical of its family, Lck kinase activity is highly regulated by its conformational changes. And the protein exists in

four different states as defined by the phosphorylation states of its two regulatory tyrosines: autoinhibited (pY505), primed, active (pY394), or DPho-active (pY505 and pY394). Stirnweiss and colleagues approached the study of Lck dynamic with a conformational FRET reporter. Unfortunately, the reporter does not distinguish between the 4 different states. It merely reports on either an open (likely active) or a closed (likely autoinhibited). The reporter observed a 20% increase in the 'open' form upon CD3 engagement, an increase from 16% to 19.2% in JCAM1.6. As mentioned, under unstimulated conditions, 16% of the Lck protein is already pY294-active. That's not including a large population of DPho-active Lck proteins. As a reference, in Jurkats, before stimulation 23% of Lck proteins are pY394-active and 29% DPho-active. So the additional 20% increase in pY394 at the plasma membrane, what does that mean for intracellular kinase activity? The conformational reporters offered no additional information.

Thus a reporter of Lck kinase activity was designed. PLck phosphorylation of the substrate peptide would trigger a FRET response. Fragments of the ZIP reporter from the Vale group were salvaged to generate the LckR_FRET reporter. However, different methods were employed to quantify the FRET responses. The Vale group measured the lifetime of the eGFP in fixed samples: to quantify how eGFP lifetime shortens in response nonradiative energy transfer to mCherry. To capture real-time FRET responses, another method was used, measuring the acceptor, or mCherry, intensity versus the donor, or YPET, intensity. As discussed in the introduction, beyond conformational regulations, spatial organizations of pLck during IS formation also plays an important role on the overall effect of Lck kinase activity. Thus, a real-time reporter would be more appropriate to study the interactions. The next chapter focuses on the challenges of working with primary T-cells and studies in Jurkats to understand how CD3 and CD28 engagements spatiotemporally affect pLck kinase activity in real-time.

Chapter 3

3. The LckR_FRET Reporter

3.1 Introduction

LckR_FRET must first be transfected into the cells. And many factors affect transfection, such as cell type, cell growth cycle, and osmotic conditions of the transfection media. T-cells, central to immune response to foreign pathogens, are naturally intolerant of transfections. Naïve T-cells are even more difficult to work with because they are metabolically resting before activation. And actively dividing cells take up genetic materials more readily than quiescent cells. Investigators have generally utilized viral transduction, especially lentiviral vectors for both dividing and non-dividing cells. Even then, T-cells first must be stimulated to activate and to divide generating lymphoblasts. And human peripheral blood CD4+ T-cells and mouse splenic CD4+ T-cells respond differently to CD3 and CD28 engagement after stimulation. Beyond the need to stimulate T-cells, viral transduction is very labor, time, and cost intensive. Even upon successful transduction, cells infected with lentivirus are difficult to work with, as

environmental stresses will trigger the virus to go lytic, and kill-off the host cell. Finally, there are the safety concerns of working with a retrovirus, which requires P2 containment. (Zhao, Zheng et al. 2006). Ultimately, non-viral gene transfer was opted for the LckR_FRET reporter.

It is still a real challenge to modify primary T-cells using non-viral gene transfer. The most common method is electroporation; the exposure of an intense electric field transiently permeabilizes the cellular membrane. This was the method used by Bashour to study the diffusion of Lck_YFP. The method had low gene transfer efficiency and poor viability due to cytotoxicity. However, the only method available for primary T-cells without stimulation. To illustrate the challenge, Bashour transfected T-cells with Lck_YFP to measure its diffusion rate within human and mouse T-cells. The diffusion rate were measured using less than 30 cells. To put into perspective, Bashour completed more than a dozen rounds of transfection to collect the data. And for each round of transfection, a suspension of roughly 10 million T-cells were used. While highly inefficient, the method gave wonderful insight into Lck dynamic in clinically relevant cells.

The difficulty of working with primary cells also forced many researchers to use lymphoblastic cells line, the mostly commonly used T-cell lines to study Lck dynamics are the Jurkat cells and its variants. However, Jurkat cells have corrupt signaling pathways when compared to health, non-cancerous lymphocytes. Ueda and colleagues were studying the effect of CD28 engagement by B7-2 or CD85 on phosphoinositide 3-kinase (PI3K) activity (p85-p110 heterodimer) and its downstream effect on IL-2 secretions (Ueda, Levine et al. 1995). PI3K catalyzes the conversion of phosphatidylinositol (4,5)-bisphosphate (PIP2) to

phosphatidylinositol(3,4,5)-triphosphate (PIP3). Thus, to measure PI3K activity, PIP3 concentration was quantified. And to capture the dynamics of the pathway, Wortmannin, a pharmacologic inhibitor of PI3K was used.

In Jurkat cells, while Wortmannin inhibited PIP3 in a concentration dependent manner (Fig. 3.1A), it increased IL-2 secretions (Fig. 3.B).

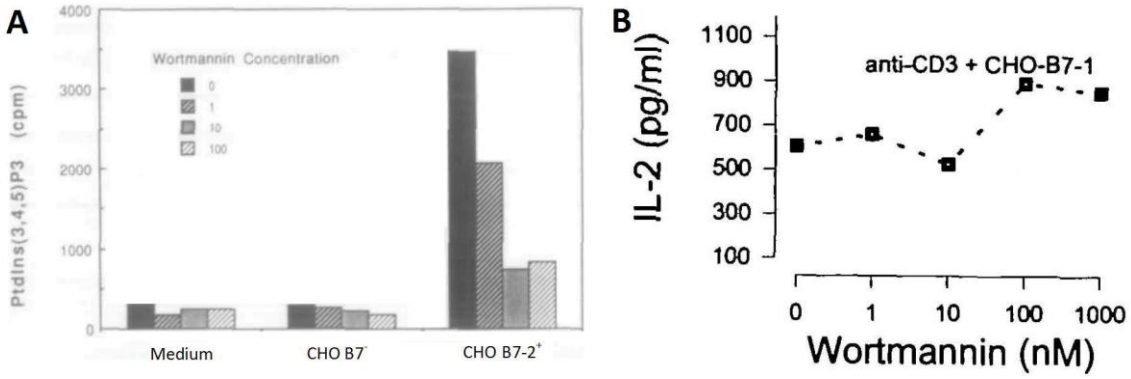

Figure 3.1: A. Wortmannin inhibition of B7-2 induced PIP3 conversion was concentration dependent. B. Wortmannin, despite PIP3 inhibition, resulted in increased IL-2 secretion. From (Ueda, Levine et al. 1995).

In contrast, in primary human T-cells, Wortmannin inhibits both PIP3 and IL-2 (Fig. 3.2). Jurkat cells were sensitive to CD28 engagement; however the functional pathways appeared to be different from primary T-cells, thus emphasizing the importance of working with primary cell.

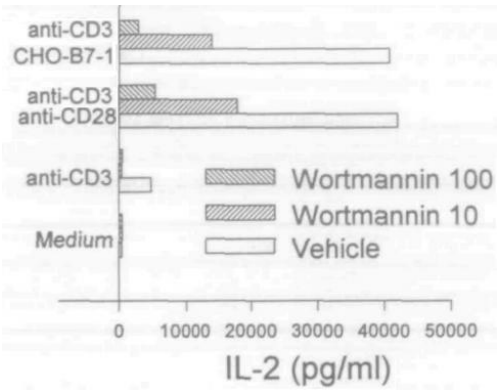

Figure 3.2: Wortmannin inhibition of IL-2 secretions in primary T-cells. From (Ueda, Levine et al. 1995).

3.2 Materials and Method

3.2.1 Micropatterned Glass Preparation

Glass coverslides were prepared as previously described. To create micropatterned surfaces, stamps were incubated in a solution with a total protein concentration of 28 µg/mL. For mouse T-cells, activating antibodies against CD3 (clone 145-2C11) and CD28 (clone 37.51) were purchased from eBioscience. The stamped surfaces were backfilled with mouse ICAM-1 (R&D Systems CD54 Fc Chimera Protein) to promote adhesion at 2 µg/ml for 2h. For human T-cells, activating antibodies against CD3 (clone OKT3 from M Sheetz' laboratory, Columbia University) and CD28 (clone 9.3 from BioXCell, BE0248). L were also purchased. Again, the surfaces were backfilled with human ICAM-1 (R&D Systems CD54 Fc Chimera Protein) at 2 µg/ml for 2h.

For COL pattern, stamps with 2µm diameter dots at either a 10µm pitch for mouse T-cells or a 15µm pitch for human T-cells were used. The incubation mixtures for the stamps were made at 1:10 (wt/wt) α-CD3:α-CD28 for mouse T-cells, and 1:3 (wt/wt) α-CD3:α-CD28 for human T-cells.

For SEG pattern, an inert antibody was used to standardize the total protein concentration. In this case, donkey anti-sheep IgG (Life Technology A16045) was used. And two rounds of stamping were performed to generate the pattern. First, stamps with 2µm diameter dots were incubated with α-CD:α-IgG at either 1:10 or 1:3, depending on the species of the primary T-

cells. Next, stamps with 1µm diameter dots at a 5µm pitch were incubated with α-IgG: α-CD28, again at either 1:10 or 1:3.

Adjustments were made for Jurkat cells because of the large cell size. Stamps with 2µm diameter dots and a 15µm pitch were used for the α-CD3 antibody. And stamps with 2µm diameter dots and a 10µm pitch were used for the α-CD28 antibody. Human ICAM-1 was eliminated because Jurkat cells do not require adhesion proteins to land and spread.

3.2.2 T-cell Isolation

Mouse T-cells were collected from the lymph nodes and spleens of 6-week old C57BL/6 males. CD4+ T-cell isolation was performed with negative-selection Dyno beads (Invitrogen, 11415D), which gave predominately naïve mouse T-cells (Bashour, Tsai et al. 2014). Human CD4+ T-cells were purified from Leukopacks (New York Blood Center) using negative selection Rosette-Sep kits (StemCell Technologies 15062). The purified T-cells were a mixture of naïve and memory cells (though higher percentages of the population were naïve T-cells), and highly patient-dependent.

All the cells were cultured in RPMI 1640 (Gibco 32404), supplemented with 10% FBS, 10mM HEPES, 50 U/mL Penicillin & Streptomycin, 2mM L-glutamine, and 50µM β-Mercaptoethanol.

3.2.3 Nucleic Acid Transfection

Electroporation was performed using two commercial systems: Neon Transfection System (Invitrogen) and Amaxa/Nucleofector Technology (Lonza). Because of poor transfection efficiency and viability of T-cells, *in* vitro transcribed LckR_FRET mRNA was used for gene transfer instead of DNA plasmid. Also, naïve T-cells without stimulation cannot survive overnight, which is needed for an incorporated DNA plasmid to express a protein of interest.

Neon had recommended or optimized settings for Jurkats. Unfortunately, none were available for unstimulated human and mouse primary T-cells. Optimization protocols were performed without much success (see discussion below).

Amaxa offered an optimized protocol for C57BL/6 unstimulated splenocytes. For the control plasmid, (pMAX-GFP), Lonza reported the viability at 35% and with only 20% transfection efficiency using program X-001. When transfecting LckR_FRET mRNA, the cytotoxicity and transfection efficiency were even worse. Discussion with Lonza technical support yielded no further progress as they suggested either stimulate the naïve T-cells to generate lymphoblasts or switch to viral transduction. Amaxa also offered an alternative protocol for unstimulated human peripheral blood T-cells: program V24. While GFP mRNA was efficiently transfected, the cells did not tolerate LckR_FRET, a much larger construct.

Post transfection, T-cells recovered for 5 h in prewarmed fully supplemented media (see above) without Penicillin or Streptomycin.

3.2.4 Immunostaining

Immunostainings were performed in Jurkat cells to study pLck distribution. The Jurkat cells were seeded onto the micropatterned surface for 30 minutes, fixed with 1:1 4% paraformaldehyde: PHEM buffer for 15 minutes, and perforated with 0.1% Triton-X in PBS. Next, the cells were blocked 2h to overnight with 5% BSA. Then primary staining was performed at 1:200 dilution using antibodies targeting phosphorylated Lck Y394 (Novus Biological NBP1-60894). Finally a secondary staining was performed at 1:500 dilutions against pLck (AF488 α-rabbit) before washing and imaging.

3.2.5 IL-2 Secretion Assay

IL-2 secretion assays performed used to measure T-cell activation at a medium time-scale. IL-2 was indirectly captured using an IL-2 secretion kit (Miltenyi 130-090-763 or 130-090-987). The IL-2 binding antibodies were mounted onto CD45, a protein ubiquitously expressed on T-cells. The mounting of α-IL-2 antibodies was performed per the manufacturer's recommendation. However, adaptations were made to the manufacturer's protocol because the kit was intended for FACS analysis for cells in a suspension buffer, instead of adherent cells on a coverslide. Instead, T-cells were seeded onto micropatterned glass surfaces, and maintained under standard cell culture conditions for 6h. Next, detecting agent was added to examine IL-2 secretion on a cell-to-cell basis. Finally, the cells were fixed for imaging. IL-2 secretion was captured using 20x objective and quantified using MetaMorph; IL-2 fluorescent intensity was

measured for at least 200 cells per condition, and for each cell the intensity was averaged around the whole cell.

3.2.6 FRET Measurement and Analysis

Image acquisitions were completed as previously described. And FRET Analysis was adopted from Na and colleagues (Na and Wang 2008) as described in Chapter 2. And custom Matlab codes were written to process the timelapse images. See Appendix A

Without a beam splitter, donor and acceptor images were acquired within 1s of each other. Diffusion of Lck is roughly 0.26 $\mu m^2/s$ in Jurkat cells that's Lck-deficient (Zimmermann, Paster et al. 2010). Since $D = x^2/4T$ (D – diffusion, x – distance, and T-time), at 100X (.08µm/pixel) it's a 13-pixel movement.

During timelapse imaging, interval of acquisition must balance photobleaching of the fluorescent proteins against the time scale of pLck diffusion between CD3 and CD28. With an acquisition interval of 30 seconds, the Lck protein would have diffused roughly 5.5µm.

3.3 Results

3.3.1 Transfection of Mouse Splenocytes

Non-viral gene transfer of LckR_FRET requires *in vitro* transcribed mRNA. The Neon Transfection System was selected over the Amaxa Nucleofactor System. Neon permits a

reaction volume ~10µl; in comparison, Amaxa requires a 100µl reaction volume. Instead of using 2-4µg of LckR_FRET mRNA per reaction, Amaxa required +40µg, an unsustainable amount given the limitations of the *in vitro* mRNA production system.

The Neon Transfection System did not provide an optimized setting for unstimulated mouse primary T-cells. Thus, an optimization protocol was performed initially using GFP mRNA before switching to LckR_FRET mRNA. Five parameters were optimized: cell density, mRNA concentration, pulse voltage, pulse width, and number of pulse. All of which affected transfection efficiency and cell viability.

Table 3.1: Optimization of transfection parameters for mouse splenocytes

		Cell Count	mRNA (µg)	Voltage (mV)	Width (ms)	Pulse Number
	Jurkat Control	500,000	2	1325	30	1
Voltage	A	1,000,000	2	500	20	1
	B	1,000,000	2	750	20	1
	C	1,000,000	2	1000	20	1
mRNA & Cell	A	500,000	2	750	20	1
	B	500,000	4	750	20	1
	C	1,000,000	4	750	20	1
Pulse Voltage, Width, &	A	1,000,000	4	750	20	1
	B	1,000,000	4	750	30	1
	C	1,000,000	4	750	30	2
	D	1,000,000	4	850	30	1
	E	1,000,000	4	950	30	1

Jurkats were used (Neon recommended setting available) as a control for LckR_FRET mRNA quality and cellular transfection (Fig. 3.3 Jurkat control). Initial reactions found that at a low voltage (i.e., 500mV), the T-cells exhibited good viability, but a poor transfection efficiency. On the other hand, high voltage (i.e., 1000mV) resulted in very poor viability (Fig. 3.3).

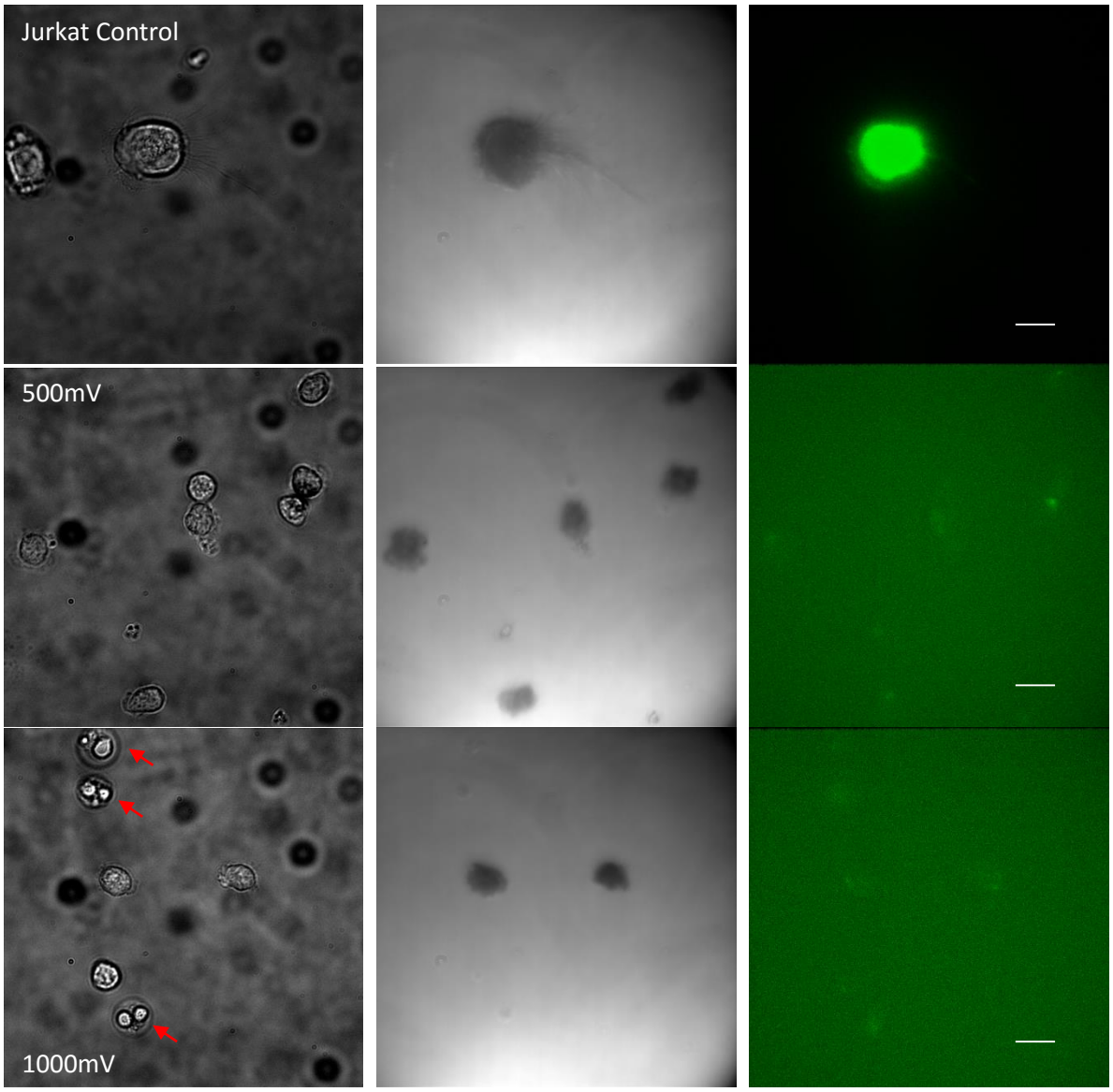

Figure 3.3: Representative images of transfected mouse splenocytes. Images were taken in Brightfield, interference reflection microscopy (IRM), and epifluorescence (for GFP). IRM reports cellular adhesion, a good indicator of cellular viability. Red arrows point to apoptotic cells. Scale Bar = 10µm.

Next, an optimal mRNA concentration (4µg) and cell count per reaction (1M) was found. While 750mV pulse voltage gave good viability, its transfection efficiency was very poor (<10%). Small increases in pulse voltage, width, and number did not greatly increase the transfection efficiency, but greatly compromised the viability. Accepting the poor transfection efficiency,

eGFP mRNA was replaced with LckR_FRET mRNA. Viability further decreased and no transfected cells were observed. Discussions with Invitrogen technical support were unfruitful. They suggested moving into a lentiviral transduction system.

Despite the limitations of the *in vitro* mRNA production system, the study moved into the Amaxa/Nucleofector Technology system. Unlike the Neon system, where users can control up to five parameters, Amaxa gives pre-programmed protocols with a set cell count and a small range of recommended mRNA concentrations. Initially reactions with GFP mRNA were completed using the recommended program, X-001. While transfection of GFP mRNA was possible, LckR_FRET mRNA had very poor transfection efficiency and viability (Fig. 3.4). Technical support at Lonza suggested two alternative programs, U-001 and W-001. Again, transfection was possible with GFP mRNA, but not LckR_FRET mRNA, a construct that roughly three times as large as the control.

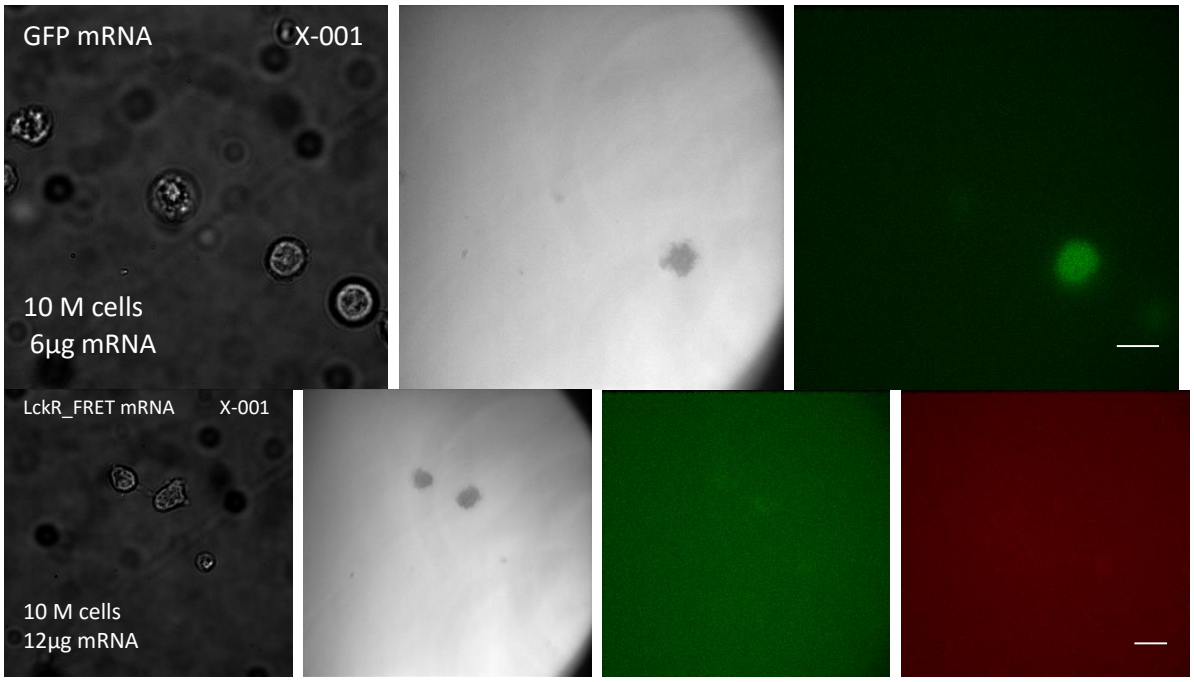

Figure 3.4: Representative images of transfected mouse splenocytes. Images were taken in Brightfield, IRM, and epifluorescence (for GFP or YPET and mCherry). Mouse spleenocytes tolerated GFP, but not LckR_FRET. Scale Bar = 10µm.

3.3.2 Transfection of Human T-cells

Again, the Neon Transfection System did not provide an optimized setting for unstimulated human peripheral blood T-cells. Thus another optimization protocol was performed.

Table 3.2: Optimization of transfection parameters for human peripheral blood T-cells

		Cell Count	mRNA (µg)	Voltage (mV)	Width (ms)	Pulse Number
	Jurkat Control	500,000	2	1325	30	1
Voltage	A	1,000,000	2	1325	20	1
	B	1,000,000	2	2050	20	1
	C	1,000,000	2	2100	20	1
LckR_FRET mRNA	A	1,000,000	2.00	2100	20	1
	B	1,000,000	2.75	2100	20	1
	C	1,000,000	3.50	2100	20	1

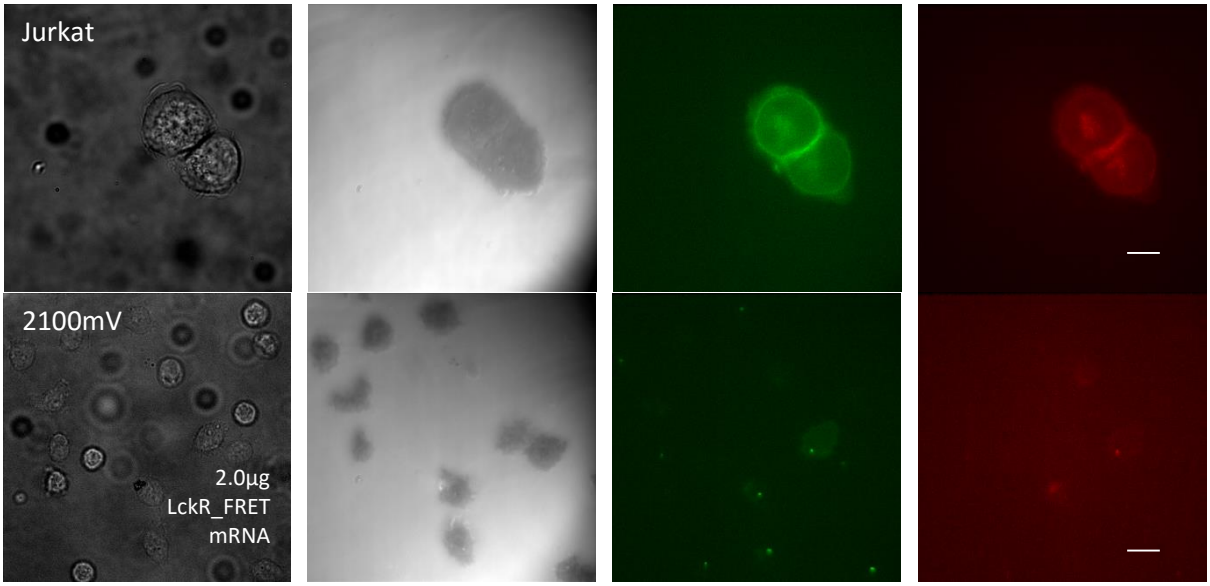

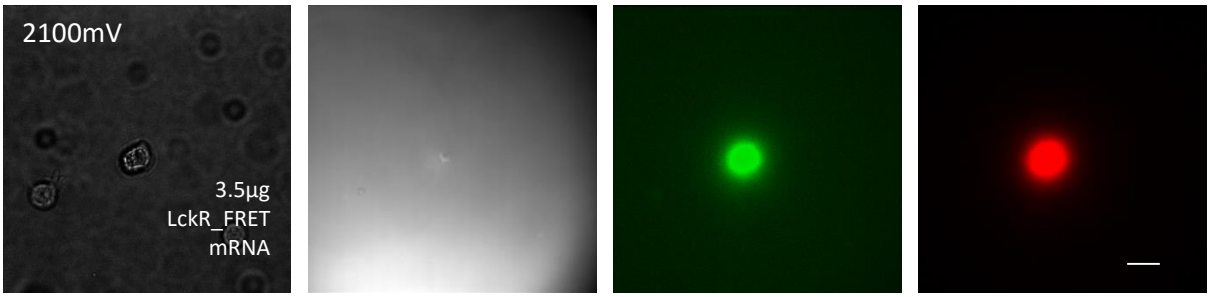

Figure 3.5: Representative images of transfected human peripheral blood CD4+ T-cells. Images were taken in Brightfield, IRM, and epifluorescence (for YPET and mCherry). While transfection was achieved at 2200mV and 3.5µg of mRNA, the cell was not viable as seen in IRM. Scale Bar = 10µm.

Using GFP mRNA, 2100mV was found to be an appropriate pulse voltage. GFP was replaced with LckR_FRET mRNA. At 2µg, the viability was acceptable, but with poor transfection efficiency. Unfortunately upon addition of more mRNA (3.5µg), the viability vastly decreased (Fig. 3.5). Lonza representatives again recommended using lentiviral systems.

Again the study moved into the Amaxa/Nucleofector Technology system. Initial optimization were completed in recommended program V-24. While the cellular viability was satisfactory, the transfection efficiency was poor. To compensate for the poor transfection efficiency, additional mRNA were added. Instead of the recommended 1-5µg of plasmid, 16µg of LckR_FRET mRNA were added. While the transfection efficiency increased slightly with the huge increase in LckR_FRET mRNA concentration, the cells were still too dim for imaging and subsequent analysis.

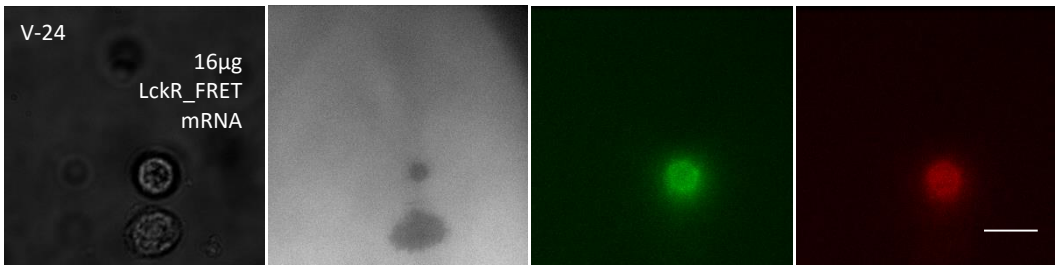

Figure 3.6: Representative images of transfected human peripheral blood Cd4+ T-cells using the Amaxa system. Images were taken in Brightfield, IRM, and epifluorescence (for GFP or YPET and mCherry). Despite a large quantity of LckR_FRET mRNA, the transfection efficiency was still poor. Scale Bar = 10µm.

3.3.3 Jurkat Cells Are Responsive to Micropatterned Surfaces

Unable to transfect primary T-cells with LckR_FRET, the study moved back into Jurkat cells. And the T-cell line does have a compromised signaling cascade, as demonstrated by the Wortmannin study. However, the LckR_FRET reporter probes Lck kinase activity, which occurs very early in the signaling cascade, within the first 30 minutes after T-cell activation. Even the Wortmannin study suggested that early enzymatic activities (i.e., PI3K activity) were less compromised in Jurkat cells.

Before continuing onto dynamic real-time imaging and analysis of Jurkat cells responding to microscale spatial cues, previous studies were replicated in the T-cell line, as performed prior in human and mouse primary T-cells.

Initially, immunostainings were performed to understanding the time scale of Lck activation in Jurkats. And it was found that when compared to mouse T-cells, pLck signaling was more sustained in Jurkat cells. In mouse T-cells, pLck staining peaked around 5 minutes and

disappeared after 15 minutes (Lee, Holdorf et al. 2002). However, in Jurkats, pLck staining was still visible after 15 minutes, and mostly disappeared after 30 minutes. In conclusion, an appropriate duration for a timelapse to study LckR_FRET reporter in Jurkats would be roughly 15 minutes.

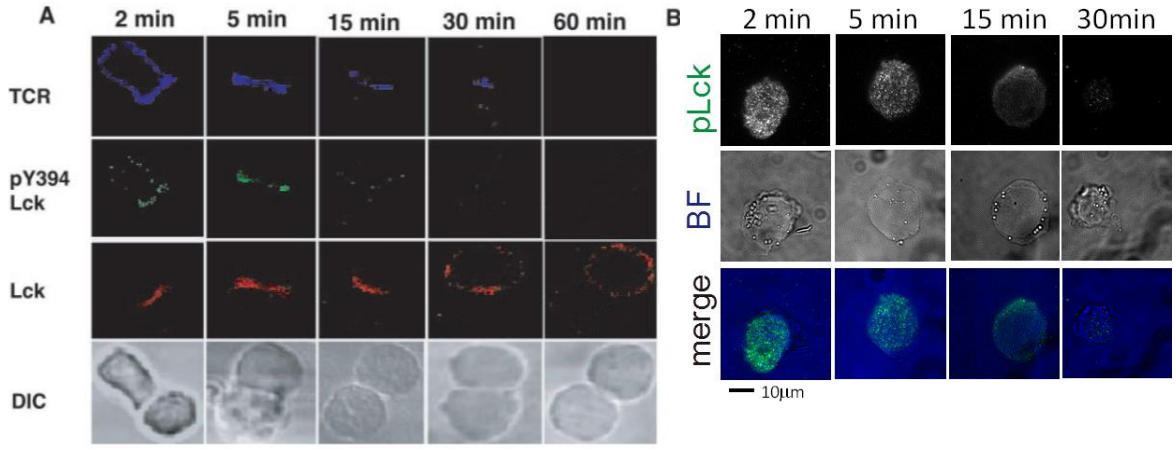

Figure 3.7: A. Mouse transgenic splenic T-cell were activated by APCs from B10.BR mice. From (Lee, Holdorf et al. 2002). B. Jurkat cells were seeded onto activating surfaces. All the cells are fixed at the indicated time, perforated, blocked and stained with pLck.

Next, IL-2 secretion assays were performed to measure cellular response to micropatterned surfaces. As mentioned in Chapter 1, mouse T-cells prefer SEG pattern to COL pattern; specifically the cells favor peripheral presentation of CD28 (Fig. 3.8A). In contrast, human peripheral blood CD4+ cells respond strongly to COL pattern because IL-2 secretions require co-engagement of CD3 and CD28 (Fig. 3.8B). Like non-leukemic primary T-cells, human lymphoblastic Jurkat cells also require CD28 for IL-2 secretion, as evident by the lack of response on α-CD3 surfaces. However, unlike both human and mouse primary T-cells, for Jurkats, adhesion and spreading are uncoupled from cellular activation and costimulation.

While few primary T-cells could be found on α-CD3 surfaces, Jurkat cells readily adhere without IL-2 secretion. Like primary human T-cells, stronger IL-2 secretion was observed on COL micropatterns, 1.5x fold increase over the intensities observed on SEG surfaces. However, unlike human primary cells, Jurkat cells had significant IL-2 secretion on SEG surfaces, about 100 fold brighter in intensity than on CD3 surfaces ($p<0.0001$).

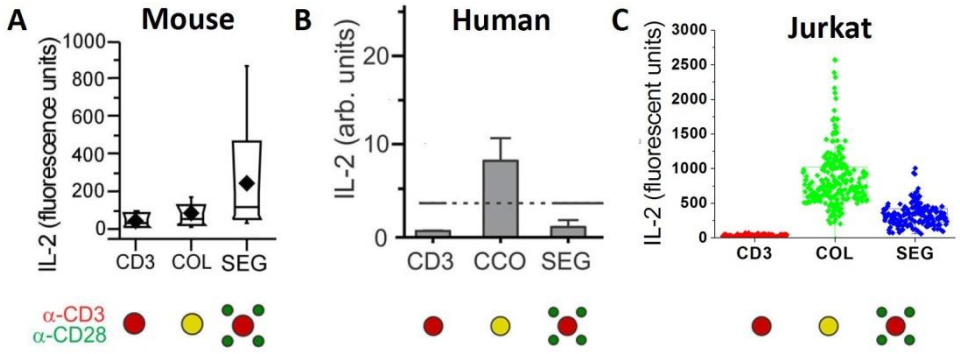

Figure 3.8: Cellular response to micropatterned surface. A. mouse splenocytes favored peripheral presentation of CD28. From (Shen, Thomas et al. 2008). B. Human peripheral blood lymphocytes favored co-presentation of CD3 and CD28. From (Bashour, Tsai et al. 2014). C. Jurkat cells, while like human primary cells responded most strongly to COL surfaces, had significant IL-2 secretion on SEG patterns.

Previous work in our lab partially attributed the observed differences between human and mouse T-cells on differential Lck diffusion between the species. In mouse T-cells, rapid diffusion ($0.37\mu m^2/s$) of pLck was able to overcome the basal phosphatase activities, resulting in scattered distribution of pLck (Fig. 3.8) and stronger IL-2 secretion on SEG patterns. However in human T-cells, Lck diffused much slower ($0.04\ \mu m^2/s$). The pLck distribution favored CD3, and any significant IL-2 secretion required CD3/CD28 co-engagement. For Jurkat cells, Lck diffusion was measured to be $0.26\ \mu m^2/s$ (Zimmermann, Paster et al. 2010); the rate was closer to that of mouse T-cells. This could explain the significant secretion of IL-2 on SEG micropatterns. The

rapid diffusion of Lck permitted responsiveness to the SEG surface. However, the phosphatase activities could ultimately limit the overall pLck kinase activity. Thus immunostaining of Jurkats on different micropatterned surfaces more closely resemble that of human primary T-cells (Fig. 3.9). In Jurkats, pLck preferentially localizes to CD3. However, a low concentration of pLck could be found throughout the interface. On COL pattern, Jurkat cells center on CD3-CD28 dots. However, on SEG patterns, a small population of cells does not center on CD3 dots. And neither does the pLck staining, instead, the concentrated cluster of pLck protein is found off the α-CD3 surface at the center of the cell (Fig. 3.9), a phenomenon which will be discuss in detail later.

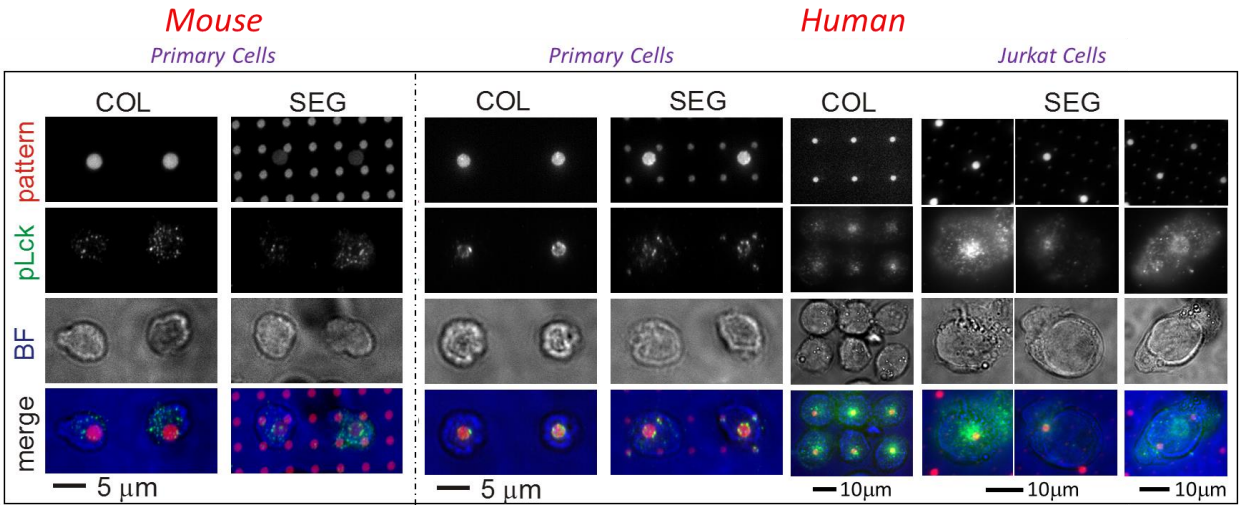

Figure 3.9: PLck staining of mouse naïve T-cells, human primary T-cells and Jurkat cells. While pLck was found throughout the mouse T-cell –glass interface, pLck preferentially co-localize with CD3 in human primary cells. From (Bashour, Tsai et al. 2014). In human lymphoblastic cell line, Jurkat E6.1, pLck also favored CD3. However, there existed a low concentration of pLck throughout the cell-glass interface.

3.3.4 LckR_FRET reporter in Jurkat cells

Jurkat cells were transfected with LckR_FRET mRNA. A few parameters were optimized for biologically relevant data acquisitions. Without a beam splitter, donor and acceptor spectra

emissions were measured sequentially. Given the diffusion rate of pLck (0.26 $\mu m^2/s$), acquisition was completed under 1s total, equivalent of about 13 pixel shift.

Next, during timelapse imaging, interval of acquisitions must balance the photobleaching of the fluorescent proteins against the diffusion of the Lck proteins. Given the diffusion rate of Lck in Jurkats, a time interval of 30s was selected. In 30s, Lck would have traveled roughly 5.5μm. With a 2μm α-CD3 dot at the center of an array of 2μm α-CD28 dots with a 10μm pitch, the distance between α-CD3 and α-CD28 is roughly be 7.1μm.

The acquisition technique over-bleaches the donor. For a given time point, YPET is exposed twice to a 450nm excitation laser, in order to measure both YPET and mCherry emissions. Wang and colleagues were able to correct for the photobleaching. For the Src FRET reporter, because no Src proteins were expressed in the nucleus, the averaged intensity of the region was used to normalize the subsequent time points. Unfortunately, Lck is found throughout the cell-glass interface. To limit the effect of photobleaching, the duration of timelapse imaging was limited to roughly 15-25 minutes. Also immunostainings revealed that pLck signaling already started to disappear 15 minutes after activation (Fig. 3.7).

Beyond a corrupt CD28 signaling pathway (Ueda, Levine et al. 1995), Jurkats behave very differently from primary human T-cells. Primary T-cells are cultured in suspension. TCR/α-CD3 engagement acts as a stop signal to leave the suspension and adhere onto surfaces. Without CD28 co-stimulation, the primary T-cells rapid disengage. Even with CD28 co-stimulation, but without ICAM-1 engagement, the T-cells form poor contact and fail to spread. And either CD28

or ICAM-1 can induce T-cell activation and subsequent adhesion, independent of CD3 priming. In contrast, unstimulated Jurkat cells readily adhere to untreated glass surfaces. And cellular adhesion to glass surfaces also induces low level of Lck activation (as revealed by pLck immunostainings).

Because Jurkats readily adhere to glass surfaces, it was difficult to capture cells landing and responding to micropatterned protein dots, as the proteins occupy a small percent of the total surface area. Starvation regiments were performed to suppress the basal metabolic rate as suggested by literature, and in an effort to suppress non-specific adhesion-induced Lck activation. Shan and colleagues cultured Jurkat overnight in 2.5% FBS media (Shan, Czar et al. 2000). August and colleagues serum starved the cells in 0.5% FBS media for 4h (August and Dupont 1994). Chu and colleagues starved Jurkat cells for 2h in serum-free RPMI 1640 (Chu, Wu et al. 2004). Despite trying the different resting regiments, pLck immunostainings revealed robust activation of Lck, independent of CD3 or CD28 engagement.

Efforts were made to quantify pLck kinase activity in cells that landed between the micropatterened protein dots, also referred to as 'null' cells. Two populations of null cells were observed. Some null cells land and spread onto glass without ever coming into contract with micropatterned protein dots (Fig. 3.11A). Others land and repeatedly attach and detach, or bounce on the glass surfaces (Fig. 3.10). And FRET ratios were calculated on a pixel-to-pixel basis then averaged for a given ROI: either on an α-CD3 dot or at center of a cell.

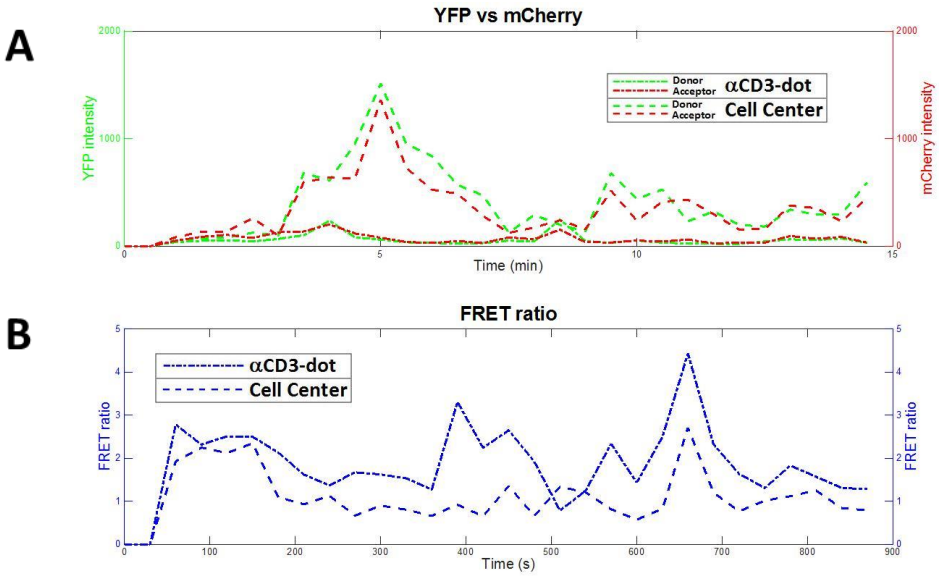

Figure 3.10: Plots of a representative null cell bouncing on the glass surface. The cell is not in contact with any micropatterned proteins (trace of the closest micropatterned dot). And the FRET ratio is sensitive to cells stepping on and off the glass surface.

Null cells that bounce on the glass surfaces help to illustrate that the FRET ratio is sensitive to cells stepping on and off a ROI. While the FRET ratio had a small dynamic range (Fig. 2.9), artificially high FRET ratios were produced from the highly ambulatory null cells (Fig. 3.10B). Thus the bouncing null cells were excluded from the analysis.

Another limitation elucidated by Fig. 3.10 is seen in traces for the ROI on the α-CD3 dot. While neither donor nor acceptor intensities were captured, as an artifact of the FRET analysis, high FRET ratio was generated by the background noises, as seen in the traces for $ROI_{\alpha\text{-}CD3}$. It can also be inferred that cells with low level of LckR_FRET expression will also produce artificially high FRET ratios. Thus these cells were also excluded from the analysis.

Null cells also simply land and spread (Fig. 3.11A). Unsurprisingly, the FRET ratio of the non-ambulatory null cells varies minimally. Then the FRET ratios were averaged from after the cells land (~1-3 minutes) and to before photobleaching (~15 minutes) generates artificial high ratios. The average FRET ratio for non-ambulatory null cells was 0.522 ± 0.177 (mean $\pm$ stdev).

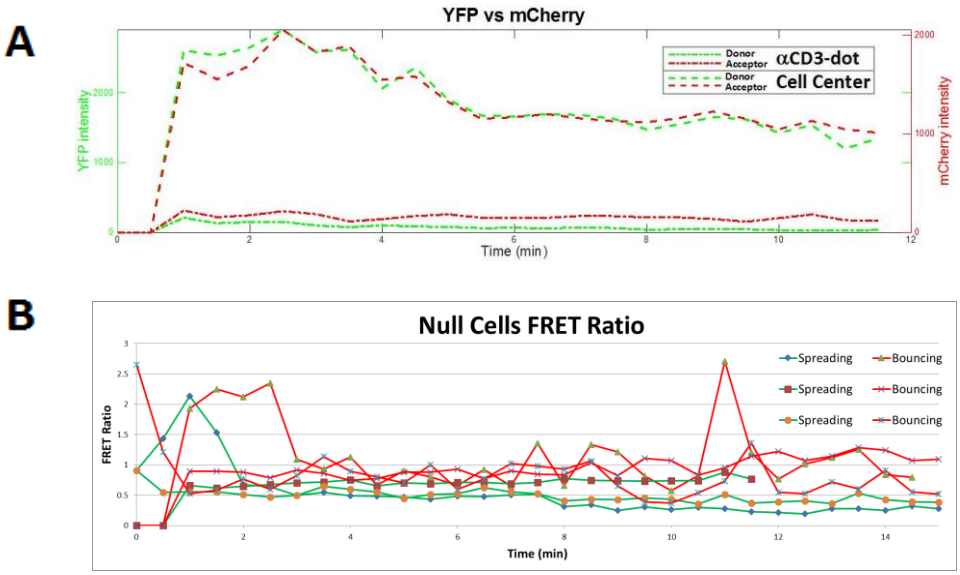

Figure 3.11: A. Plots of a representative null cell landing and spreading on the glass surface. Again the cell is not in contact with any micropatterned proteins (--- closest micropatterned surface). B. FRET ratio traces of null cells.

Another large population of seeded Jurkat cells, interact with micropatterned protein dots intermittently (Fig. 3.12). And like null cells bouncing on the glass surface, artificial high ratios were generated. Thus these cells were also excluded from the analysis.

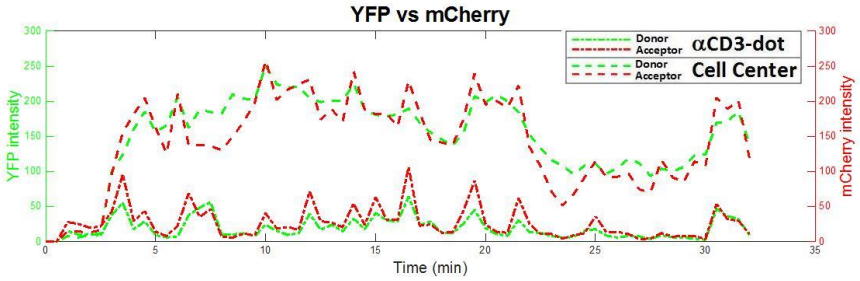

Figure 3.12: A cell interacting intermittently with the micropatterned proteins (--- αCD3-dot).

For cells that consistently interact with the micropatterned dots, three types of surfaces were studies: α-CD3 only surfaces, COL surfaces, SEG surfaces. Again, only few cells were captured on these three surfaces, once the nulls and the partially interactive cells were eliminated. For Jurkats seeded on CD3 micropatterned surfaces, the average FRET ratio was 0.576 ± 0.251 (mean $\pm$ stdev).

On COL surfaces, if cells land and find the micropatterned proteins, they tended to spread around the protein dots for sustained contact with the surface (Fig. 3.13A). While CD3-CD28 co-engagements are not necessary for surface adhesion, upon contact with the protein dots, the region becomes a site for sustained high pLck kinase activity. Fig. 3.13A shows a typical Jurkat cell landing on COL surfaces. Upon being in contact with the α-CD3/α-CD28 dot (T = ~1 min), the cell spread onto the dot. FRET ratio heat map revealed that the pLck kinase activity was very strong throughout the cell upon initial landing and spreading. Then after about 7 minutes, pLck activity dropped off across the interface, except on top of the α-CD3 protein dot (Fig. 3.13B). And the prolonged contact with the protein dots resulted in average FRET ratios with a small variance: 0.525 ± 0.069 (mean $\pm$ stdev).

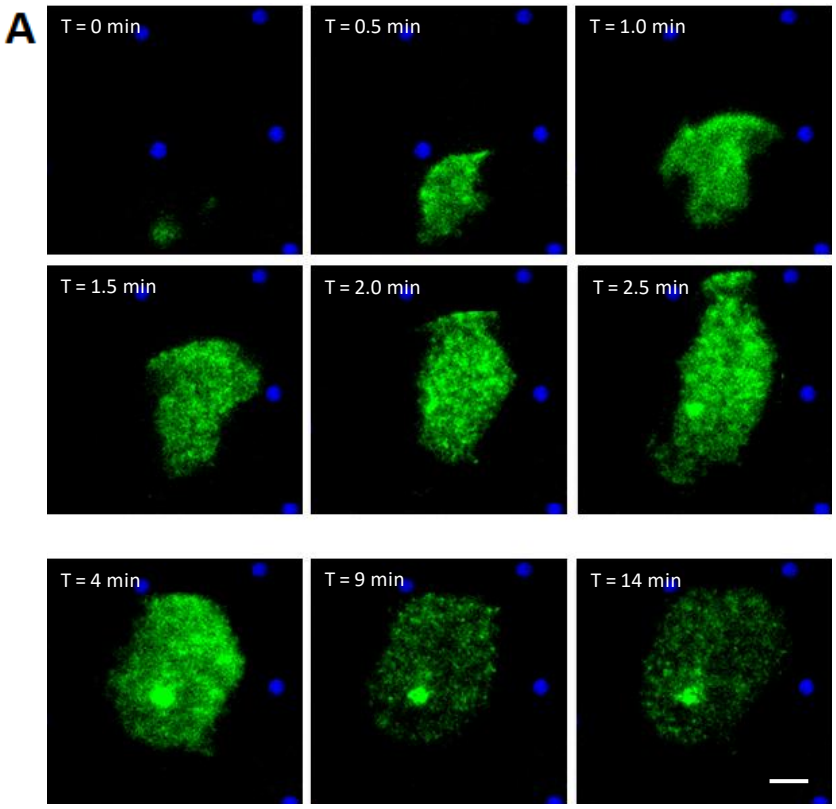
A
T = 0 min
T = 0.5 min
T = 1.0 min
T = 1.5 min
T = 2.0 min
T = 2.5 min
T = 4 min
T = 9 min
T = 14 min

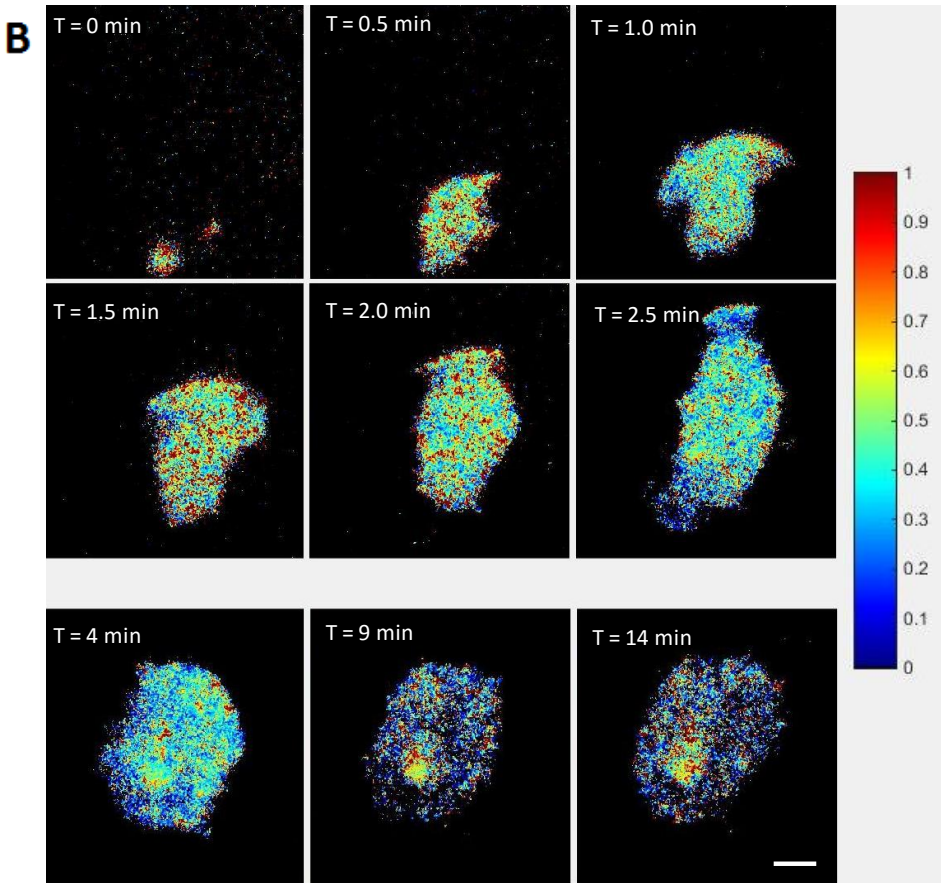
B
T = 0 min
T = 0.5 min
T = 1.0 min
T = 1.5 min
T = 2.0 min
T = 2.5 min
T = 4 min
T = 9 min
T = 14 min
1
0.9
0.8
0.7
0.6
0.5
0.4
0.3
0.2
0.1
0

Figure 3.13: Montage of a Jurkat cell interacting with a COL micropatterned glass coverslide. A. Only the donor (YPET) intensity was shown. B. Heat map of FRET ratios. Scale bar = 5µm.

However, Jurkat cells behave very differently on SEG surfaces. The cells were more migratory. And sometimes, Jurkat cells simply spread out away from the α-CD3 dots and interact with the proteins with its lamellipodia (Fig. 3.14).

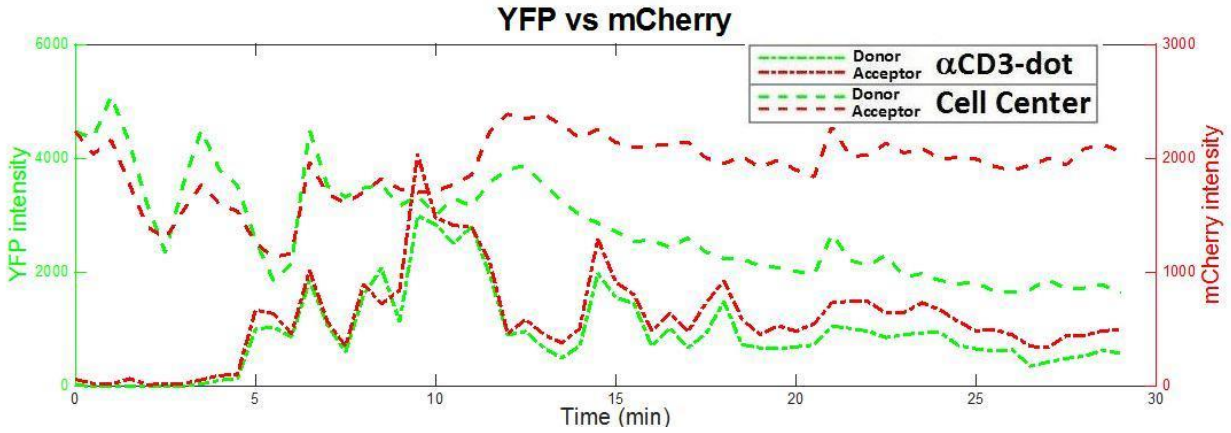

Figure 3.14: Plots of a representative cell on a SEG surface. The cell landed onto the surface. At around T = 5 min, it came into contact with the α-CD3 dot (--------). Then the cell sustained the contact with a varying degree of intensities, depending on the size of the lamellipodia.

Again, Jurkats readily land and spread without CD3 engagement, which induce an increase in FRET ratio across the cell. However, the heightened pLck activity quickly disappears after about 4 minutes. Around T = 5 min, the cell comes into contract with the α-CD3 proteins. The CD3 engagement, induces the classic centripetal retrograde flow, associated with immunological synapse formation (Fig. 3.15A T = 10-25 min). Correspondingly, an increase in FRET ratio is observed at the center of the cell (Fig. 3.15B T=10-25 min). And this could explain the cells observed in fixed pLck immunostainings where the concentrated dot of pLck proteins was found off the α-CD3 at the center of the cell (Fig. 3.9).

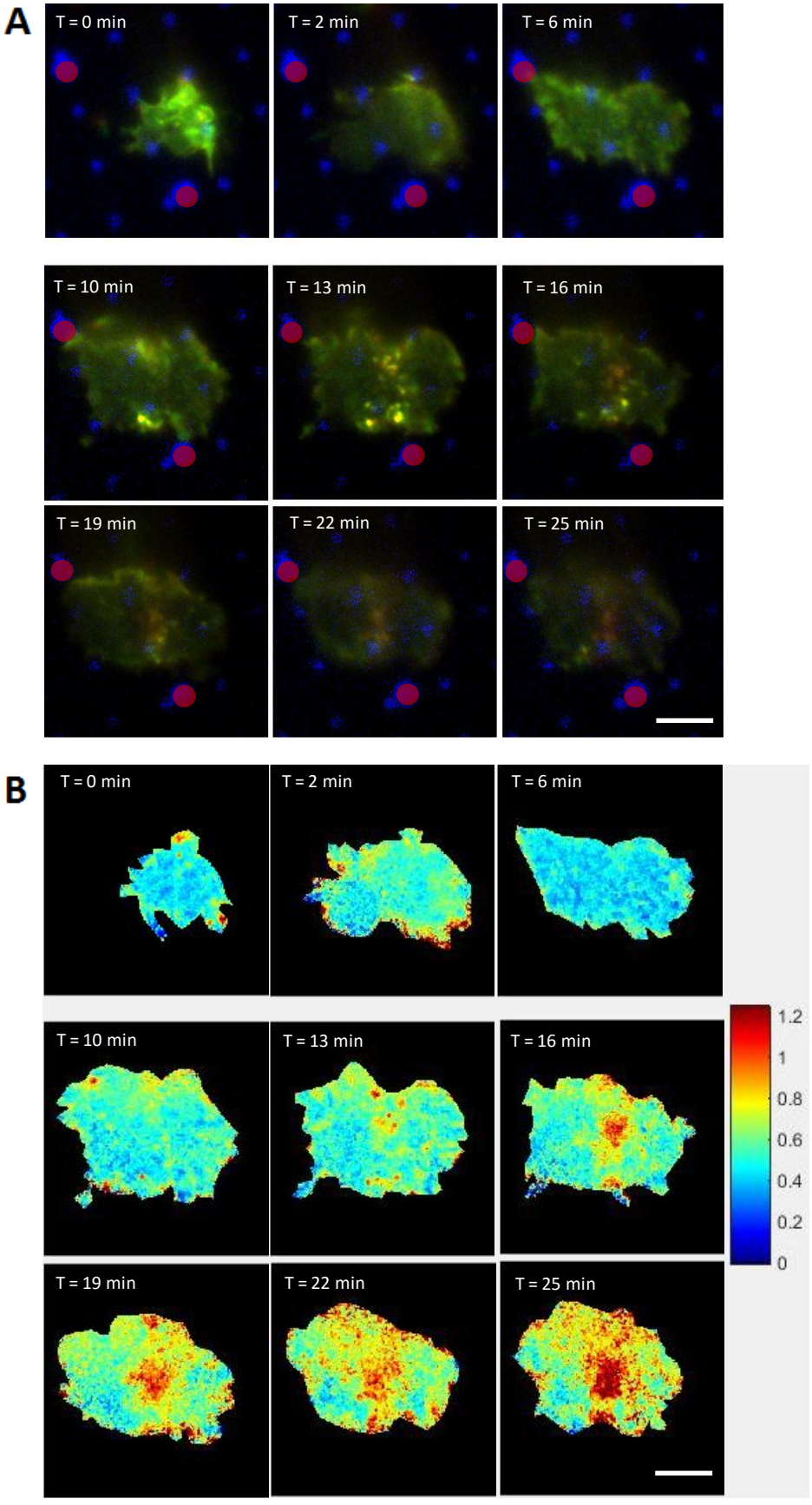
A
T = 0 min
T = 2 min
T = 6 min
T = 10 min
T = 13 min
T = 16 min
T = 19 min
T = 22 min
T = 25 min
B
T = 0 min
T = 2 min
T = 6 min
T = 10 min
T = 13 min
T = 16 min
T = 19 min
T = 22 min
T = 25 min
1.2
1
0.8
0.6
0.4
0.2
0

Figure 3.15: The same representative cell from Fig. 3.14 on a SEG surface. The cell landed and began to spread. At around 10min, contact with α-CD3 dot initiated centripetal retrograde flow. A. Montage of a Jurkat cell on SEG patterns, with green for YPET intensity and red for mCherry intensity. B. Heat map of FRET ratio. Scale bar = 5µm.

The FRET ratios were averaged from after the cells land contracted both CD3 and CD28 dots, and for 10 minutes afterward. However, because of photobleaching from longer timelapse imagings (takes longer to land, then locate both CD28 and CD3 proteins), the FRET ratios steadily rose. And the average FRET ratios reflected the effect: 0.662 ± 0.095(mean $\pm$ stdev).

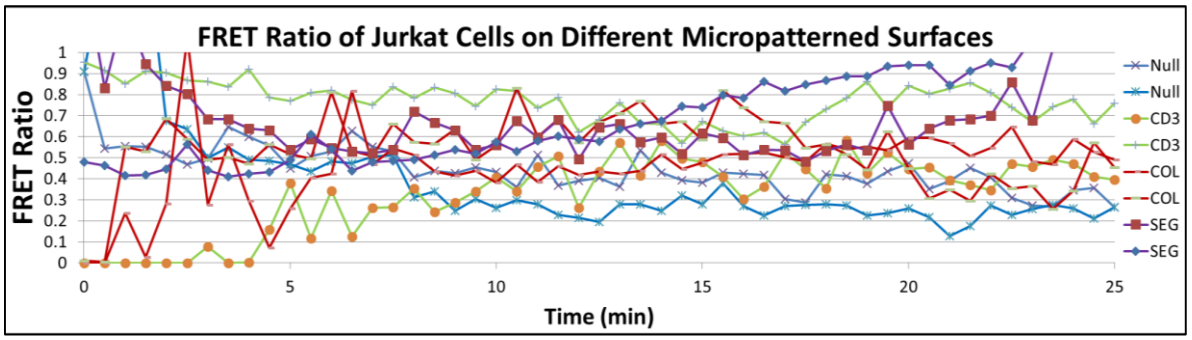

Figure 3.16: FRET ratios of Jurkat cells on micropatterned surfaces: null, CD3, COL, and SEG. The differences were statistically insignificant.

Comparing the average FRET ratios across the different micropatterned surfaces, they were not statistically significant (Fig. 3.16). However, downstream assays measuring IL-2 secretions revealed differences in cellular activation on the three surfaces (Fig. 3.8). Two probable explanations emerged. One, the dynamic range for the LckR_FRET reporter was insufficient in teasing out the differences. The problem was further aggravated by variations in LckR_FRET expression levels and cellular movement. Two, while the magnitude of the pLck kinase activity was the same among the surfaces, the duration could be different. Unfortunately, in an effort

to minimize photobleaching, longer duration of image acquisition was not considered. Another construct was designed to capture the duration of the pLck kinase activity. Its design and synthesize are detailed in the next chapter.

3.4 Discussion

Activation and expansion of primary T-cells for adoptive immunotherapy have always motivated the research from our laboratory. Beyond using chemical and biological cocktails to induce the desired cellular responses, this thesis aims to understand how spatial cues can modulate T-cell activation. To be clinically relevant, attempts were made to transfect LckR_FRET into primary T-cells. However, the endeavor was stymied by technical challenges. T-cell, as a master regulator of immune responses against foreign pathogen, was extremely resistant to gene transfers. Gene uptake mimics a viral infection, thus most methods induced tremendously level of T-cell death. And despite performing multiple rounds of optimization protocols in the Neon Transfection System and exploring alternative programs in the Amaxa system, the efforts ultimately failed.

LckR_FRET was ultimately transfected into Jurkat cells. The T-cell lines does have a compromised signaling network, as demonstrated by the Wortmannin study. However, the LckR_FRET reporter focus on Lck kinase activity, which occurs very early in the signaling cascade. And Wortmannin study seems to suggest that early enzymatic activities were less compromised (i.e., PI3K activity). Unfortunately, Jurkat, a human lymphoblastic cancerous T-cell line, behaves very differently from primary T-cells. Human T-cells remain in suspension, until

CD3 engagement, which acts as a stop signal. And the cell lands and adhere to the surface. Without CD28 costimulation, the cell would rapidly disengage. And even with both signals, ICAM-1 binding with LFA-1 is crucial for a stable interaction, aiding the cell in forming a tight seal around the IS and spread out across the interface. In contrast, Jurkat cells readily adhere without CD3-induced activation. Still IL-2 secretion assays revealed that Jurkat cells require CD28 engagement for a robust activation. Because Jurkats readily adhere to glass surfaces, it was a challenge to capture cells landing and responding to micropatterned protein dots, as the proteins occupy a small percent of the total surface area.

Nonetheless, few interesting observations were made. Upon Jurkat cell spreading, Lck was activated throughout the interface. On COL surfaces, most of the pLck kinase activity dropped off after roughly 7 minutes. Heightened activity remained on top of the α-CD3/α-CD28 dots. On SEG surfaces, again, pLck activity increased upon spreading, within minutes, the activity all but dropped off. Upon contact with α-CD3 dots, FRET ratio again increased, and the classic centripetal retrograde flow was observed, with heightened pLck activity concentrated at the center of the cell.

However, analysis of average FRET ratios revealed no differences among the various surface conditions. Immediately, limitations of the FRET reporter and the analysis were examined. It's possible that the LckR_FRET reporter lacks the sensitivity to differentiate the FRET responses. This is further complicated by the susceptibility of the FRET ratios to variation in LckR_FRET expression levels and cellular movement. Another possibility is that pLck activity is similar during the interval, but changes afterward. FRET ratios were averaged for the first 15 minutes,

to compensate for the inability to correct for photobleaching. Thus, not just the magnitude, but also the duration of pLck activity should be examined. In an effort to address some of these questions, anther construct was designed. Instead of a FRET reporter, a recruitment reporter was synthesized.

Chapter 4

4. The Tandem SH2-Domain Recruitment Reporter

4.1 Introduction

With the Lck membrane targeting peptides at the N-terminus, the LckR_FRET reporter moves with the protein to report on total Lck distribution throughout the surface. And the FRET responses help to isolate spatial regions of high pLck kinase activity. For Jurkat cells, high pLck kinase activity is localized to the center of the cells, and for COL surfaces on top of the α-CD3/α-CD28 dots. However, there are limitations to the LckR_FRET reporter. For one, the dynamic range of the probe is quite small. For some cells, no regions of high pLck kinase activity was observed when examining the FRET ratio color maps. Also, unable to correct for photobleaching, FRET ratios started to artificially creep up, about 20 minutes after cellular

activation. Another construct was designed to probe pLck kinase activity. The new probe exploits the dynamic interactions induced by Lck activation. CD3, a receptor ubiquitously expressed on surface of Jurkats. Upon Lck activation, its ITAMs are phosphorylated, inducing the recruitment of ZAP70, through its tandem SH2-domain. (Fig. 4.1A).

Zap70 is a Syk-family protein tyrosine kinase (PTK). Its expression is predominately limited to thymocytes and peripheral T-cells (Au-Yeung, Deindl et al. 2009); in contrast, other PTKs involved in T-cell signaling are more ubiquitously expressed in various types of immune cells. Upon phosphorylation of the crucial tyrosines, Zap70 is recruited by the doubly phosphorylated ITAMs. The recruitment not only localizes Zap70 to CD3 for pLck to activate the protein, but also relieves the autoinhibited conformation of Zap70. Two critical downstream adaptor proteins are then phosphorylated: linker for activation of T-cells (LAT) and SH2-domain containing leukocyte phosphoprotein of 76kDa (SLP-76). The downstream signaling cascade results in cytokine production, T-cell differentiation and differentiation. Clinically Zap70-deficient patients suffer from severe combined immunodeficiency (SCID), while Zap70 hypermutation has been associated with poor prognosis in leukemia. Also because Zap70 has limited cell type expressions, the protein is an attractive drug target.

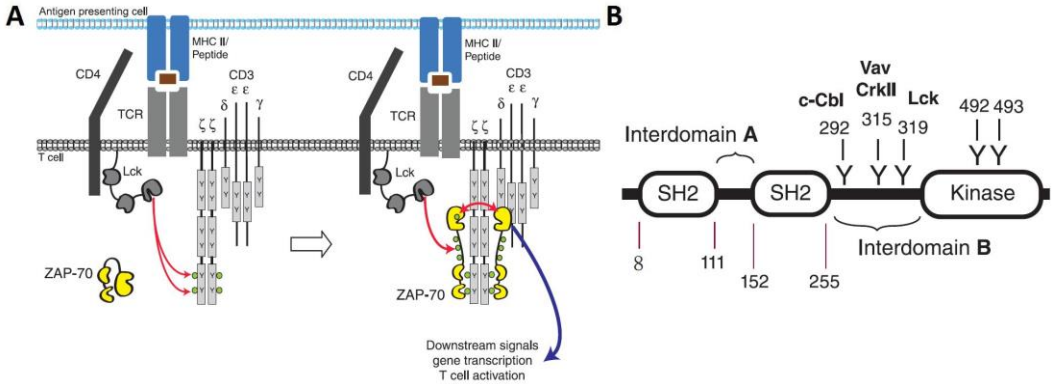

Figure 4.1: A. Zap70 recruitment upon Lck activation. The tandem SH2 domains are recruited to the pITAM. B. Schematic of Zap70 protein: tandem SH2-domain, interdomain B with crucial regulatory tyrosines, and kinase domains. From (Au-Yeung, Deindl et al. 2009).

Structurally, Zap70 has two SH2-domains (linked by interdomain A) and a C-terminal kinase domain. Between which is interdomain B containing 3 critical regulatory tyrosines (Fig. 4.1B). Y292 is associated with autoinhibition, while Y315 and Y319 are showed as positive regulators in mutational analysis. Without a membrane-targeting domain, the tandem SH2-domains are responsible for Zap70 recruitment. And both domains are necessary for high avidity binding; it insures preferential accumulation at the pITAMs, instead of other singly phosphorylated sites.

Bunnell and colleagues studied T-cell activation with eGFP tagged proteins (Bunnell, Hong et al. 2002). At one point during the study, they examined full-length Zap70_eGFP in Jurkat cells on glass coverslides coated with α-CD3 antibodies. Zap70 was initially recruited to the surface in TCR-rich clusters within 15s of initial formation of contact (Figure 4.2A).

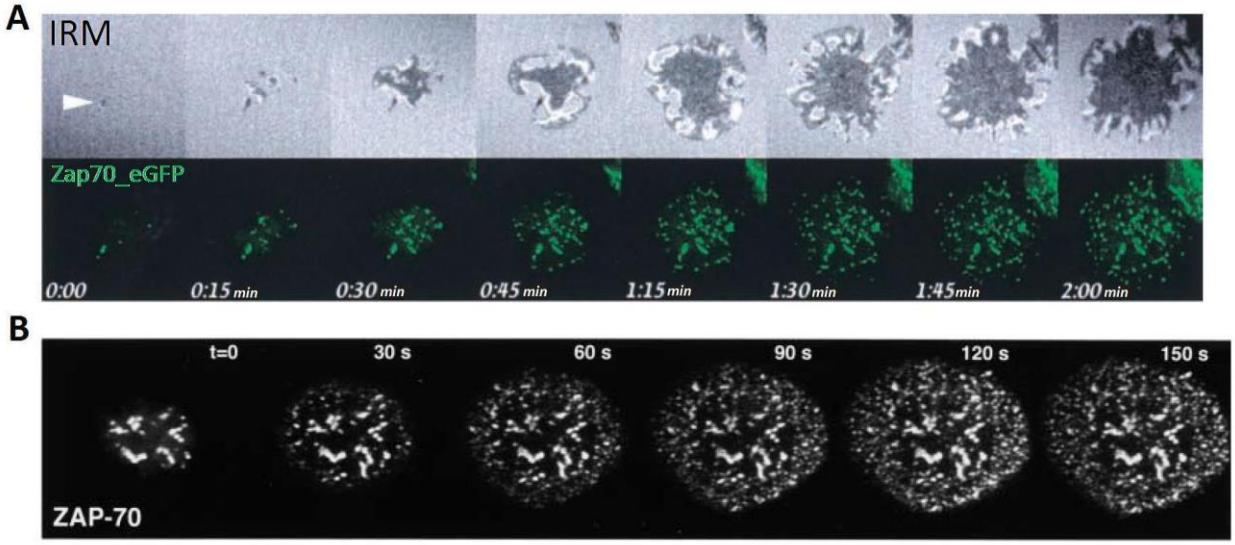

Figure 4.2: A. Zap70 recruited to TCR in tight contact with the surface, as seen in IRM imaging. And the recruitment occurred within 15s. B. The signal persists without moving laterally. From (Bunnell, Hong et al. 2002).

Zap70 signal persisted for at least 20min without moving laterally, uncoupling from the TCR, which has migrated to the cSMAC (Fig. 4.2B). FRAP studies of Zap70_eGFP revealed that the bleached region recovered rapidly, indicating a rapid equilibration between bleached and unbleached pools of Zap70. Full-length Zap70 would not be a good alternative reporter of pLck activity as Zap70 diffuses evenly throughout the interface for subsequent signal propagations. However, the tandem SH2-domain remains a strong candidate to monitor pITAM state, an indirect indicator of pLck kinase activity.

4.2 Materials and Method

4.2.1 SH2-ZAP-YPET Plasmid Preparation.

A custom plasmid was synthesized by Invitrogen via GeneArt. In a pMK-T backbone with Kanamycin resistance, AscI and Sfgl flanked 784bp of interest. Both the LckR_FRET reporter and the custom plasmid were digested with AscI and SgfI/AsisI (New England Biolab, R0534 and R0630). Ligation of the two fragments was performed as previously described.

The DNA sequence was validated using 5 primers: CTGCTTCTCGCTTCTGTTC, CGTCCTTGAAGAAGATGGTC, CATCAAGGCCAACTTCAAGA, CGAGTAGAACTCGCAGAGC, and GGTGGAGAAGCTCATTGCTA.

4.2.2 Immunostaining

Immunostaining were performed in Jurkat cells to study SH2_YPET colocalization. The fixing and the immunostainings were performed as previously described. Additional immunostainings were done for pZAP20 using antibodies against Zap70 Y319/Syk Y352 (Cell Signaling, 27011).

4.2.3 Data Acquisition and Analysis for Zap70 Recruitment

Data acquisition was completed as previously described.

Before Lck activation, Zap70 is found throughout the cytosol. And upon activation, Zap70 through its tandem SH2-domain is recruited to the doubly phosphorylated ITAMs, located just below the plasma membrane. To image proteins recruited to the cellular membrane, total internal reflection florescence microscopy (TIRFM) is used. TIRFM is spatially restricted by its excitation or evanescent field. This is achieved when a laser beam is shined off-axis at an angle greater than the critical angle, which is a function of the differences in refractive indices between the sample and the cover slip (Snell's Law). At off-axis angle greater than the critical angle, the light beam undergoes total internal reflection, thus reflected back instead of through the sample. However, some of the incident energy penetrate to create an evanescent field where the intensity decays exponentially (Fig. 4.3B) (Mattheyses, Simon et al. 2010):

$$I_z = I_0^{-z/d}, \text{ and } d = (\lambda_0/4\pi) * \left(n_2^2 \sin^2\theta - n_1^2\right)^{-1/2}$$

Where n_1 and n_2 is the refractive indices of the sample and the coverslide, respectively. And λ_0 is the wavelength of the excitation light in a vacuum.

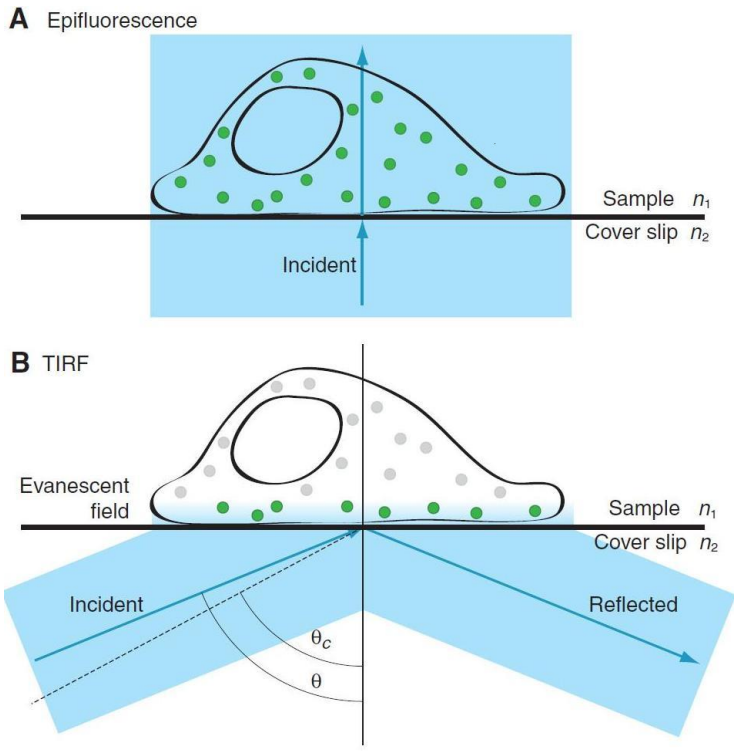

Figure 4.3: A. In epifluorescence, the light source penetrates the cover slip to illuminate a field of view without spatial constraint. B. TIRF imaging, the beam undergoes total internal reflection. Some of the incident energy generate an evanescent field. Its depth is a function of the differences in refractive induces of the interface, and its intensity decays exponentially. From (Mattheyses, Simon et al. 2010).

For a standard setup, TIRF penetrates a depth of approximately 100nm. TIRF is able to spatially visualize proteins proximal to the plasma membrane; however, with plasma membrane to be only about 10nm thick, the technique also captures proteins in the cytosol. To extract proteins being actively recruited to the membrane versus ones in the cytosol, epifluorescence is used. Epifluorescence illustrates through the glass cover slip and is not spatially restricted, in the z-axis (Fig. 4.3A). Thus recruitment is revealed by changes in the ratio of TIRF to epifluorescence (Merrifield, Feldman et al. 2002).

To map SH2_YPET recruitment as an indicator of pLck kinase activity, background was subtracted via MetaMorph. Then TIRF/Epifluorescence (TIRF/EF) ratio was calculated on a pixel-to-pixel basis.

4.3 Results

4.3.1 Designing and Synthesizing the Zap70 Recruitment (SH2_YPET) Reporter

The LckR_FRET reporter already contain the tandem SH2-domain from Zap70. Thus it was modified to remove both the Lck targeting domain and the ITAM3. To quantify SH2 (Zap70) recruitment, the fluorescent tag must be TIRF compatible (excitable by a 450nm laser), thus YPET was selected. Also the fluorescent protein has better quantum yield and extinction coefficient than either mCherry or eGFP (Fig. 4.3) (Table 4.1).

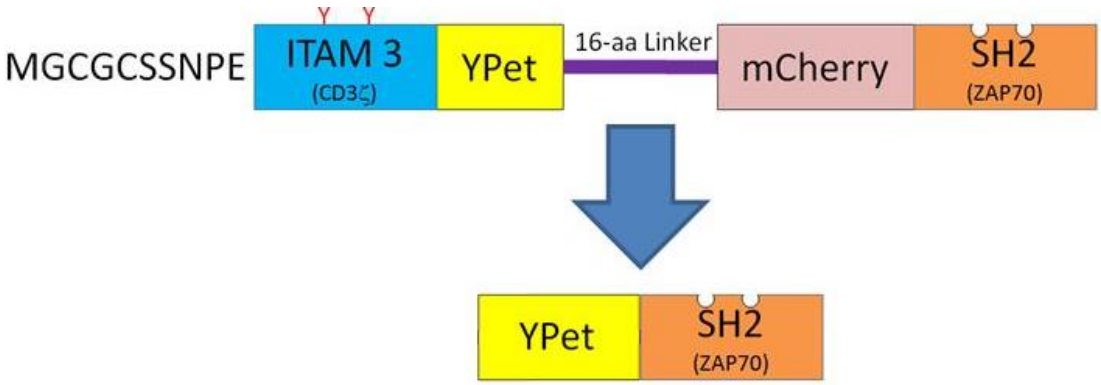

Figure 4.4: Schematic of reporter redesign from a pLck FRET reporter to a Zap70 recruitment biosensor.

Table 4.1: Sequence for YPET_ SH2 recruitment reporter.

```
-61     GGCGCGC Cagtcctccg acaaTAATAC GACTCACTAT AGGGagacaa gcttcgaatt
  1  ATGgtgagca aaggcgaaga gctgttcacc ggcgtggtgc ccatcctggt ggagctggac
 61  ggcgacgtga acggccacaa gttcagcgtg agcggcgagg gcgagggcga cgccacctac
121  ggcaagctga ccctgaagct gctgtgcacc accggcaagc tgcccgtgcc ctggcccacc
181  ctggtgacca ccctgggcta cggcgtgcag tgcttcgccc ggtaccccga ccacatgaag
241  cagcacgact tcttcaagag cgccatgccc gagggctacg tgcaggagcg gaccatcttc
301  ttcaaggacg acggcaacta caagacccgg gccgaggtga agttcgaggg cgacaccctg
361  gtgaaccgga tcgagctgaa gggcatcgac ttcaaggagg acggcaacat cctgggccac
421  aagctggagt acaactacaa cagccacaac gtgtacatca ccgccgacaa gcagaagaac
481  ggcatcaagg ccaacttcaa gatccggcac aacatcgagg acggcggcgt gCAGCTGgcc
541  gaccactacc agcagaacac ccccatcggc gacggccccg tgctgctgcc cgacaaccac
601  tacctgagct accagagcgc cctgttcaag gaccccaacg agaagcggga ccacatggtg
661  ctgctggagt tcctgaccgc cgccggcatc accgagggca tgaacgagct ctataagaaG
721  CGATCGCacc ggtatacaag tttgtacaaa aaagcaggct ccgcggccgc ccccttcacc
781  atgccagacc ccgcggcgca cctgcccttc ttctacggca gcatctcgcg tgccgaggcc
847  gaggagcacc tgaagctggc gggcatggcg gacgggctct tcctgctgcg ccagtgcctg
901  cgctcgctgg gcggctatgt gctgtcgctc gtgcacgatg tgcgcttcca ccactttccc
961  atcgagcgcc agctcaacgg cacctacgcc attgccggcg gcaaagcgca ctgtggaccg
1021 gcagagctct gcgagttcta ctcgcgcgac cccgacgggc tgccctgcaa cctgcgcaag
1081 ccgtgcaacc ggccgtcggg cctcgagccg cagccggggg tcttcgactg cctgcgagac
1141 gccatggtgc gtgactacgt gcgccagacg tggaagctgg agggcgaggc cctggagcag
1201 gccatcatca gccaggcccc gcaggtggag aagctcattg ctacgacggc ccacgagcgg
1261 atgccctggt accacagcag cctgacgcgt gaggaggccg agcgcaaact ttactctggg
1321 gcgcagaccg acggcaagtt cctgctgagg ccgcggaagg agcagggcac atacgccctg
1381 tccctcatct atgggaagac ggtgtaccac tacctcatca gccaagacaa ggcgggcaag
1441 tactgcattc ccgagggcac caagtttgac acgctctggc agctggtgga gtatctgaag
1501 ctgaaggcgg acgggctcat ctactgcctg aaggaggcct gccccaacag cagtgcccca
1561 gggcaccatc atcatcatca tTAAgcggcc gcgacTCTAG AGTCGACctg caggcatgc
```

Theoretically, as the SH2_YPET biosensors cycle on and off the pITAMs, phosphatases are able to dephosphorylate/deactivate the ITAMs, pLck, and Zap70. Thus the ability of pITAM to continue to recruit SH2_YPET is being used as an alternative reporter of pLck kinase activity.

The probe reveals the duration of pLck kinase activity associated with CD3/ITAM. However, it does not take into consideration CD28-associated pLck kinase activity.

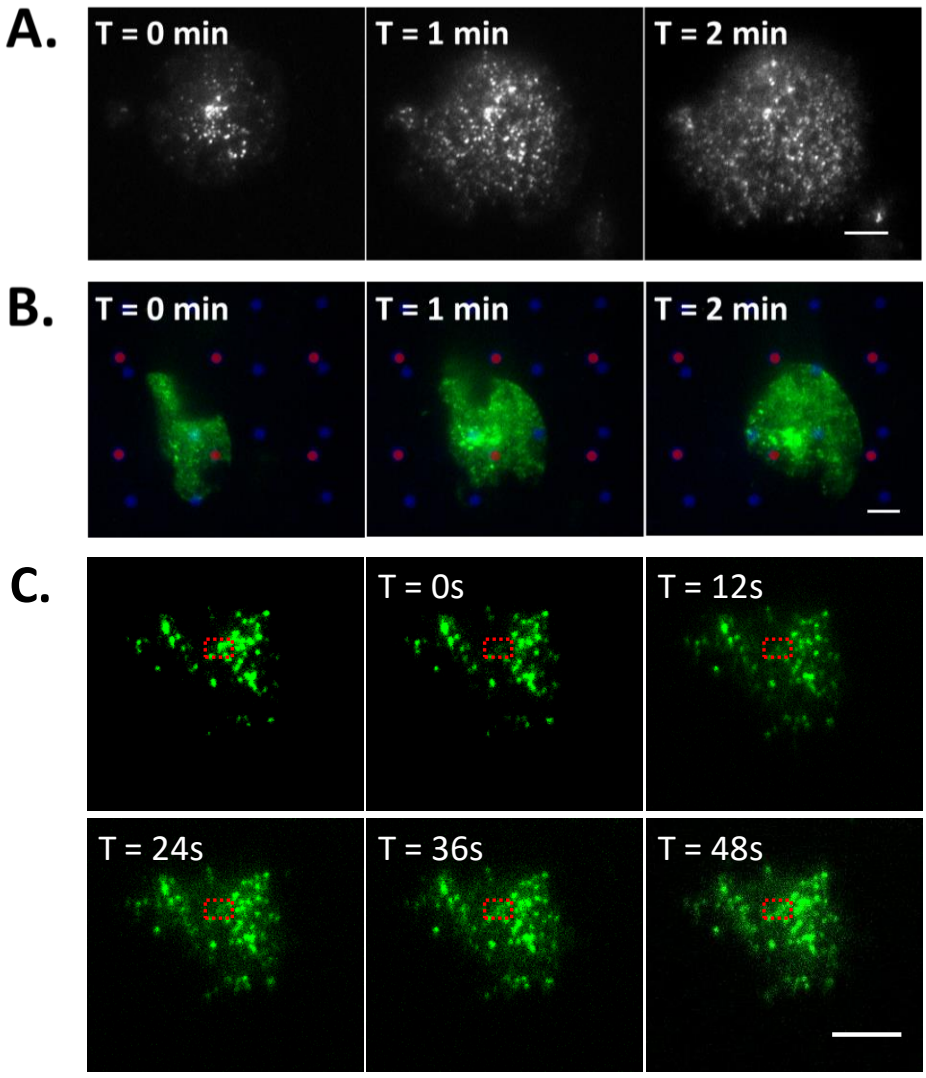

Figure 4.5: A. SH2_YPET transfected Jurkat cell on surface completely coated with activating antibodies. Clusters of ZH2_YPET were laterally static. B. In contrast, SH2_YPET was very fluid in Jurkat cell exposed to SEG micropatterns C. The fully coated surface was used to check whether SH2_YPET molecules were stably bound to pITAM. Its recovery in about 2 minutes suggested active exchange between bleached and unbleached pools of SH2_YPET. Scale bar = 5µm.

For SH2_YPET to be a dynamic and real-time reporter of pLck activity, it's important to test whether individual molecules are stably bound to pITAM. Jurkats transfected with SH2_YPET mRNA were placed on two different surfaces. While the SH2_YPET reporter was very dynamic on micropatterned surfaces, especially on SEG patterns (Fig. 4.5B), the reporter was more laterally static on fully coated surfaces (Fig. 4.5A). To check for SH2_YPET cycling, FRAP was performed to monitor fluorescent recovery. The recovery was nearly complete after 2 minutes (Fig. 4.5C). Thus the probes were being rapidly exchanged between bleached and unbleached pools of SH2_YPET, allowing for dynamic reporting of pLck kinase activity.

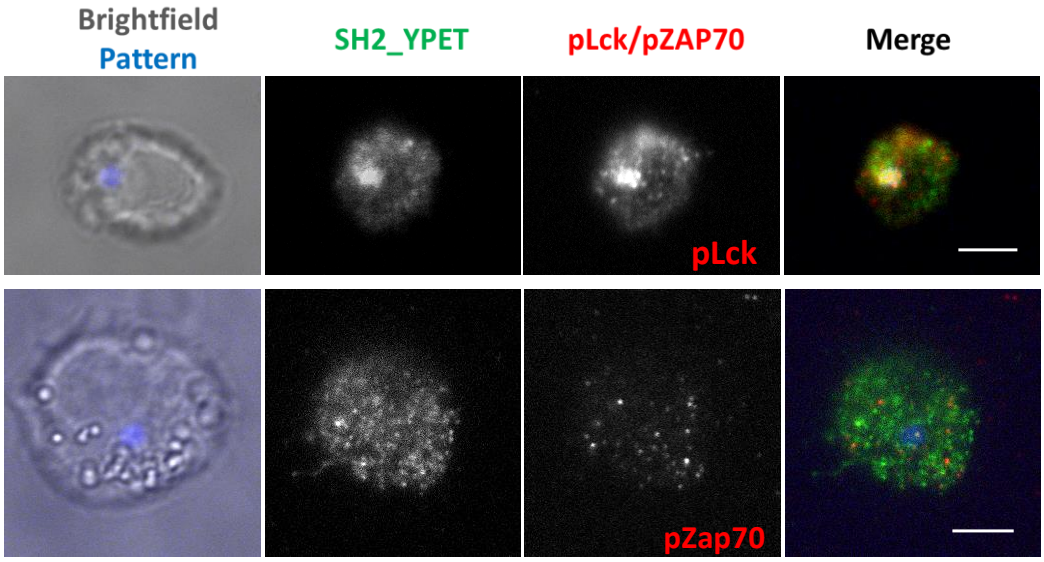

Figure 4.6: SH2_YPET distribution is unique from both pZap70 and pLck. Its distribution more closely resembles that of pLck than pZap70. While pZap70 has mostly disappeared 15 minutes after seeding, pLck concentrated on the micropatterned protein dots with some found throughout the cell. Scale bar = 5µm.

While the SH2_YPET reporter only contains the tandem SH2-domain from Zap70, studies were completed to ensure that it does not diffuse and behave like Zap70. According to Bunnell, Zap70 is initially recruited to the TCR, its distribution changed with time as the protein remain

laterally static. Immunostainings were performed 15 minutes after seeding to study the distribution of SH2_YPET versus pLck or pZAP70. The SH2_YPET reporters did not diffuse with full-length Zap70 proteins. After 15 minutes, pZAP70 had all but disappeared from the cell. Instead, the recruitment probe had a similar distribution as pLck, concentrated on the micropatterned protein dots with some proteins found throughout the cell.

The final plasmid for SH2_YPET was then sequenced.

```
  1 MVSKGEELFT GVVPILVELD GDVNGHKFSV SGEGEGDATY GKLTLKLLCT TGKLPVPWPT
 61 LVTTLGYGVQ CFARYPDHMK QHDFFKSAMP EGYVQERTIF FKDDGNYKTR AEVKFEGDTL
121 VNRIELKGID FKEDGNILGH KLEYNYNSHN VYITADKQKN GIKANFKIRH NIEDGGVQLA
181 DHYQQNTPIG DGPVLLPDNH YLSYQSALFK DPNEKRDHMV LLEFLTAAGI TEGMNELYKK
241 RSHRYTSLYK KAGSAAAPFT MPDPAAHLPF FYGSISRAEA EEHLKLAGMA DGLFLLRQCL
301 RSLGGYVLSL VHDVRFHHFP IERQLNGTYA IAGGKAHCGP AELCEFYSRD PDGLPCNLRK
361 PCNRPSGLEP QPGVFDCLRD AMVRDYVRQT WKLEGEALEQ AIISQAPQVE KLIATTAHER
421 MPWYHSSLTR EEAERKLYSG AQTDGKFLLR PRKEQGTYAL SLIYGKTVYH YLISQDKAGK
481 YCIPEGTKFD TLWQLVEYLK LKADGLIYCL KEACPNSSAP GHHHHHH
```

4.3.2 SH2_YPET Recruitment Reporter Analysis

Again a large population of cells landed between the micropatterned dots. Without stimulation, minimal changes were observed in epifluorescence intensity. And TIRF intensity increased upon landing then reminded largely unchanged after the cell fully spread out (~2 minutes) (Fig. 4.7).

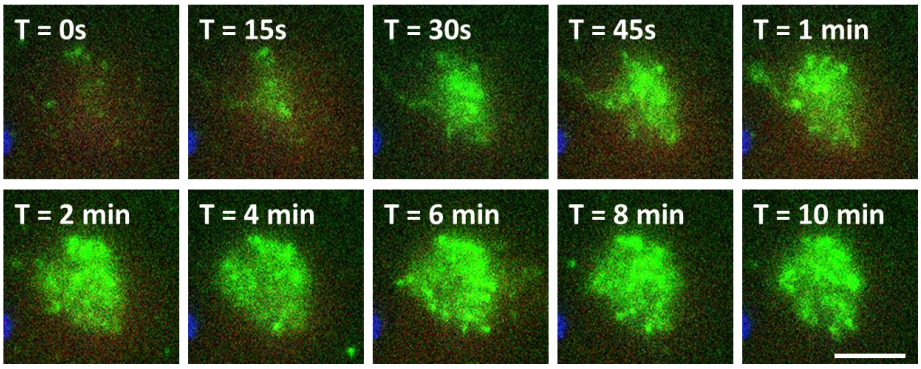

Figure 4.7: Null cells transfected with SH2_YPET mRNA were seeded on micropatterned surfaces. No intense increases in TIRF of SH2_YPET (in green) was observed beyond the initial cell landing and spreading. Epifluorescence of SH2_YPET (in red) remained largely unchanged. Scale bar = 5µm.

SH2_YPET appears to be a more sensitive reporter than LckR_FRET. This was illustrated by studies on CD3 only surfaces. Immunostainings revealed pLck colocalizing on α-CD3 micropatterned dots. However, because LckR_FRET has a narrow dynamic range, no heightened FRET response was observed in FRET ratio color maps (Fig. 4.8).

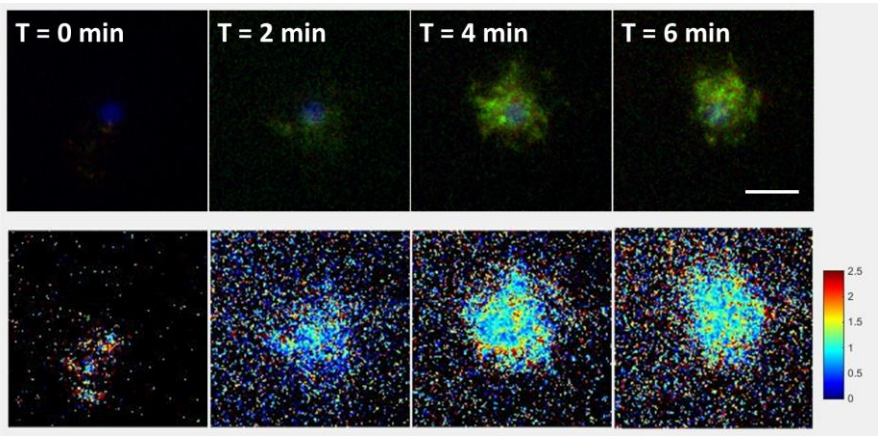

Figure 4.8: Jurkat cell transfected with LckR_FRET on α-CD3 (blue) only surface with YPET in green and mCherry in red. The FRET reporter was unable to detect a high concentration of kinase activity on the α-CD3 dot as seen in the color map. Scale bar = 5µm.

However, the SH2_YPET reporter was able to capture the increased pLck activity on the stamped α-CD3 dots (Fig. 4.9). Though, the method to quantify SH2_YPET recruitment does have its limitations. Specifically, the analysis is spatially sensitive. For example, as the cell lands on a stamped protein dot, the epifluorescence intensity starts to increase before the TIRF intensity, suggesting active recruitment to the surface. However, when cell continues to spread, but only interact with the protein dot at the cell edge, the epifluorescence intensity decreases significantly around the dot. This is due to the cell body shifting away from the stamp, possibly masking recruitment to the membrane and certainly distorting the recruitment ratio (Fig. 4.9).

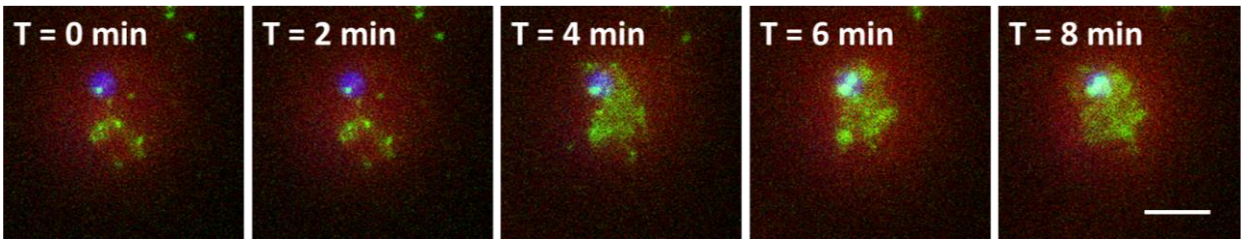

Figure 4.9: Jurkat cell transfected with SH2_YPET on α-CD3 (blue) only surface. When a cell only interacts with micropatterned surface at the lamellipodia, the recruitment ratio exhibits spatial distortion. Note the gradient in epifluorescence intensity (red) as a function of cell radius. Scale bar = 5μm.

As previously described, when seeded onto COL surfaces, Jurkat cells settle onto the stamped protein dots (Fig. 4.10). An increase in epifluorescence intensity precedes any TIRF intensity, as pLck kinase activity increased upon cell landing on the surface. As seen in FRET, pLck was found throughout the cell (see T = 2m), with concentrated activity at the stamped protein. While pLck activity slowly dropped off across the interface, the recruitment remained strong at the α-CD3/α-CD28 dot (Fig. 4.10).

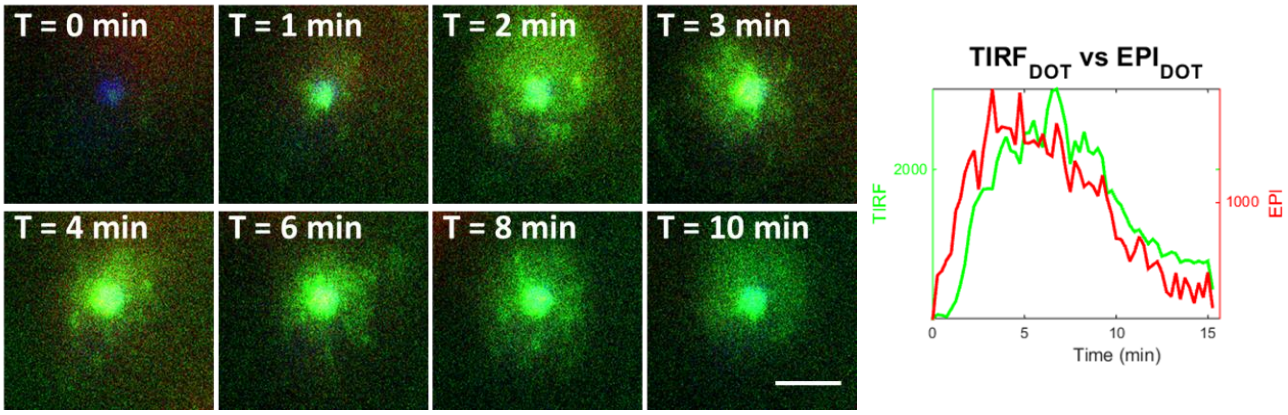

Figure 4.10: Jurkat cell transfected with SH2_YPET (TIRF intensity in green and epifluorescence intensity in red) on COL pattern (blue). The cell lands and spreads around the stamped protein. Initially, pLck was found throughout the interface, with heightened kinase activity on the α-CD3/α-CD28 dot. While pLck activity gradually dropped off across the interface, recruitment remained strong at the dot. A trace of averaged intensities on the dot was plotted. Scale bar = 5μm.

However, the ratio was still sensitive to SH2_YPET expression level, thus the recruitment ratio had to be normalized. When several traces of averaged intensity on α-CD3/α-CD28 dots were overlaid, a characteristic curve arose. Roughly 7.5 minutes after cell landing, the recruitment ratio reached its peak and started to slowly decay. The full width at half maximum was roughly 15 minutes.

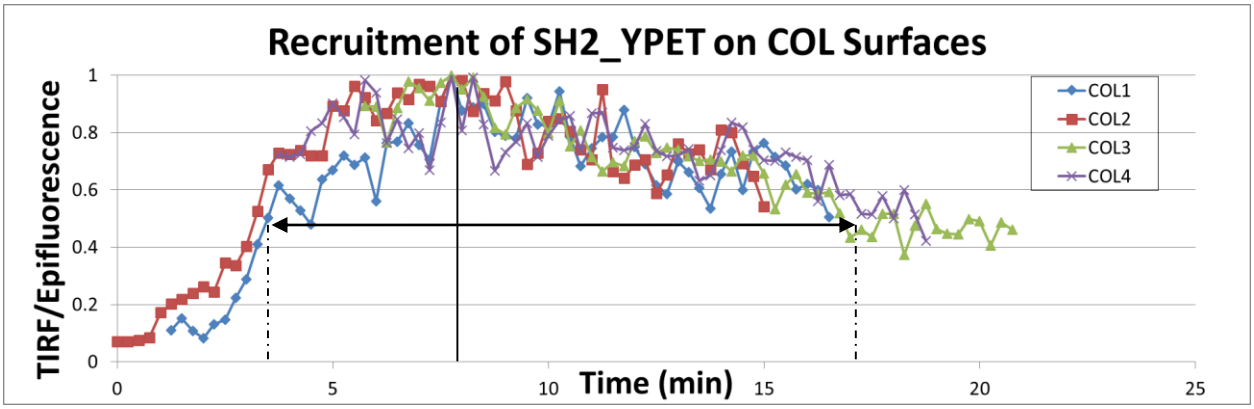

Figure 4.11: TIRF/Epifluorescence ratio of Jurkat cells on COL surfaces.

Also as previously described, Jurkat cells are very migratory on SEG patterns. Upon contact with α-CD3 (T = 0), an increase in pLck kinase activity resulted in a marked rise in SH2_YPET recruitment to the center of the cell as the cell continued to move (Fig. 4.12).

While concentrated region of SH2_YPET recruitment occurred near the center of the cell, the recruitment ratio was still spatially distorted. As the cell migrates, its cell body shifted resulting in rapid drops in SH2_YPET epifluorescence. Thus, the recruitment ratio lacked a characteristic shape.

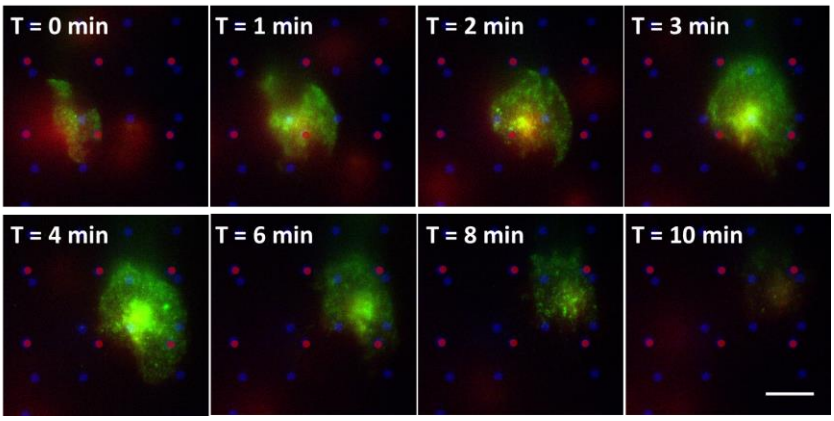

Figure 4.12: Jurkat cell on SEG pattern (blue for α-CD28 and pink for α-CD3). As previously discussed, the cell initiated contact with α-CD3 dot and increased recruitment of reporter was observed near the center of the cell. Scale bar = 10μm.

Unable to compare recruitment ratios between COL and SEG patterns, the decay of peak TIRF intensity examined. If a pattern induced a more sustained pLck kinase activity, the decay should be slowed by more SH2_YPET recruitment. Again normalization was performed to account for differences in SH2_YPET expression level. Below are traces of averaged intensity for regions of concentrated SH2_YPET recruitment. For COL patterns, this colocalized with both the printed α-

CD3/α-CD28 protein dot and the center of the cells. For SEG pattern, ROI was often the center of the cell. Looking at the signal decay on COL patterns (green curves), the traces were closely clustered together and dropped off more slowly. In contrast, SEG dropped off more rapidly (red curves). In conclusion pLck kinase activity was more sustained on COL patterns versus SEG patterns.

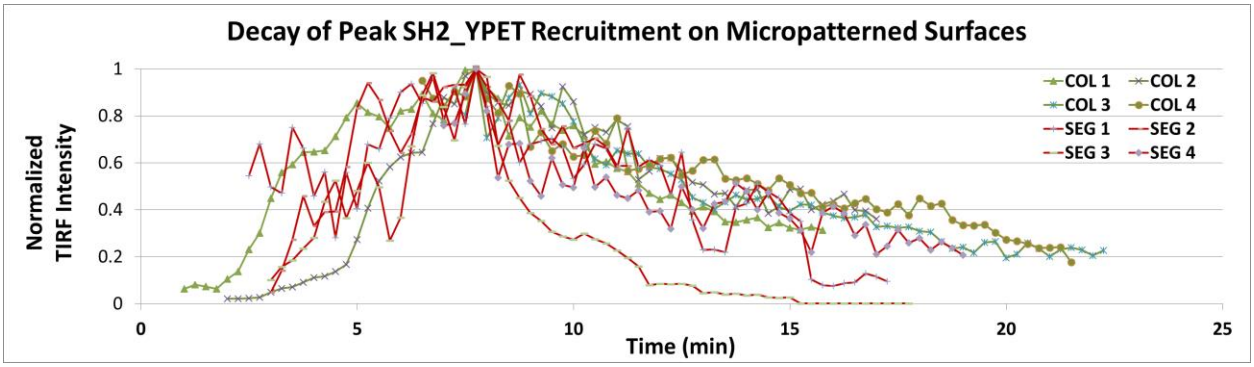

Figure 4.13: Normalized TIRF intensity of Jurkat cells on COL (in green) and SEG (in red) patterns. The decay in signal was slower on COL patterns versus SEG patterns.

4.4 Discussion

SH2_YPET recruitment reporter was constructed to answer some of questions that arose from the LckR_FRET reporter. The FRET plasmid was sufficient at demonstrating the importance of α-CD3 in inducing a spike in pLck activity. Jurkat cells naturally adhere on glass coverslides. And without stimulation, pLck kinase activity was observed in Jurkats upon landing and spreading on untreated glass surfaces. However, CD3 signal was required for a spike in pLck activity. This was demonstrated on SEG patterns, where Jurkat cells land and spread on α-CD28 surfaces, and only the contact with α-CD3 dots, 10 minutes after landing, induced a centripetal retrograde flow and a spike in pLck kinase activity. However no differences in FRET ratio were observed

between cells on COL and SEG surfaces. Alternatively, the lack of difference could be due to biosensor insensitivity; or for the duration in question, the FRET ratios were the same.

SH2_YPET reporter was designed to study the duration of pLck kinase activity. PLck phosphorylates pITAM, which recruits the tandem SH2-domain. As dynamic, real-time reporter of pLck kinase activity, SH2_YPET reporter must not be stably bound to the pITAMs. Instead it should be rapidly exchanged, allowing for phosphatase to deactivate/dephosphorylate on the pITAMs. Photobleaching studies were performed to assess fluorescent recovery. On fully coated glass cover slide, pITAM appeared to be laterally static, thus a good surface for the FRAP studies. Recovery was observed in about 2 minutes, implying a rapid exchange between bleached and unbleached pools of SH2_YPET proteins.

Close examination of Jurkat cells on various surfaces revealed limitations to the analysis. TIRF microscopy while spatially restricted still captured proteins in the cytosol, because despite a penetration depth of roughly 100nm, the average thickness of the plasma membrane is only 10nm. To visualize active SH2_YPET recruitment, epifluorescence intensity was acquired. And the recruitment ratio was calculated dividing the TIRF intensities by the epifluorescence intensities. An increase in ratio signified active recruitment, while decrease described particle endocytosis or internalization.

However, in cells that had spread but was still actively sampling the surrounding areas, the cell body/bulk would shift rapidly result in sharp changes in epifluorescence intensity, thus distorting the recruitment ratio. And data analysis necessitated comparison between largely

immobile and rapidly migrating cells, specifically those exposed to COL and SEG patterns, respectively. An alternative analysis was required. Instead of quantifying the recruitment ratio, decay of the peak TIRF intensity was measured. If pLck kinase activity was more sustained, SH2_YPET would continue to be recruited and retained for a slower signal decay. Comparison between traces on both COL and SEG patterns revealed more rapid decay of TIRF intensity in cells seeded on SEG patterns. The shorter pLck activation could account for the observed poor IL-2 secretions and cellular activation on SEG patterns.

Chapter 5

5. Conclusion and Future Directions

The primary aim of the two reporters was to understand the spatial role of CD28 in T-cell modulating T-activation. Motivated by the awesome potential of immunotherapy for cancer treatments, this dissertation attempts to understand how spatial cues could be used to modify cellular activation for adoptive immunotherapy.

For Jurkat cells, co-engagement of CD3 and CD28 (as on COL surfaces) was needed to induce strong IL-2 secretions, a marker of robust T-cell activation. Previous work in our lab identified activated pLck as the intermediary between CD3- and CD28- associate signaling pathways. Lck is a well-studied member of the Src family kinases. However many questions remain about the protein. At the most basic level, its activation is not well understood. The protein is able to autophosphorylate *in vitro* and a population of activated protein exists before stimulation

(Nika, Soldani et al. 2010). However, what is happening during activation to induce pLck kinase activity for subsequent signaling cascades? And how is it regulated? Many studies propose spatial organization as a means to control pLck activity (Dustin, Chakraborty et al. 2010, Rossy, Williamson et al. 2012, Bashour, Tsai et al. 2014). A dynamic, real-time reporter of pLck activity was needed.

Many groups utilize FRET reporters to investigate cellular activities in real-time. A related reporter was the biosensor constructed by Stirnweiss and colleagues to study Lck conformation. They reported a 20% increase in 'open' conformation being recruited to the membrane upon activation. However, no information on intracellular Lck kinase activity was available. Thus my thesis focused on designing and synthesizing a FRET reporter of pLck kinase activity.

The Src reporter from Wang and colleagues was studied in constructing the LckR_FRET reporter. LckR_FRET reporter exhibited an increase in FRET ratio in response to cellular activation. And using micropatterned surfaces, one is able to visualize in real-time, the importance of CD3 engagement on heightened pLck activity. However, limitations of the system prevented the visualization of differences in FRET ratio between Jurkats seeded on COL patterns and those seeded on SEG patterns. The FRET ratio was also sensitive to expression level, cellular movement, and photobleaching of the YPET proteins. Guided by IL-2 secretion assays, it's known that CD28 is required for IL-2 secretion. And the spatial organization of CD3 and CD28 modulates the strength of the activation. IL-2 secretion on COL pattern was ~2.5x that of SEG patterns. However, the FRET ratios, averaged from when the cells have completely spread to about 15 minutes after landing, were indistinguishable between the two surfaces.

Two possible explanations were proposed for the lack of differences in FRET ratios. One, because the dynamic range for the FRET reporter was quite narrow, differences in pLck activity was masked. Two, while the magnitude of the pLck kinase activity was the same, the duration of the activity could be different between the two surfaces.

Next, a recruitment probe was constructed to study the duration of pLck activity. The ITAMs of the CD3 receptors, found throughout the plasma membrane, are well-known targets of pLck kinase activity. And pLck-activated pITAMs rapidly recruit tandem SH2-domain of Zap70 to the membrane. The SH2_YPET reporter revealed a more sustained pLck activity on COL pattern.

What remain unaddressed are the differences in pLck kinase activity on the two surfaces, immediately after T-cell activation. Beyond a more prolonged pLck activity on COL patterns, could the surface induce a stronger spike initially? In another word, is the FRET response larger on COL patterns? To answer that question, the LckR_FRET expression level must be better controlled. One approach would be to switch into a lentiviral transduction system for a more stable expression of the construct. Also, Jurkats could be sorted by LckR_FRET expression levels using FACS. Looking forward into the future, one big question at the system level is the mechanism of the observed prolonged pLck activity. How does CD28 mediate the process? Could CD28 help to recruit pLck? However, both reporters did not reveal heightened pLck activity on CD28 dots in the SEG patterns. And why does the segregation of CD28 engagement from CD3 result in more cellular movement and migration? If future studies were able to elucidate the relevant pathways, they could be targeted during *in vitro* T-cell culturing to improve the efficacy of lymphocyte expansions for adoptive immunotherapies.

Bibliography

1. Abbas, A. K., A. H. Lichtman and S. Pillai (2007). Cellular and molecular immunology. Philadelphia, Saunders Elsevier.

2. Alegre, M. L., K. A. Frauwirth and C. B. Thompson (2001). "T-cell regulation by CD28 and CTLA-4." Nature Reviews Immunology **1**(3): 220-228.

3. Au-Yeung, B. B., S. Deindl, L. Y. Hsu, E. H. Palacios, S. E. Levin, J. Kuriyan and A. Weiss (2009). "The structure, regulation, and function of ZAP-70." Immunol Rev **228**(1): 41-57.

4. August, A. and B. Dupont (1994). "Activation of src family kinase lck following CD28 crosslinking in the Jurkat leukemic cell line." Biochem Biophys Res Commun **199**(3): 1466-1473.

5. Bashour, K. T., J. Tsai, K. Shen, J. H. Lee, E. Sun, M. C. Milone, M. L. Dustin and L. C. Kam (2014). "Cross talk between CD3 and CD28 is spatially modulated by protein lateral mobility." Mol Cell Biol **34**(6): 955-964.

6. Boggon, T. J. and M. J. Eck (2004). "Structure and regulation of Src family kinases." Oncogene **23**(48): 7918-7927.

7. Boomer, J. S. and J. M. Green (2010). "An enigmatic tail of CD28 signaling." Cold Spring Harb Perspect Biol **2**(8): a002436.

8. Bunnell, S. C., D. I. Hong, J. R. Kardon, T. Yamazaki, C. J. McGlade, V. A. Barr and L. E. Samelson (2002). "T cell receptor ligation induces the formation of dynamically regulated signaling assemblies." Journal of Cell Biology **158**(7): 1263-1275.

9. Chu, P. C., J. Wu, X. C. Liao, J. Pardo, H. R. Zhao, C. F. Li, M. K. Mendenhall, E. Pali, M. Shen, S. Yu, V. C. Taylor, G. Aversa, S. Molineaux, D. G. Payan and E. S. Masuda (2004). "A novel role for p21-activated protein kinase 2 in T cell activation." Journal of Immunology **172**(12): 7324-7334.

10. Consensus CDS, C. "CCDS1260.1 Human CD3-zeta." from http://www.ncbi.nlm.nih.gov/CCDS/CcdsBrowse.cgi?REQUEST=CCDS&ORGANISM=0&BUILDS=CURRENTBUILDS&DATA=CCDS1260.1.

11. Consensus CDS, C. "CCDS48427.1 Mouse CD3-zeta." from http://www.ncbi.nlm.nih.gov/CCDS/CcdsBrowse.cgi?REQUEST=CCDS&DATA=CCDS48427.

12. Dustin, M. L., A. K. Chakraborty and A. S. Shaw (2010). "Understanding the structure and function of the immunological synapse." Cold Spring Harb Perspect Biol **2**(10): a002311.

13. Fazilleau, N., L. Mark, L. J. McHeyzer-Williams and M. G. McHeyzer-Williams (2009). "Follicular Helper T Cells: Lineage and Location." Immunity **30**(3): 324-335.

14. Janeway, C. (2005). Immunobiology : the immune system in health and disease. New York, Garland Science.

15. June, C. H. (2007). "Adoptive T cell therapy for cancer in the clinic." Journal of Clinical Investigation **117**(6): 1466-1476.

16. Kalos, M., B. L. Levine, D. L. Porter, S. Katz, S. A. Grupp, A. Bagg and C. H. June (2011). "T Cells with Chimeric Antigen Receptors Have Potent Antitumor Effects and Can Establish Memory in Patients with Advanced Leukemia." Science Translational Medicine **3**(95).

17. Klebanoff, C. A., N. Acquavella, Z. Yu and N. P. Restifo (2011). "Therapeutic cancer vaccines: are we there yet?" Immunol Rev **239**(1): 27-44.

18. Koretzky, G. A. and P. S. Myung (2001). "Positive and negative regulation of T-cell activation by adaptor proteins." Nature Reviews Immunology **1**(2): 95-107.

19. Lee, K. H., A. D. Holdorf, M. L. Dustin, A. C. Chan, P. M. Allen and A. S. Shaw (2002). "T cell receptor signaling precedes immunological synapse formation." Science **295**(5559): 1539-1542.

20. Mattheyses, A. L., S. M. Simon and J. Z. Rappoport (2010). "Imaging with total internal reflection fluorescence microscopy for the cell biologist." J Cell Sci **123**(Pt 21): 3621-3628.

21. Maude, S. L., N. Frey, P. A. Shaw, R. Aplenc, D. M. Barrett, N. J. Bunin, A. Chew, V. E. Gonzalez, Z. Zheng, S. F. Lacey, Y. D. Mahnke, J. J. Melenhorst, S. R. Rheingold, A. Shen, D. T. Teachey, B. L. Levine, C. H. June, D. L. Porter and S. A. Grupp (2014). "Chimeric antigen receptor T cells for sustained remissions in leukemia." N Engl J Med **371**(16): 1507-1517.

22. Maus, M. V., S. A. Grupp, D. L. Porter and C. H. June (2014). "Antibody-modified T cells: CARs take the front seat for hematologic malignancies." Blood **123**(17): 2625-2635.

23. Merrifield, C. J., M. E. Feldman, L. Wan and W. Almers (2002). "Imaging actin and dynamin recruitment during invagination of single clathrin-coated pits." Nat Cell Biol **4**(9): 691-698.

24. Mozaffarian, D., E. J. Benjamin, A. S. Go, D. K. Arnett, M. J. Blaha, M. Cushman, S. de Ferranti, J. P. Despres, H. J. Fullerton, V. J. Howard, M. D. Huffman, S. E. Judd, B. M. Kissela, D. T. Lackland, J. H. Lichtman, L. D. Lisabeth, S. M. Liu, R. H. Mackey, D. B. Matchar, D. K. McGuire, E. R. Mohler,

C. S. Moy, P. Muntner, M. E. Mussolino, K. Nasir, R. W. Neumar, G. Nichol, L. Palaniappan, D. K. Pandey, M. J. Reeves, C. J. Rodriguez, P. D. Sorlie, J. Stein, A. Towfighi, T. N. Turan, S. S. Virani, J. Z. Willey, D. Woo, R. W. Yeh, M. B. Turner, A. H. A. S. Comm and S. S. Subcomm (2015). "Heart Disease and Stroke Statistics-2015 Update A Report From the American Heart Association." Circulation **131**(4): E29-E322.

25. Na, S. and N. Wang (2008). "Application of fluorescence resonance energy transfer and magnetic twisting cytometry to quantify mechanochemical signaling activities in a living cell." Science Signaling **1**(34): pl1.

26. National Cancer Institute, N. (2015). "Annual Report to the Nation on the Status of Cancer, 1975-2011." **March 30, 2015**.

27. Nika, K., C. Soldani, M. Salek, W. Paster, A. Gray, R. Etzensperger, L. Fugger, P. Polzella, V. Cerundolo, O. Dushek, T. Hofer, A. Viola and O. Acuto (2010). "Constitutively active Lck kinase in T cells drives antigen receptor signal transduction." Immunity **32**(6): 766-777.

28. O'Shea, J. J. and W. E. Paul (2010). "Mechanisms underlying lineage commitment and plasticity of helper CD4+ T cells." Science **327**(5969): 1098-1102.

29. Parham, P. and C. Janeway (2009). The immune system. London ; New York, Garland Science.

30. Pot, C., L. Apetoh and V. K. Kuchroo (2011). "Type 1 regulatory T cells (Tr1) in autoimmunity." Semin Immunol **23**(3): 202-208.

31. Restifo, N. P., M. E. Dudley and S. A. Rosenberg (2012). "Adoptive immunotherapy for cancer: harnessing the T cell response." Nat Rev Immunol **12**(4): 269-281.

32. Rosenberg, S. A., J. C. Yang, R. M. Sherry, U. S. Kammula, M. S. Hughes, G. Q. Phan, D. E. Citrin, N. P. Restifo, P. F. Robbins, J. R. Wunderlich, K. E. Morton, C. M. Laurencot, S. M. Steinberg, D. E. White and M. E. Dudley (2011). "Durable Complete Responses in Heavily Pretreated Patients with Metastatic Melanoma Using T-Cell Transfer Immunotherapy." Clinical Cancer Research **17**(13): 4550-4557.

33. Rossy, J., D. J. Williamson and K. Gaus (2012). "How does the kinase Lck phosphorylate the T cell receptor? Spatial organization as a regulatory mechanism." Front Immunol **3**: 167.

34. Sakaguchi, S., T. Yamaguchi, T. Nomura and M. Ono (2008). "Regulatory T cells and immune tolerance." Cell **133**(5): 775-787.

35. Sethi, A., N. Kulkarni, S. Sonar and G. Lal (2013). "Role of miRNAs in CD4 T cell plasticity during inflammation and tolerance." Front Genet **4**: 8.

36. Shan, X. C., M. J. Czar, S. C. Bunnell, P. H. Liu, Y. S. Liu, P. L. Schwartzberg and R. L. Wange (2000). "Deficiency of PTEN in Jurkat T cells causes constitutive localization of Itk to the plasma membrane and hyperresponsiveness to CD3 stimulation." Molecular and Cellular Biology **20**(18): 6945-6957.

37. Shaner, N. C., P. A. Steinbach and R. Y. Tsien (2005). "A guide to choosing fluorescent proteins." Nature Methods **2**(12): 905-909.

38. Shen, K., V. K. Thomas, M. L. Dustin and L. C. Kam (2008). "Micropatterning of costimulatory ligands enhances CD4+ T cell function." Proc Natl Acad Sci U S A **105**(22): 7791-7796.

39. Soni, A. (2014). "Trends in Use and Expenditures for Cancer Treatment among Adults 18 and Older, U.S. Civilian Noninstitutionalized Population, 2001 and 2011. ." Medical Expenditure Panel Survey: Agency for Healthcare Research and Quality **Statistical Brief #443**.

40. Soroosh, P. and T. A. Doherty (2009). "Th9 and allergic disease." Immunology **127**(4): 450-458.

41. Stirnweiss, A., R. Hartig, S. Gieseler, J. A. Lindquist, P. Reichardt, L. Philipsen, L. Simeoni, M. Poltorak, C. Merten, W. Zuschratter, Y. Prokazov, W. Paster, H. Stockinger, T. Harder, M. Gunzer and B. Schraven (2013). "T Cell Activation Results in Conformational Changes in the Src Family Kinase Lck to Induce Its Activation." Science Signaling **6**(263).

42. Tesmer, L. A., S. K. Lundy, S. Sarkar and D. A. Fox (2008). "Th17 cells in human disease." Immunol Rev **223**: 87-113.

43. Tran, K. Q., J. H. Zhou, K. H. Durflinger, M. M. Langhan, T. E. Shelton, J. R. Wunderlich, P. F. Robbins, S. A. Rosenberg and M. E. Dudley (2008). "Minimally cultured tumor-infiltrating lymphocytes display optimal characteristics for adoptive cell therapy." Journal of Immunotherapy **31**(8): 742-751.

44. Tseng, S. Y., M. L. Liu and M. L. Dustin (2005). "CD80 cytoplasmic domain controls localization of CD28, CTLA-4, and protein kinase C theta in the immunological synapse." Journal of Immunology **175**(12): 7829-7836.

45. Ueda, Y., B. L. Levine, M. L. Huang, G. J. Freeman, L. M. Nadler, C. H. June and S. G. Ward (1995). "Both Cd28 Ligands Cd80 (B7-1) and Cd86 (B7-2) Activate Phosphatidylinositol 3-Kinase, and

Wortmannin Reveals Heterogeneity in the Regulation of T-Cell Il-2 Secretion." International Immunology **7**(6): 957-966.

46. Wang, Y., E. L. Botvinick, Y. Zhao, M. W. Berns, S. Usami, R. Y. Tsien and S. Chien (2005). "Visualizing the mechanical activation of Src." Nature **434**(7036): 1040-1045.

47. Weiner, H. L. (2001). "Induction and mechanism of action of transforming growth factor-beta-secreting Th3 regulatory cells." Immunological Reviews **182**: 207-214.

48. Yao, Z. Q. and J. P. Moorman (2013). "Immune exhaustion and immune senescence: two distinct pathways for HBV vaccine failure during HCV and/or HIV infection." Arch Immunol Ther Exp (Warsz) **61**(3): 193-201.

49. Yudushkin, I. A. and R. D. Vale (2010). "Imaging T-cell receptor activation reveals accumulation of tyrosine-phosphorylated CD3 zeta in the endosomal compartment." Proceedings of the National Academy of Sciences of the United States of America **107**(51): 22128-22133.

50. Zhao, Y. B., Z. L. Zheng, C. J. Cohen, L. Gattinoni, D. C. Palmer, N. P. Restifo, S. A. Rosenberg and R. A. Morgan (2006). "High-efficiency transfection of primary human and mouse T lymphocytes using RNA electroporation." Molecular Therapy **13**(1): 151-159.

51. Zhou, L., M. M. W. Chong and D. R. Littman (2009). "Plasticity of CD4(+) T Cell Lineage Differentiation." Immunity **30**(5): 646-655.

52. Zhu, J. F. and W. E. Paul (2010). "Heterogeneity and plasticity of T helper cells." Cell Research **20**(1): 4-12.

53. Zimmermann, L., W. Paster, J. Weghuber, P. Eckerstorfer, H. Stockinger and G. J. Schutz (2010). "Direct Observation and Quantitative Analysis of Lck Exchange between Plasma Membrane and Cytosol in Living T Cells." Journal of Biological Chemistry **285**(9): 6063-6070.

Appendix

A. Matlab Codes for Timelapse FRET Analysis

A.1 FRET_MM_NoMask.m

The .m file performs cross correlation and FRET ratio calculation on a pixel-to-pixel basis.

```
clear; clc;

%%  Pre-treating the data  using MetaMorph%%

% select an area as the background using trace region icon

% BACKGROUND SUBTRACTION
% Go to 'Process' menu
% --> Background and Shading Correction...
% --> select source image
%     select full stack (subtract background from each image of the
stack)
% --> Operation: -> Statistical Correction
% --> Parameters: -> Region Statistics -> Average -> Region number: 1

% 3X3 MEDIAN FILTER SMOOTHING
% Go to 'Process' menu
% --> Basic Filters...
% --> select 'Statistical Correction' stack
%     select full stack (smoothing of the whole stack)
% --> Operation: -> Median
% --> Parameters: -> filter width: 3 -> filter height: 3 -> sub-sample
ratio: 1

Donor = 'COL1_1Donor_MF.tif';
%%______CHANGE NAME
Acceptor = 'COL1_1Acceptor_MF.tif';
%%______CHANGE NAME
Stamp = 'COL1_1Stamp_MF.tif';
%%______CHANGE NAME
```

```
%%  Crop the YFP image so it can be used as the template in normxcorr2
%%

figure
num_image = max(size(imfinfo(Donor)));
[YFPcr rect] = imcrop(imadjust(imread(Donor,1))); % YFPcr: adjusted
image intensity (like in imageJ)
title('Crop the YFP/Donor image');
[isize jsize] = size(YFPcr);

%%         cross correlation between mCherry and YFP images
%%

tic

% Initialize variables
offsets = zeros(num_image,3);
offsets1 = zeros(num_image,3);

for i=1:num_image

    YFPcrop = imcrop(imread(Donor,i), rect); % YFPcrop: intensity
unadjusted image

    mFP = imadjust(imread(Acceptor,i)); % Read in the mCherry image as
the base
    A = normxcorr2(YFPcrop,mFP); % Template is YFP cropped image, base
is mCherry

    [max_A, imax] = max(abs(A(:)));
    [ipeak, jpeak] = ind2sub(size(A),imax(1));
    corr_offset1 = [ (ipeak-size(YFPcrop,1)) (jpeak-size(YFPcrop,2))
]; % How the template image needs to translate [i distance, j
distance]
    offsets(i,1:2) = corr_offset1;
    offsets(i,3) = max_A;
    rect_new = [corr_offset1(2)+.51,
corr_offset1(1)+.51,rect(3),rect(4)];
    mFPcrop = imcrop(imread(Acceptor,i), rect_new); % Crop the mCherry
image unadjusted
```

```
    % Calculate FRET ratio, mCherry/YFP on a pixel-by-pixel basis
    FRETratio = (double(mFPcrop) ./ double(YFPcrop));
%unadjusted/unadjusted
    FRETratio(isnan(FRETratio)) = 0;
    FRETratio(isinf(FRETratio)) = 0;

    % Apply the cell mask to the FRET ratio
    FRETcell{i} = FRETratio;

    % stamp for later
    stampCro = imcrop(imadjust(imread(Stamp,i)), rect);
     i

end
toc % read elapsed time from stopwatch
save('FRETcell_COL1_1.mat')
%%______CHANGE NAME
close all
```

A.2 FRET_plot_stampNoSB.m

The .m file generates a heat map from the FRET ratios. And it overlay the stamping on top.

```
%%                    Plot figure and set properties
%%

cmap  = jet(256);
cmap(1,:) = [0 0 0]
bot = 0;
cap = 2;
set(gcf,'Color','white')
set(gca,'YColor','blue')

aviobj = VideoWriter('COL1_1_MF_noCB');
%%______CHANGE NAME
aviobjS = VideoWriter('COL1_1_MF_S');
%%______CHANGE NAME
aviobj.FrameRate = 5;
```

```
aviobjS.FrameRate = 5;

open(aviobj);
for i=1:num_image
    figure
    imshow(FRETcell{i},[bot cap],'Colormap',cmap, 'Border', 'tight');
    F = getframe;
    writeVideo(aviobj,F);
    close
    i
end
close(aviobj);

open(aviobjS);
for k=1:num_image
    figure
    imshow(stampCro, 'Border', 'tight')
    G = getframe;
    writeVideo(aviobjS,G);
    close
    k
end
close(aviobjS);

%% convert avi to tif
pause

%% superimpose stamp onto FRET image

aviobjO = VideoWriter('COL1_1_MFandS');
%%______CHANGE NAME
aviobjO.FrameRate = 5;

open(aviobjO);
for i=1:num_image
    h = figure;
    bg = imread('COL1_1_noCB.tif',i);
    %______CHANGE NAME
    im = imread('COL1_1_MF_S.tif',i);
    %______CHANGE NAME
    imshow(bg, 'Border', 'tight');
```

```
    hold on
    iim2 = image(im,'XData',[0 0],'YData',[0 0]);
    alpha(iim2, 0.15);
    F = getframe(h);
    writeVideo(aviobjO,F);
    i
    close
end
close(aviobjO);
```

A.3 FRET_plot_videoSB.m

The .m file generates an .avi of the FRET ratio heat map with its scale or color bar.

```
%%                    Plot figure and set properties
%%

cmap  = jet(256);
cmap(1,:) = [0 0 0]
bot = 0;
cap = 2;
set(gcf,'Color','white')
set(gca,'YColor','blue')

aviobj = VideoWriter('COL1_1');
%%______CHANGE NAME
aviobj.FrameRate = 5;
open(aviobj);
for i=1:num_image
%for i=1:1
    h = figure;
    imshow(FRETcell{i},[bot cap],'Colormap',cmap), colorbar
    F = getframe(h);
    writeVideo(aviobj,F);
    close
    i
end
close(aviobj);
```

A.4 FRET_MMROI_cd3vcd28.m

The .m file completes FRET ratio calculation for 2 regions of interest.

```
load('FRETcell_COL1_1.mat')
%%______CHANGE NAME

%%            Define a region of interest for FRET mask              %%

%  Define ROI of the cell body
figure
bg2 = imcrop(imadjust(imread(Donor,16)),rect);
im2 = imcrop(imread(Stamp,1),rect);


imshow(bg2, 'Border', 'tight');
hold on
iim2 = image(im2,'XData',[0 0],'YData',[0 0]);
alpha(iim2, 0.4);

title('Select the CD3 dot')
[CD3cell xi1body yi1body]=roipoly;

title('Select the CD28 dot')
[CD28cell xi2body yi2body]=roipoly;

tic

for i=1:num_image

    % Apply the cell mask to the FRET ratio
    FRETroiCD3{i} = FRETcell{i}.*CD3cell;
    FRETroiCD28{i} = FRETcell{i}.*CD28cell;
    % Calculate the mean FRET in the region of interest
    FRETmeanCD3(i) = mean2(FRETroiCD3{i}(CD3cell==1));
    FRETmeanCD28(i) = mean2(FRETroiCD28{i}(CD28cell==1));

    % YFP
    YFPalone{i} = imcrop(imread(Donor,i), rect); %PD
    YFPvalue = double(YFPalone{i});
```

```
    % Apply the mask to the YFP value
    YFProiCD3{i} = YFPvalue.*CD3cell;
    YFProiCD28{i} = YFPvalue.*CD28cell;
    % Calculate the mean YFP in the region of interest
    YFPmeanCD3(i) = mean2(YFProiCD3{i}(CD3cell==1));
    YFPmeanCD28(i) = mean2(YFProiCD28{i}(CD28cell==1));

    % mCherry
    mFPalone{i} = imcrop(imread(Acceptor,i), rect_new); %PD
    mFPvalue = double(mFPalone{i});
    % Apply the mask to the mCherry value
    mFProiCD3{i} = mFPvalue.*CD3cell;
    mFProiCD28{i} = mFPvalue.*CD28cell;
    % Calculate the mean mCherry in the region of interest
    mFPmeanCD3(i) = mean2(mFProiCD3{i}(CD3cell==1));
    mFPmeanCD28(i) = mean2(mFProiCD28{i}(CD28cell==1));

    i
end

colFRETCD3 = FRETmeanCD3';
colFRETCD28 = FRETmeanCD28';

colYFPCD3 = YFPmeanCD3';
colYFPCD28 = YFPmeanCD28';

colmFPCD3 = mFPmeanCD3';
colmFPCD28 = mFPmeanCD28';

toc % read elapsed time from stopwatch

save('FRET_CD3vCD28.mat')
%%______CHANGE NAME after running...
```

A.5 FRET_MMROI_plot_cd3vcd28.m

The .m file plot the data from FRET_MMROI_cd3vcd28.m.

```
figure
```

```
t = 0:.5:((num_image-1)*.5);
subplot(3,1,1)
[haxes,hline1,hline2] = plotyy(t,[colYFPCD3 colYFPCD28],t, [colmFPCD3
colmFPCD28]);
set(hline1(1),'LineStyle','-.','LineWidth',2,'Color','green'); % set
linewidth and color
set(hline1(2),'LineStyle','--','LineWidth',2,'Color','green'); % set
linewidth and color
set(hline2(1),'LineStyle','-.','LineWidth',2,'Color','red'); % set
linewidth and color
set(hline2(2),'LineStyle','--','LineWidth',2,'Color','red'); % set
linewidth and colorset(haxes(1),'ycolor','k'); % set axis color
set(haxes(1),'ycolor','g'); % set axis color
set(haxes(2),'ycolor','r'); % set axis color
ylabel(haxes(1),'YFP intensity','Color','green','FontSize',15) % left
y-axis
ylabel(haxes(2),'mCherry intensity','Color','red','FontSize',15) %
right y-axis
xlabel(haxes(1),'Time (min)','FontSize',15) % x-axis
title('YFP vs mCherry','Fontsize',20) % title

t = 0:30:((num_image-1)*30);
subplot(3,1,2)
[haxes,hline1,hline2] = plotyy(t,[colFRETCD3 colFRETCD28],t,
[colFRETCD3 colFRETCD28]);
set(hline1(1),'LineStyle','-.','LineWidth',2,'Color','green'); % set
linewidth and color
set(hline1(2),'LineStyle','--','LineWidth',2,'Color','green'); % set
linewidth and color
set(hline2(1),'LineStyle','-.','LineWidth',2,'Color','blue'); % set
linewidth and color
set(hline2(2),'LineStyle','--','LineWidth',2,'Color','blue'); % set
linewidth and colorset(haxes(1),'ycolor','k'); % set axis color
set(haxes(1),'ycolor','b','YLim',[0 1]); % set axis color
set(haxes(2),'ycolor','b','YLim',[0 1]); % set axis color
ylabel(haxes(1),'FRET ratio','Color','blue','FontSize',15) % left y-
axis
ylabel(haxes(2),'FRET ratio','Color','blue','FontSize',15) % right y-
axis
xlabel(haxes(1),'Time (s)','FontSize',15) % x-axis
title('FRET ratio','Fontsize',20) % title
```

B. Matlab Codes for Timelapse Recruitment Analysis

B.1 Zap70_all.m

The .m file calculates ratio of TIRF to epifluorescence intensities on a pixel-to-pixel basis.

```
clear; clc;

TIRF = 'T3_TIRF.tif';
%%______CHANGE NAME
EPI = 'T3_EPI.tif';
%%______CHANGE NAME
DAPI = 'T3_Stamp.tif';
%%______CHANGE NAME

num_image = max(size(imfinfo(TIRF)));

for i=1:num_image

    M{i}= double(imread(TIRF,i));
    Mcrop = double(M{i});

    C{i} = double(imread(EPI,i));
    Ccrop = double(C{i});

    Recruit = Mcrop./Ccrop;
    Recruit(isnan(Recruit)) = 0;
    Recruit(isinf(Recruit)) = 0;
    ReMap{i} = Recruit;

    i
end

save('T3_All.mat')
%%______CHANGE NAME
```

B.2 Zap70_ROI.m

The .m file calculates ratio of TIRF to epifluorescence intensities averaged for 2 regions of interest.

```
load('T3_All.mat')
%%______CHANGE NAME


%%            Define a region of interest          %%


%  Define ROI of the cell body
figure
bg2 = imadjust(imread(TIRF,30));
im2 = imadjust(imread(DAPI,1));
imshow(bg2, 'Border', 'tight');
hold on
iim2 = image(im2,'XData',[0 0],'YData',[0 0]);
alpha(iim2, 0.5);

%%% frame with largest cell body
title('Select the cell body_dot')
[BWcellD xibodyD yibodyD]=roipoly;

%%% frame with largest cell body
title('Select the cell body_dot')
[BWcellN xibodyN yibodyN]=roipoly;

close

for i=1:num_image

    MembraneD{i} = M{i}.*BWcellD;
    MembraneN{i} = M{i}.*BWcellN;
    M_meanD(i) = mean2(MembraneD{i}(BWcellD==1));
    M_meanN(i) = mean2(MembraneN{i}(BWcellN==1));

    CytosolD{i} = C{i}.*BWcellD;
    CytosolN{i} = C{i}.*BWcellN;
```

```
    C_meanD(i) = mean2(CytosolD{i}(BWcellD==1));
    C_meanN(i) = mean2(CytosolN{i}(BWcellN==1));

    RecruitD{i} = ReMap{i}.*BWcellD;
    RecruitN{i} = ReMap{i}.*BWcellN;
    R_meanD(i) = mean2(RecruitD{i}(BWcellD==1));
    R_meanN(i) = mean2(RecruitN{i}(BWcellN==1));
    i
end

M_meanD = M_meanD';
M_meanN = M_meanN';
C_meanD = C_meanD';
C_meanN = C_meanN';
R_meanD = R_meanD';
R_meanN = R_meanN';

figure
t = 0:.25:((num_image-1)*.25);

subplot(3,2,1)
[haxes,hline1,hline2] = plotyy(t,M_meanD,t, C_meanD);
set(hline1,'LineWidth',2,'Color','green'); % set linewidth and color
set(hline2,'LineWidth',2,'Color','red'); % set linewidth and color
set(haxes(1),'ycolor','g'); % set axis color
ylim(haxes(1), [min(M_meanD), max(M_meanD)]);
set(haxes(2),'ycolor','r'); % set axis color
ylim(haxes(2), [min(C_meanD), max(C_meanD)]);
ylabel(haxes(1),'TIRF','Color','green','FontSize',12) % left y-axis
ylabel(haxes(2),'EPI','Color','red','FontSize',12) % right y-axis
xlabel(haxes(1),'Time (min)','FontSize',12) % x-axis
title('Percentage TIRF_D_O_T vs EPI_D_O_T','Fontsize',17) % title

subplot(3,2,2)
[haxes,hline1,hline2] = plotyy(t,M_meanN,t, C_meanN);
set(hline1,'LineWidth',2,'Color','green','LineStyle',':'); % set
linewidth and color
set(hline2,'LineWidth',2,'Color','red','LineStyle',':'); % set
linewidth and color
set(haxes(1),'ycolor','g'); % set axis color
ylim(haxes(1), [min(M_meanN), max(M_meanN)]);
```

```
set(haxes(2),'ycolor','r'); % set axis color
ylim(haxes(2), [min(C_meanN), max(C_meanN)]);
ylabel(haxes(1),'TIRF','Color','green','FontSize',12) % left y-axis
ylabel(haxes(2),'EPI','Color','red','FontSize',12) % right y-axis
xlabel(haxes(1),'Time (min)','FontSize',12) % x-axis
title('Percentage TIRF_N_O_N_-_D_O_T vs EPI_N_O_N_-
_D_O_T','Fontsize',17) % title

subplot(3,2,3)
P = plot(t,M_meanD,'g',t,M_meanN,'g');
P(1).LineWidth = 2; P(2).LineWidth = 2;
P(2).LineStyle =':';
xlabel('Time (min)','FontSize',12);
ylabel('TIRF Intensity','FontSize',12) % left y-axis
ylim([0, max(M_meanD)]);
title('Intensity TIRF_D_O_T vs TIRF_N_O_N_-_D_O_T','Fontsize',17) %
title

subplot(3,2,4)
P = plot(t,C_meanD,'r',t,C_meanN,'r');
P(1).LineWidth = 2; P(2).LineWidth = 2;
P(2).LineStyle =':';
xlabel('Time (min)','FontSize',12);
ylabel('EPI Intensity','FontSize',12) % left y-axis
title('Intensity EPI_D_O_T vs EPI_N_O_N_-_D_O_T','Fontsize',17) %
title

subplot(3,2,[5,6])
P = plot(t,R_meanD,'b',t,R_meanN,'b');
P(1).LineWidth = 2; P(2).LineWidth = 2;
P(2).LineStyle =':';
xlabel('Time (min)','FontSize',12);
ylabel('TIRF Intensity','FontSize',12) % left y-axis
ylim([0, max(R_meanD)]);
title('TIRF/EPI_D_O_T vs TIRF/EPI_N_O_N_-_D_O_T','Fontsize',17) %
title

save('T3_ROI.mat')
%%_______CHANGE NAME
```